FINAL TECHNICAL REPORT

(1) ONR Grant Number: N00014-99-1-0738

(2) Titles of Proposed Research:

(i) "Innovative Relaxor-Based PiezoCrystals: Phase Diagrams, Crystal Growth, Domain Structures and Electric Properties"

(ii) "Piezo- and Ferroelectric Materials Based on Morphotropic Phase Boundary: Synthesis, Characterization and Structure – Property Relations"

(3) Duration of Effort: May 15, 1999 to May 14, 2005, extended to Mar. 31, 2006.

(4) Institution: Simon Fraser University, Burnaby, BC, V5A 1S6, Canada
Type of Business: Educational

(5) Technical Point of Contact:

Dr. Zuo G. Ye
Department of Chemistry
Simon Fraser University,
8888 University Drive, Burnaby, BC, V5A 1S6, Canada
Tel: (604)-291-3351; Fax: (604)-291-3765; Email: zye@sfu.ca

(6) Administrative Point of Contact:

Mrs. Ellen Loosley
Office of Research Services
Simon Fraser University,
8888 University Drive, Burnaby, BC, V5A 1S6, Canada
Tel: (604)-291-3842; Fax: (604)-291-3477; Email: loosley@sfu.ca

FINAL TECHNICAL REPORT

(1) ONR Grant Number: N00014-99-1-0738

(2) Titles of Proposed Research:

(i) "Innovative Relaxor-Based PiezoCrystals: Phase Diagrams, Crystal Growth, Domain Structures and Electric Properties"

(ii) "Piezo- and Ferroelectric Materials Based on Morphotropic Phase Boundary: Synthesis, Characterization and Structure – Property Relations"

(3) Duration of Effort: May 15, 1999 to May 14, 2005, extended to Mar. 31, 2006.

(4) Institution: Simon Fraser University, Burnaby, BC, V5A 1S6, Canada
Type of Business: Educational

(5) Technical Point of Contact:

Dr. Zuo G. Ye
Department of Chemistry
Simon Fraser University,
8888 University Drive, Burnaby, BC, V5A 1S6, Canada
Tel: (604)-291-3351; Fax: (604)-291-3765; Email: zye@sfu.ca

(6) Administrative Point of Contact:

Mrs. Ellen Loosley
Office of Research Services
Simon Fraser University,
8888 University Drive, Burnaby, BC, V5A 1S6, Canada
Tel: (604)-291-3842; Fax: (604)-291-3477; Email: loosley@sfu.ca

REPORT DOCUMENTATION PAGE

Form Approved
OMB No. 0704-0188

1. REPORT DATE *(DD-MM-YYYY)*	2. REPORT TYPE	3. DATES COVERED *(From - To)*
15-07-2006	Final Technical Report	May 1999 - March 2006

4. TITLE AND SUBTITLE
1). "Innovative Relaxor-Based PiezoCrystals: Phase Diagrams, Crystal Growth, Domain Structures and Electric Properties";
2). "Piezo- and Ferroelectric Materials Based on Morphotropic Phase Boundary: Synthesis, Characterization and Structure - Property Relations"

5a. CONTRACT NUMBER

5b. GRANT NUMBER
N00014-99-1-0738

5c. PROGRAM ELEMENT NUMBER

6. AUTHOR(S)
Ye, Zuo G.

5d. PROJECT NUMBER

5e. TASK NUMBER

5f. WORK UNIT NUMBER

7. PERFORMING ORGANIZATION NAME(S) AND ADDRESS(ES)
Simon Fraser University
8888 University Drive
Burnaby, British Columbia
V5A 1S6, CANADA

8. PERFORMING ORGANIZATION REPORT NUMBER
31-559016

9. SPONSORING/MONITORING AGENCY NAME(S) AND ADDRESS(ES)
Office of Naval Research
Materials Division, ONR 332
One Liberty Center
875 North Randolph Street, Suite 1425
Arlington, VA 22203-1995

10. SPONSOR/MONITOR'S ACRONYM(S)
ONR

11. SPONSOR/MONITOR'S REPORT NUMBER(S)

12. DISTRIBUTION/AVAILABILITY STATEMENT
Approved for Public Release; distribution is Unlimited.

13. SUPPLEMENTARY NOTES
Work performed in collaboration with Dr. John Y. Yamashita, Senior Research Scientist, Corporate R & D Center, Toshiba Corp., Japan, who has been an international industrial adviser of this project.

14. ABSTRACT

This final technical report is on the research work carried out in the area of design, synthesis and characterization of novel piezo- and ferroelectric materials, especially in the form of single crystals, with a view to developing new materials resources for the next generation of electromechanical transducers in a wide range of Navy and civilian applications. Our contributions have covered the following main areas: (a) Thermodynamic analysis and establishment of relevant phase diagrams, which provide information on the solubility and saturation rate, crucial for the growth of large and high quality piezocrystals. (b) Growth of piezocrystals by various techniques, and design and synthesis of new material systems which have been proven to be very interesting as potential high Tc and high performance piezocrystal resources. (c) Investigation of the complex morphotropic phase diagrams, phase symmetry, domain structures and phase transitions of the most important piezocrystal solid solution systems, which helps illustarte the microscopic mechanisms underlying the extraordinary piezo- and ferroelectric properties. (d) Characterization of a broad spectrum of physical properties, in particular the puzzling structure, dynamics and relaxation of polar nanoregions in relaxors, which has led to the discovery of a new phenomenon of double freezing of two overlapping relaxation processes.

15. SUBJECT TERMS
Piezoelectrics; Single crystal growth; Phase diagrams; Domain structure; Phase transitions; Morphotropic phase boundary; Polar nanoregions; Relaxor ferroelectrics; Electromechanical transducers.

16. SECURITY CLASSIFICATION OF:			17. LIMITATION OF ABSTRACT	18. NUMBER OF PAGES	19a. NAME OF RESPONSIBLE PERSON
a. REPORT	b. ABSTRACT	c. THIS PAGE			Loosley, Ellen
					19b. TELEPHONE NUMBER *(Include area code)*
U	U	U	SAR	85	(604)-291-3842

Table of Contents

Contract Information

Contract Number	N00014-99-1-0738
Titles of Research	(1) Innovative Relaxor-Based PiezoCrystals: Phase Diagrams, Crystal Growth, Domain Structures and Electric Properties (2) Piezo- and Ferroelectric Materials Based on Morphotropic Phase Boundary: Synthesis, Characterization and Structure – Property Relations
Principal Investigator	Dr. Zuo G. Ye
Organization	Simon Fraser University

Technical Section

1. Technical Objectives

This research program contained two consecutive parts which were closely related to each other.

1.1) Part 1: "Innovative Relaxor-Based PiezoCrystals: Phase Diagrams, Crystal Growth, Domain Structures and Electric Properties"

The first part of the grant covered the period from May 15, 1999 to May 14, 2002.

The primary objective of this proposal was about the investigation of the single crystals of relaxor-based solid solutions, in particular, the $Pb(Mg_{1/3}Nb_{2/3})O_3$ - $PbTiO_3$ [PMN-PT], $Pb(Zn_{1/3}Nb_{2/3})O_3$ - $PbTiO_3$ [PZN-PT], and $Pb(Sc_{1/2}Nb_{1/2})O_3$ - $PbTiO_3$ [PSN-PT] systems. These piezocrystals showed extremely large piezoelectric strain (> 1.5 %) and very high electromechanical coupling factor (k_{33} > 92%), and were being considered as potential materials for the next generation of electromechanical transducers for a broad range of applications both of defense and civilian relevance. The detailed technical plans of this program included the following parts:

1.1.1). To investigate the thermodynamic properties and the melting behavior of the relaxor-based piezocrystals, PZNT and PMNT, and to establish the relevant phase diagrams as guidance for the growth of large and high quality piezoelectric single crystals. The first target system studied in the present FY is PZN-PT of morphotropic composition, i.e. 0.91PZNT-0.09PT [PZNT91/9] and PbO.

1.1.2). To optimize the crystal growth parameters and conditions for the flux and Bridgman growth methods, and to develop new growth processes to grow large and high quality piezocrystals at reasonable cost. The systems investigated are PMNT65/35, PZN, PZNT91/9 and PZNT95.5/4.5.

1.1.3). To analyze and understand the complex domain structures of the piezocrystals, especially the intriguing morphotropic domain structure. The manifold purposes of this investigation lies in: (a) to illustrate the domain and polarization switching under application of electric field for a better understanding of microscopic mechanism of the extremely high piezoelectric performance in piezocrystals; (b) to ultimately correlate the domain structures to the piezoelectric properties of the crystals and to the performance of the devices.

1.1.4). To study the dielectric and piezoelectric properties of the piezocrystals and the related solid solution systems in order to gain a deeper insight into the relaxor behavior and the relation between the nano- and mesostructures and the enhanced piezoelectric properties.

1.2) Part 2: "Piezo- and Ferroelectric Materials Based on Morphotropic Phase Boundary: Synthesis, Characterization and Structure – Property Relations".

The second part of the grant initially covered the period from May 15, 2002 to May 14, 2005, and then was extended to March 31, 2006.

This program was a continued effort in the investigation of the crystal chemistry, crystal growth, crystal structure, domain structures and structure–property relations of novel piezo-/ferroelectric single crystals, with a view to a broad range of electromechanical transducer applications, such as in Navy missions and in medical echo imaging and diagnosing. The overall objectives of this effort included:

1.2.1) Development of effective and improved synthetic routes for the preparation of the recently-developed relaxor-based piezocrystals and the new piezoelectric solid solution materials;

1.2.2) Systematic characterization of a broad spectrum of physical properties of the materials synthesized, ranging from the dielectric, piezo- and ferroelectric properties, to the structure of MPB phases, and to the mesoscopic domain structures, in order to assess their potential applications in electromechanical transducers;

1.2.3) Investigation and understanding of the relationship between the crystal and domain structures and the macroscopic properties, which is essential not only to the development and implementation of new electromechanical devices based on the novel piezocrystals, and to the design of new materials with more enhanced properties.

2. Technical Rationale, Approach and Progress

This Section describes the technical rationale proposed, the technical approach implemented and the technical results and progress obtained. The Section is organized based on the main tasks and efforts which have been performed to achieve the *Technical Objectives*.

2.1). Thermodynamic Properties and Phase Diagrams of Piezocrystal Systems

2.1.1) Technical Rationale

In 1997, single crystals of relaxor-based solid solutions, $Pb(Mg_{1/3}Nb_{2/3})O_3$ - $PbTiO_3$ [PMN-PT], $Pb(Zn_{1/3}Nb_{2/3})O_3$ - $PbTiO_3$ [PZN-PT], were reported to exhibit extremely large piezoelectric strain (> 1%) and very high electromechanical coupling factor (k_{33} > 90%). The excellent performance makes these crystals potential materials for the next generation of electromechanical transducers for such a broad range of applications as powerful undersea SONAR system, high-resolution ultrasonic imaging, etc., both of defense and civilian relevance. At the time of our proposal submission, little attention had been paid to the more fundamental aspects of the crystal chemistry, crystallophysical properties and structure-property relations of these innovative materials. It was, however, well known that these innovative piezocrystals are formed from solid solutions between relaxor ferroelectrc complex perovskites and ferroelectric $PbTiO_3$. They belong to a complex multi-component system containing PbO, ZnO (or MgO or Sc_2O_3), Nb_2O_5 and TiO_2, and the thermodynamic behavior of such a system can be very complex, and the crystal growth is a complicated process. Most of the growth techniques used consist of using lead oxide PbO as flux or high temperature solutions, which was shown to be an efficient solvent for the complex perovskites. Despite the enormous progress which had been made by some research groups in growing large size PNZT and PMNT crystals by the flux method and modified Bridgman technique, the growth results were hardly reproducible, and the quality of the crystals was still a serious problem. For instance, large size crystals usually contained inclusions of flux or an undesirable pyrochlore phase, which made the crystal wafers opaque. The presence of the opaque inclusions deteriorates the piezoelectric performance of the crystals, decreases the reliability of the piezoelectric devices and increases the cost of crystal growth. This was limiting the industrial production of the crystals and their applications, especially in defense areas where both the performance and the reliability of the devices are vital.

The reason for such problems was that there was no phase diagrams available between the piezocrystal compounds and the flux PbO, from which we could systematically control the growth pathway and growth parameters, as was shown by the P.I. in the growth of PMN crystals based on the pseudo-binary phase diagram PMN-PbO. It was obvious that accurate knowledge of the melting behavior and the phase diagrams would point out the optimal growth pathway and thermodynamic parameters to be controlled for the growth of large size and high quality piezocrystals, without inclusions of undesirable phases or flux. Large scale and cost-effective crystal production would then become possible for the innovative piezocrystals to become the next generation of materials for high performance electromechanical transducers.

Therefore, in the first major project of our effort, we proposed to investigate *in a systematic way* the thermodynamic behavior of the piezocrystal compounds and related systems, to determine the congruent or incongruent melting behavior and phase stability of PZN-PT, PMN-PT and other related systems. The problems of the complex multi-component systems for the crystal growth were simplified by considering the possible pseudo-binary systems between PZN-PT, PMN-PT or PSN-PT and the main flux PbO.

2.1.2) Technical Approach

The thermodynamic properties and the melting behavior of various innovative piezocrystal systems, including PZNT91/9 – PbO, PZNT91/9 – PbO – Pyrochlore, PMN – PT, and PMNT65/35 – PbO, were systematically investigated by micro-Differential Thermal Analysis (DTA) combined with a simultaneous micro-Thermal Gravimetry (TG). The equipment used is a Seiko Exstar TG/DTA 6300. The thermal analysis was complemented by the phase analysis by X-ray diffraction and by the microstructure examination under optical microscope. It is important to mention that in order to accurately analyze the thermodynamic behavior of the piezocrystal systems, it was necessary to prevent the PbO flux from volatilizing at high temperatures. For that purpose, Pt microtubes (with an outside diameter of 3.0 mm, a wall thickness of 0.2mm and a length of 12mm) were specially designed and a special technique was developed to seal the Pt-tubes prior to thermal analysis.

The [(1-y)PZNT91/9 - yPbO] system was prepared with 10 wt% increment of y by mixing 5 g of stoichoimetric PbO, MgO, Nb_2O_5 and TiO_2 or homogenous stoichoimetric mixture of pure $Pb(Zn_{1/3}Nb_{2/3})_{0.91}Ti_{0.09}O_3$ powder from single crystals, and PbO. The mixtures were cold-pressed to form a thin disk. A small piece (about 10 mg) was cut out off the disk and charged into a platinum pan (2.5 mm in diameter, 125 mg in weight) for normal (open-pan) thermal measurements. Another small piece (about 10 mg) was sealed under very dry atmosphere into a platinum microtube with an outside diameter of 3.0 mm, a wall thickness of 0.2mm and a length of 12mm for a close-tube thermal analysis. Single crystals of PZNT91/9 were used for single crystal thermal analysis. After each thermal test, the sample in Pt pan was examined under microscope. XRD analysis was performed on selected samples before and after thermal analysis.

To study the thermal stability of PZNT95.5/4.5 crystals, samples (as grown crystals) of about 20 mg each were put in open Pt pans (ϕ=2.5 mm) and heated from 900 to 1300 °C at 10 °C /min. in a neutral gas (N_2) atmosphere. To study the formation of phases after thermal treatments, PZNT crystals were heated in a muffle furnace at various temperatures relevant to the measured thermal events between room temperature and 1300 °C, and then quenched to room temperature in air. X-ray powder diffractometry was undertaken on the ground quenched samples using a Philips powder diffractometer (CuKα, λ=1.5416 Å), and the patterns were analyzed based on the structural data of perovskite and pyrochlore crystals.

In order to study the high temperature phase diagram of the PMNT65/35-PbO system, XRD and Differential thermal analysis (DTA) were performed on a series of samples with the composition (100-y)PMNT65/35-yPbO ($0 \leq y \leq 100$, at an interval of 10 weight percent). Here weight percentage is used since it is a commonly used unit in the crystal growth for convenience.

XRD was performed on the Philips powder diffractometer (Cu Kα, λ = 1.5418 Å). The angular resolution on the 2θ scale for XRD was 0.05°. The scan-step was set at 0.05° intervals. Thermal analysis was carried on simultaneous TG/DTA (Exstar TG/DTA 6300, Seiko Instrument Inc.). The resolution of the DTA is 1 μV.

PMNT65/35 solid solution powders were prepared by the columbite method. X-ray diffraction measurements were carried on the PMNT65/35 samples after the powders were synthesized at 950 °C for 8 hrs. After the pure perovskite phase PMNT65/35 powders were prepared, the powders were mixed with PbO in different weight percentages, ground for 1 hr, pressed into thin pellets, cut into small pieces, and loaded into a one-end-sealed mini Pt tube (OD = 2.0 mm, ID = 1.0 mm, ~11.0 mm in length). After that, the tube was heated on a hot plate at 400 °C for 2 hrs to eliminate any moisture. Then, the open-end of the tube was quickly and tightly clamped, and hermetically sealed by propane/oxygen flame welding. During the welding process, the tube was held by two Pt plates for dissipating heat (see Figure 3.5 for the tube sealing). The sealed Pt tubes were tested by DTA in static dry air at a heating/cooling rate of 5 °C/min or 10 °C/min. After each test, the sample was examined by optical microscopy and analytical balance to check whether there is any leakage on the sealed tube. The temperature accuracy of TG/DTA is ± 0.01 °C, the errors in determining the characteristic temperatures (T_{em}, T_{fm} and T_{es}) are estimated to be ± 2 °C.

2.1.3) Technical Results and Progress

2.1.3.1) Thermal stability of $Pb(Zn_{1/3}Nb_{2/3})_{0.91}Ti_{0.09}O_3$ [PZNT91/9] Single Crystals

Figure 1 shows the open-pan TG/DTA result for $Pb(Zn_{1/3}Nb_{2/3})_{0.91}Ti_{0.09}O_3$ single crystals and Figure 2 presents the X-ray diffraction for the crystals after different thermal treatments. These figure provide us with a clear picture of the high temperature thermal stability of the PZNT91/9 crystals.

In the open-pan test, a strong endothermic DTA peak was detected at 1226 °C. The λ-shape

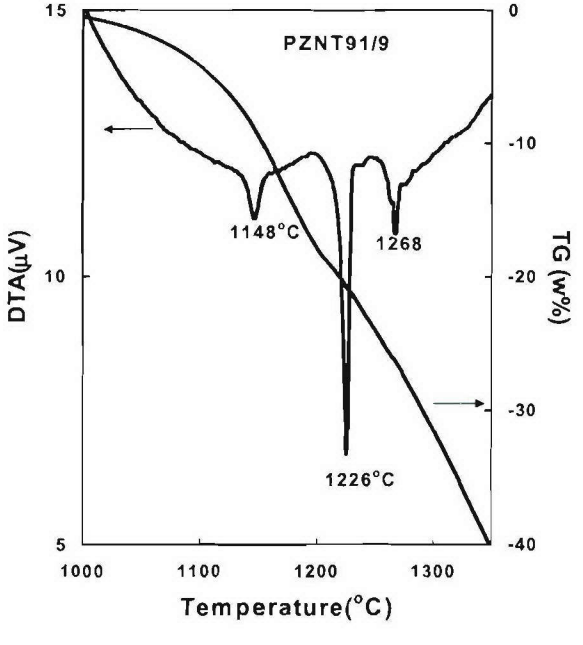

Figure 1. Simultaneous TG/DTA curves for as grown PZNT91/9 single crystals in air.

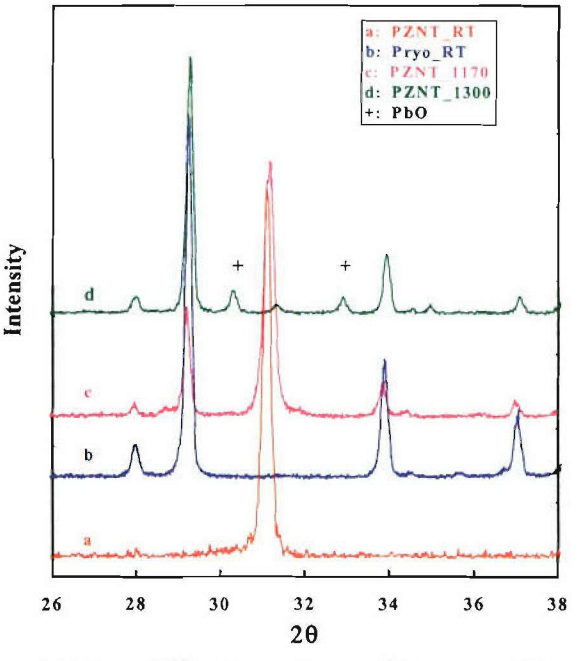

Figure 2. X-ray diffraction patterns of the perovskite and the related phases formed in the PZNT91/9 crystal system after thermal treatments: (a) Perovskite PZNT91/9; (b) a pyrochlore phase; (c) PZNT quenched from 1170°C; (d) PZNT quenched from 1300°C, yellow powder + PbO (Massicot).

suggests a major invariant melting event. In addition, two minor heat exchanges appeared at 1148°C and 1268°C, respectively. The weight loss in PZNT crystals was about 3% at 1100°C. It increased steadily upon furthers heating and research about 30 % at 1300 °C. The PZNT crystals quenched from 1170 °C did not indicate any melting behavior, but underwent a slight color change from light yellow to yellow/brown, indicating that decomposition had taken place.

X-ray diffraction pattern of the quenched sample (Fig. 2c) clearly shows the appearance of a pyrochlore phase mixed with the perovskite phase. Therefore, the broad thermal peak at 1148 °C indicates the onset of a decomposition of the perovskite crystals. PZNT sample heated at 1250 °C was melted, and the liquid was spread over the Pt pan, confirming the major melting event detected at 1226 °C. Since the perovskite phase was still in majority after the decomposition at 1170 °C, this would indicate that the perovskite PZNT91/9 melts at 1226 °C under atmospheric pressure. Two distinct phases were observed from the solidified liquid: a red/brown residue of small amount, not completely melted, and a yellow molten material that has spread on the Pt pan. Complete melting was achieved above 1268°C. Only a small amount of perovskite phase was left after melting and decomposition at 1300°C, since the quenched molten sample indicates a major pyrochlore phase (Fig. 2d). Therefore, under the atmospheric conditions, the PZNT91/9 crystal undergoes an incongruent melting at 1226°C, and a liquidus around 1268 °C. This result indicates that single crystals of PZNT is not thermal stable at high temperature under atmospheric conditions, therefore they cannot be grown directly from the melt. However, as indicated in the following Section (2.1.3.2), the perovskite phase of PZN-PT can be stabilized in the presence of a flux (PbO) and thereby it should be possible to grow PZN-PT crystals from high temperature solutions, i.e. by the flux or by the Bridgman method.

2.1.3.2) Phase Diagram of $Pb(Zn_{1/3}Nb_{2/3})_{0.91}Ti_{0.09}O_3$ - PbO Pseudo-Binary System

Figure 3(a) shows the typical low-temperature (below 950°C) TG/DTA results curves for the composition inside the pseudo-binary system (10 ~ 60wt% and 70 ~ 90wt% of PbO). Upon heating at 10 °C/min, a sharp endothermic DTA peak appeared at 830±2°C with less than 1% weight loss. During cooling down from 950°C, a sharp exothermic DTA peak with a symmetrical shape appeared at 815±2°C. This indicates a eutectic melting takes place in the pseudo-binary system at 830±2°C. Optical observation confirmed the eutectic melting and solidification.

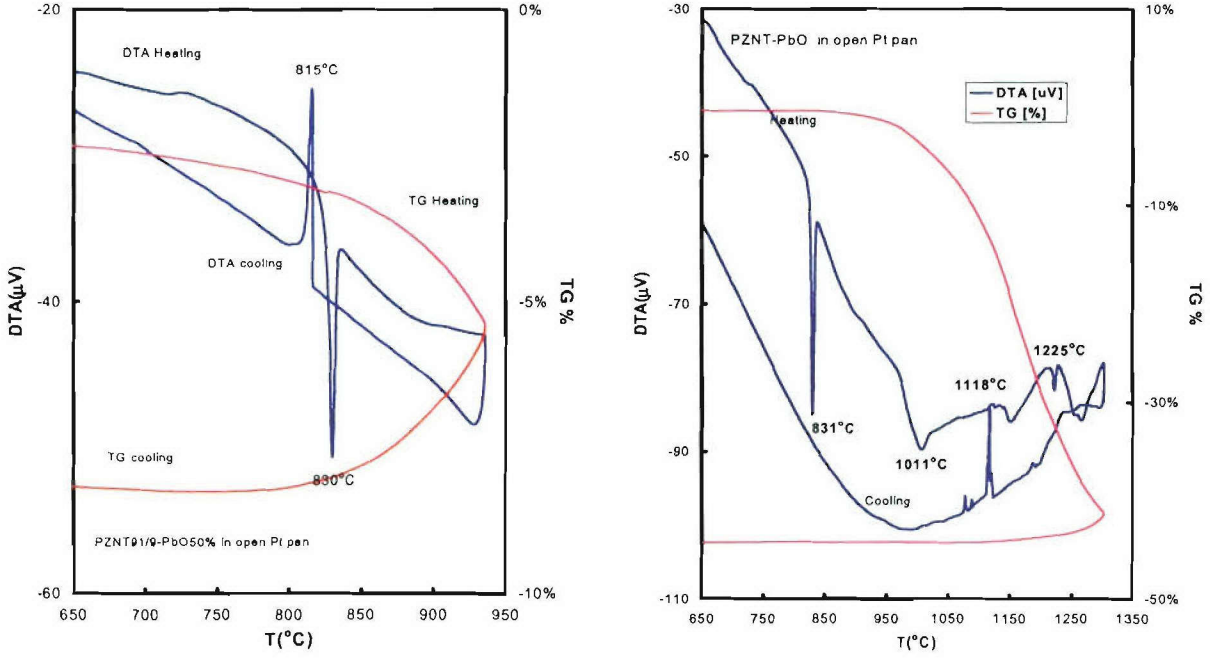

Figure 3. Typical open-pan TG/DTA result: (a) low-temperature test; (b) high-temperature test.

Figure 3(b) shows the typical high-temperature (up to 1300°C) TG/DTA results for the same compositions. Upon heating, the same sharp endothermic DTA peak appeared at 830±2°C with less than 1% weight loss. With increasing temperature, weight loss increased more sharply, and several weak endothermic peaks appeared, which became exothermic upon cooling. The microscopic observation showed that the sample was first melted and then the liquid spread over the support and crystallizes upon cooling with the evaporation of PbO flux. There was no flux left when the temperature is close to the eutectic point and thus no exothermic eutectic peak appeared.

Since the compositions change apparently at high temperature in open pans, the actual composition was estimated according to the weight loss for each DTA peak, and the melting point of verified using close-tube TG/DTA analysis.

Based on the above experimental data of DAT/TG of the PZNT91/9 - PbO system, we established a complete pseudo-binary phase diagram, as shown in Figure 4. This pseudo-binary system shows a typical eutectic-melting behavior with the eutectic composition close to 25wt%PZNT91/9 – 75wt% PbO and the eutectic temperature at 828±2°C. The perovskite $Pb(Zn_{1/3}Nb_{2/3})_{0.91}Ti_{0.09}O_3$ phase exhibits complex thermal behavior and undergoes a partial decomposition starting at 1140°C, leading to the formation of the pyrochlore phase and PbO. Upon further heating, the PZNT91/9 crystals incongruently melts at 1225±2°C resulting in a further decomposition of the perovskite phase. The decomposition of the perovskite crystals is significantly accelerated during the open pan thermal treatments at high temperatures as a result of the evaporation of PbO. The crystals of the pyrochlore $Pb_{1.5}Nb_2O_{6.5}$-type phase are thermodynamically more stable than PZNT91/9 and only undergo a partial decomposition on the crystal surface. The thermal instability of PZNT91/9 evidenced by the thermal analysis both in open and sealed Pt tubes suggests that in order to obtain pure PZNT crystal, extra PbO flux is necessary to prevent the decomposition of the perovskite phase and the formation of the pyrochlore phase. The liquidus melting behavior of $Pb(Zn_{1/3}Nb_{2/3})_{0.91}Ti_{0.09}O_3$ in the PbO flux for less than 75wt% PbO ($x_{PbO} < 0.75$) follows a liquidus curve that is represented by the equation: T_L (°C) = $-435.34\ x_{PbO}^2 - 214.34\ x_{PbO} + 1227.6$.

The established pseudo-binary phase diagram provides a useful thermodynamic guidance for the growth of high quality and large PZNT crystals either by the flux method or by a modified Bridgman or Czochralski technique using PbO as high temperature solution. Further studies are underway to determine the compositions of the different phases formed from PZNT at various temperatures within a possible ternary phase diagram including the pyrochlore phase.

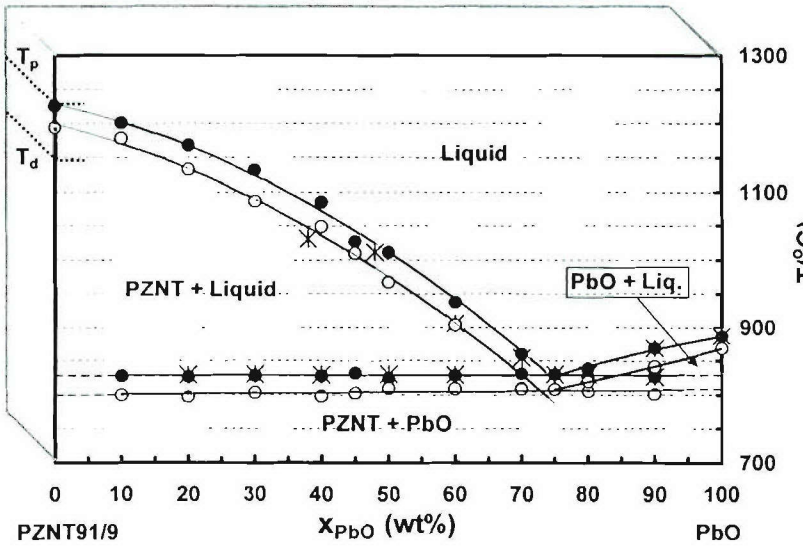

Figure 4. Pseudo-binary phase diagram of the PZNT91/9 – PbO phase diagram.

2.1.3.3) Pseudo-Binary Phase Diagram of $Pb(Zn_{1/3}Nb_{2/3})_{0.91}Ti_{0.09}O_3$ - $Pb_{1.5}Nb_2O_{6.5}$

The phase diagram in Figure 4 provides a thermodynamic explanation of the instability of the perovskite PZNT phase, which decomposes into a pyrochlore $Pb_{1.5}Nb_2O_{6.5}$-type phase and PbO. The pyrochlore phase is undesirable due to its harmful effects on the electric properties of PZNT crystals. But it is thermodynamically more stable than the perovskite phase. Therefore, in order to find an effective growth pathway for the PZNT crystals, it was necessary to understand the phase connections between PZNT, pyrochlore and PbO. As a natural extension of the pseudo-binary system, we have studied the pseudo-binary system between PZNT91/9 and $Pb_{1.5}Nb_2O_{6.5}$-type phase.

It was found that a pseudo-eutectic behavior appears in the PZNT91/9 and pyrochlore system, with a eutectic temperature around 1180 °C and the liguidus temperature varying between 1220 and 1250 (Figure 5). It would be desirable to follow up this work in the future to study the pyrochlore and PbO system and to establish the pseudo-ternary system between PZNT91/9 – pyrochlore – PbO, which should illuminate in a more clear way the formation and stability range of the perovskite phase v.s. the pyrochlore phase.

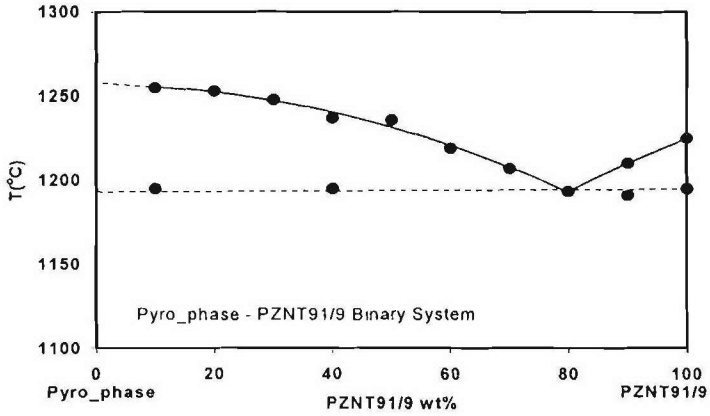

Figure 5. Partial phase diagram of the pseudo-binary phase diagram of $Pb(Zn_{1/3}Nb_{2/3})_{0.91}Ti_{0.09}O_3$ - $Pb_{1.5}Nb_2O_{6.5}$.

2.1.3.4) Thermal Stability of the $Pb(Zn_{1/3}Nb_{2/3})_{0.955}Ti_{0.045}O_3$ (PZNT95.5/4.5) Crystals

Single crystals of $Pb(Zn_{1/3}Nb_{2/3})_{0.955}Ti_{0.045}O_3$ (PZNT95.5/4.5) represent another interesting composition of the PZN-PT solid solution system, which crystallizes in the rhombohedral phase. Therefore, it was important to investigate their thermal stability. To study the melting behavior detected by DTA, PZNT95.5/4.5 crystals were heated at different characteristic temperatures, followed by air-quenching down to room temperature. X-ray diffraction was then performed on ground samples. Figure 6 shows the spectra of samples after thermal treatments at various temperatures. It can be seen that the perovskite phase of PZNT95.5/4.5 crystals decomposes into a pyrochlore phase at temperature as low as 1000 °C (Fig. 6b). Further heating resulted in a larger amount of pyrochlore phase and PbO, while the perovskite phase almost disappeared.

PZNT95.5/4.5 crystals quenched from 1000 °C did not indicate any melting, but underwent a clear color change from light yellow to brown, indicating that a phase transformation had taken place, which can be related to

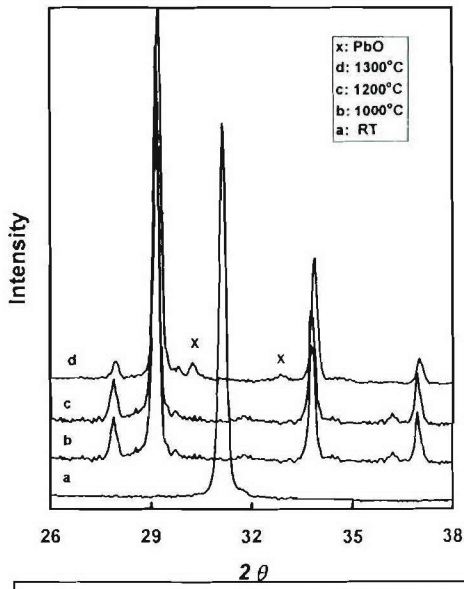

Figure 6. XRD patterns of PZNT95.5/4.5 crystals after thermal treatments at different temperatures.

the decomposition of the perovskite phase in pyrochlore phase occurring around 1000 °C, as shown in Fig. 6b. The broad thermal peak at 1143 °C would correspond to the eutectic temperature between the pyrochlore and PZNT phases. PZNT sample heated at 1250 °C was melted and cast over Pt support, confirming the major melting event detected around 1230 °C. A complete melting was achieved above 1300°C and the quenched molten indicates a major pyrochlore phase plus PbO (Figure 6d).

Compared with the thermal properties of PZNT91/9 (see Section 2.1.3.1), the PZNT95.5/4.5 crystals seem to show a lower stability and the thermal decomposition of the perovskite into pyrochlore phase occurs at lower temperature and under faster kinetics. This may be related to its lower PT content. Therefore, a high concentration of flux may be needed in order to grow the PZNT95.5/4.5 crystals in the perovskite phase.

2.1.3.5) High Temperature Phase Diagram of the (1-x)Pb($Mg_{1/3}Nb_{2/3}$)O_3–x$PbTiO_3$ [PMN–PT] Solid Solution System

The high temperature phase diagram of the (1-x)Pb($Mg_{1/3}Nb_{2/3}$)O_3–x$PbTiO_3$ solid solution system is very important to understand the composition segregation in the grown PMn-PT single crystals. In order to establish such a phase diagram, samples of (1-x)PMN-xPT (x=0, 0.10, 0.20, 0.30, 0.35, 0.40, 0.50, 0.60, 0.70, 0.80, 0.90 and 1) were synthesized to provide ceramic samples for DTA analysis. The use of polycrystalline ceramics samples so-prepared allowed us to avoid the problems of composition inhomogeneity inherently present in single crystal samples. In order to prepare the perovskite phase of the solid solutions of (1-x)PMN-xPT, a two-step columbite precursor method was used to prevent the formation of pyrochlore phase ($3PbO{\cdot}4Nb_2O_5$). XRD profiles for (1-x)PMN-xPT samples indicated that these solid solutions exhibit a clean perovskite phase when synthesized at 950 °C without any trace of pyrochlore phase, therefore suitable for thermal analysis.

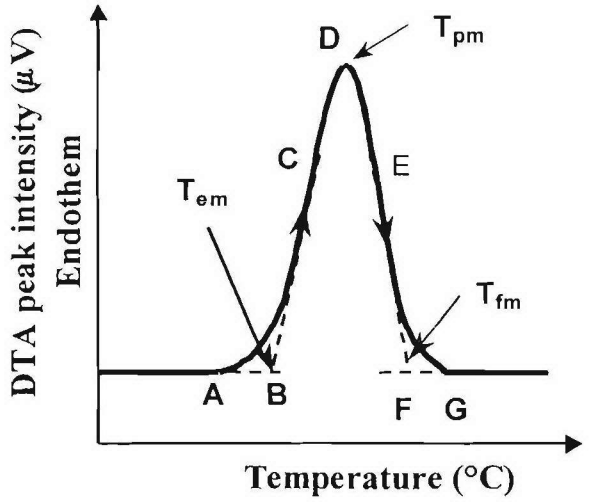

Figure 7. A typical endothermic DAT peak with characteristic temperatures indicated.

Figure 7 shows a schematic endothermic DAT peak expected for a melting event, with the characteristic temperatures of T_{em} (extrapolated onset melting temperature), T_{fm} (extrapolated end melting temperature) and T_{pm} (peak melting temperature).

Figure 8 shows the typical DTA curves for the composition of 0.7PMN-0.3PT. Upon heating, an endothermic peak appears between 1304 and 1311 °C, indicating the melting process of the compound. Upon cooling, an exothermic peak occurred between 1296 and 1290°C, corresponding to the solidifying process of the same compound. T_{em} (= 1304 °C) is the extrapolated onset melting temperature, and T_{cs} (= 1296°C) is the extrapolated onset solidifying temperature.

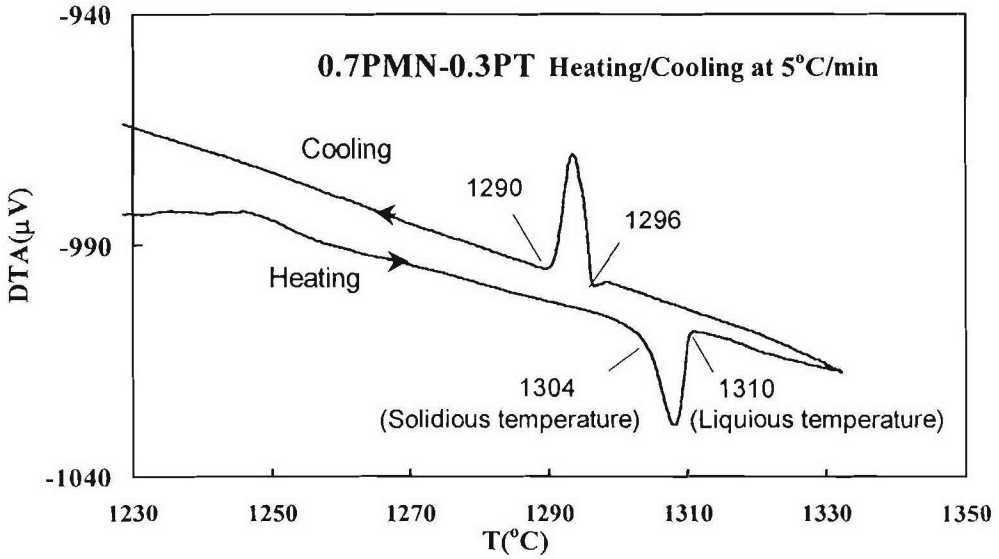

Figure 8. Typical DTA curve of 0.7PMN-0.3PT solid solution.

Based on the information obtained from DTA, the melting points of (1-x) PMN-x PT solid solutions ($0 \leq x \leq 1$, in mol fractions) are summarized in Table 1.

Table 1. Summary of the Melting Points of the (1-x)PMN-xPT Solid Solutions

x (in mol%)	Extrapolated onset melting temperature T_{em} (°C)	Extrapolated end melting temperature T_{fm} (°C)	Peak width (T_f -T_{em}) (°C)
0	1323	1323	0
10	1317	1323	6
20	1311	1316	5
30	1304	1311	7
35	1300	1308	8
40	1294	1302	8
50	1290	1299	9
60	1285	1294	9
70	1280	1287	7
75	1281	1288	7
80	1281	1288	7
90	1282	1289	7
100	1286	1286	0

All temperatures shown in Table 1 were obtained from heating curves. T_{em} is the extrapolated onset melting temperature, and T_{fm} is the extrapolated end melting temperature. (T_{fm} - T_{em}) is the width of the endothermic peak, as shown in Fig. 7. For PMN and PT, the extrapolated onset melting temperature is considered as the melting point of these two compositions.

The phase diagram of the (1-x)PMN - xPT solid solution system was then constructed based on the information given in Table 1, as shown in Fig. 9.

For each composition, the extrapolated onset melting temperature (T_{em}) in DTA curve gives the solidus temperature in Fig. 9, and the extrapolated end melting temperature (T_{fm}) provides the liquidus temperature. The solidus line and the liquidus line divides the phase diagram into three parts: solid solutions region (SS), liquid region (L) and the coexistence of solid solutions (SS) and liquid (L) regions. The separation between the solidus and liquidus lines indicates the origin of the phase segregation in the PMN-PT system, and thereby the composition fluctuation in the corresponding single crystals when grown from the liquid phase at high temperatures. It was found that for the compositions near the MPB, a phase segregation coefficient $k = C_{S1}/C_{L1} \approx 0.64 < 1$. This coefficient not only explains the origin of the composition gradient in PMN-PT single crystals grown by the Bridgman method, but also provide useful quantitative information for crystal growers to minimize the composition fluctuation which had been a major hurdle in the production of the piezocrystal on a large scale and at a cost effective way.

The phase diagram in Fig. 9 shows a minimum solidus temperature (T_{em} = 1280°C) at about 70mol% fraction of $PbTiO_3$. This melting point is lower than the melting point of PMN (T_{em} = 1323°C) and the melting point of PT (T_{em} = 1286°C). This behavior may be caused by the size factor since the difference between the ionic radius of Mg^{2+} (r = 0.72 Å) and Ti^{4+} (r = 0.61 Å) exceeds 15%.

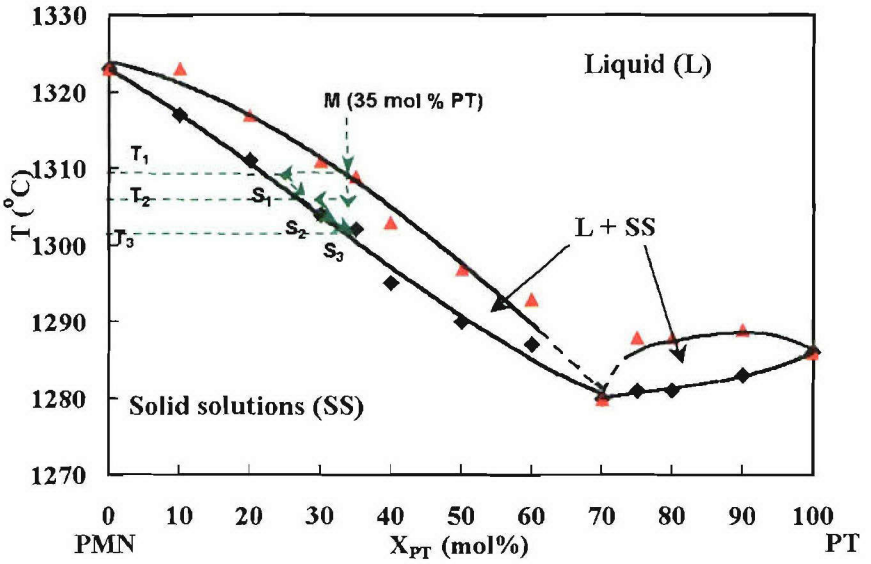

Figure 9. High temperature phase diagram of the (1-x)PMN - xPT solid solutionsystem.

2.1.3.6) Phase Diagram of the Pseudo-Binary system of (0.65PMN-35PT) – PbO

In order to find out the optimum chemical and thermodynamic conditions for the growth of PMN-PT piezocrystals, it was necessary to understand the melting behavior of the PMNT in the main flux of PbO. A series of thermal analysis were carried out for various compositions of (100-y)wt%PMNT65/35–ywt%PbO system (0 ≤y ≤100).

Based on the data obtained from DTA, the melting points of the (100-y)wt% PMNT65/35–ywt%PbO system ($0 \leq y \leq 100$) are summarized in Table 2.

In Table 2, all peak temperatures shown were obtained from the heating curves since the cooling temperature was affected by supercooling. T_E represents the eutectic temperature, obtained from the extrapolated onset melting temperature (T_{em}). T_L is the liquidus temperature, measured from the extrapolated end melting temperature (T_{fm}). The following two observations can be made from Table 2.

(a) Eutectic temperature (T_E) and liquidus temperature (T_L)

Eutectic temperature T_E was found to be averaged at 846 °C excluding y = 0, 10, 100 wt% of PbO, where the eutectic peaks were not detectable. Table 2 shows that the liquidus temperatures T_L decrease from 1302 °C (0 %wt PbO) to 1226 °C (40 wt% PbO) and increases from 845 °C (80 wt% PbO) to 888 °C (100 wt% PbO). The results indicate that PMNT65/35-PbO exhibits eutectic behaviour at high temperature.

(b) Explanation of the non-detectable peaks

The eutectic temperatures were not detectable for the composition with y = 10 wt% PbO. When the composition is close to the eutectic, the intensity of the eutectic peak becomes higher. At the eutectic composition, the intensity of the peak reaches the maximum. As the composition y = 10 wt% PbO is far away from the eutectic composition, the eutectic peak becomes too weak to be detected.

Table 2. Summary of the peak temperatures upon heating for (100-y)PMNT65/35–y%PbO (wt%) system

y (wt% PbO)	Eutectic temperature T_E (°C)	Liquidus Temperature T_L (°C)
0	Not detectable	1302
10	Not detectable	1300
20	849	1290
30	846	1281
40	850	1226
50	843	Not detectable
60	853	Not detectable
70	840	Not detectable
80	845	845
90	840	859
100	Not detectable	888

Table 2 also shows that the liquidus temperatures (T_L) were not detectable at y = 50, 60 and 70 wt% PbO. As the composition is moving relatively far away from PMNT65/35, the liquidus peak intensity decreases, and the peak becomes too weak to be detected for compositions with y_{PbO} = 50, 60 and 70 wt%. In our experiments, the DTA signals of the samples were particularly weak because of the relative small mass of the sample (~ 15 mg) compared with the mass of Pt tube (~550 mg), which makes the weak thermal events difficult to be detected.

Table 2 indicates that at high temperatures, the (100-y)wt%PMNT65/35-ywt%PbO system forms a pseudo-binary system with eutectic behavior. "Pseudo" is used since PMNT65/35 is a solid solution itself rather than a simple compound.

In order to determine the eutectic composition of the system, a "maximized peak area method" was used. This method is based on the principle that the area under the DTA peak for the eutectic melting achieves the maximum at the eutectic concentration. The normalized (by sample weight) peak areas around the eutectic composition are summarized in Table 3 and plotted in Figure 10.

Table 3 Summary of the eutectic peak area obtained from differential thermal analysis for the PMNT65/35–PbO system

PbO in weight percent (%)	40	50	60	70	80	90	100
Normalized peak area ** (μV x sec/mg)	1.6	5.1	8.0	11.5	15.3	7.6	0*

* The peak area for 100% PbO at eutectic temperature was deduced as 0 μV x sec/mg.

** Normalized by the powder sample weight.

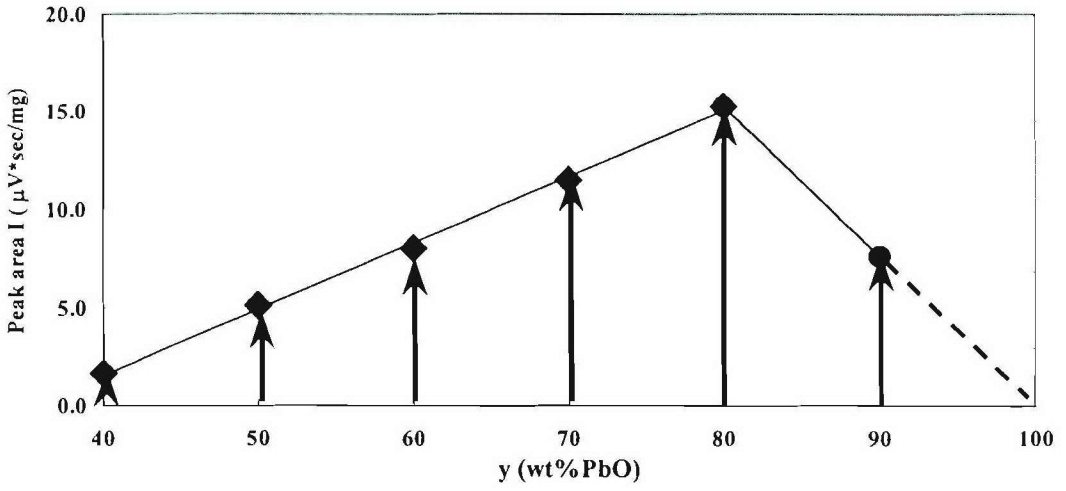

Figure 10. Determination of the eutectic composition from differential thermal analysis for the (100-y)PMNT65/35-yPbO system.

Figure 10 shows that the DTA eutectic peak area increases as the composition increases from 40 to 80 wt% of PbO. At y = 80 wt% PbO, the peak area reaches maximum. Then, from 80 to 100 wt% of PbO,

the peak area decreases. Therefore, the eutectic composition is located at y_E = 80 wt% PbO (at an interval of 10 wt% PbO).

Based on the information obtained in Section 2.4, a pseudo-binary phase diagram of the (100-y)wt%PMNT65/35–ywt%PbO system (0 ≤y ≤100) is constructed as shown in Figure 11.

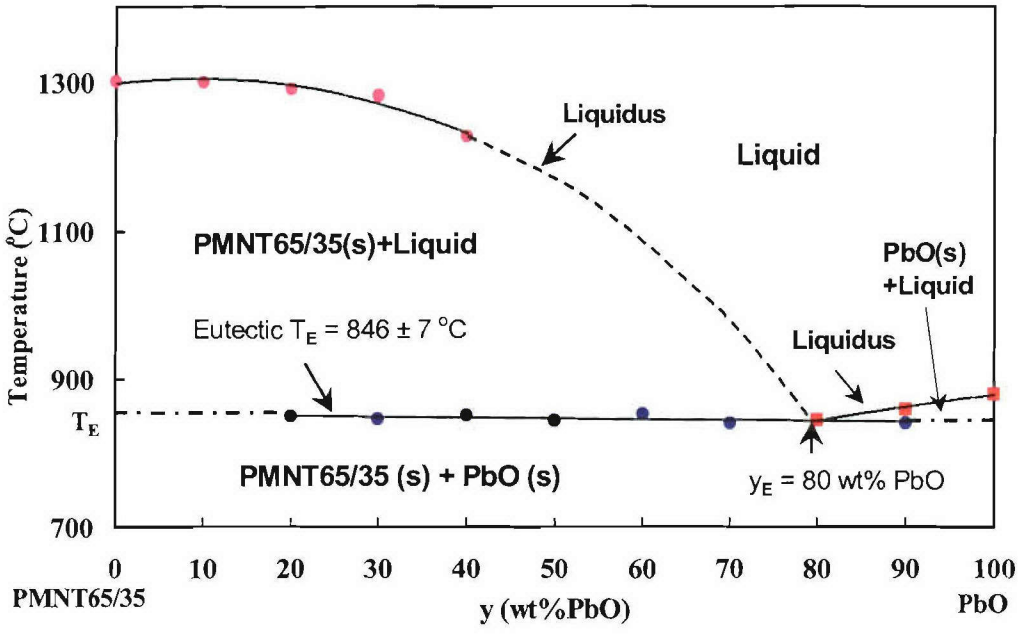

Figure 11. Pseudo-binary phase diagram of the PMNT65/35-yPbO system.

In Figure 11, T_E = 846 °C represents the eutectic temperature and was determined from the average f the eutectic temperatures at y = 20, 30, 40, 50, 60, 70, 80 and 90%wt PbO (see Table 2). Dashed line shows the extrapolated liquidus temperature curve for 50, 60 and 70 wt% PbO, where the liquidus peak could not be detected from our DTA measurements. Dash dot lines indicate the extrapolated eutectic temperatures for 0, 10 and 100wt% PbO.

Figure 11 indicates that the PMNT65/35-PbO binary system exhibits eutectic behaviour at high temperatures. The eutectic composition is located at 80wt% PbO, and the eutectic temperature (T_E) is around 846 °C. It can be seen that the melting point of PMNT65/35 (1302 °C) or PbO (888 °C) is depressed by adding PbO to PMNT65/35 or PMNT65/35 to PbO. The maximum depression of the melting points (846 °C) occurs at the eutectic composition ($y_E \approx$ 80 wt% PbO).

2.1.3.7) Significance of the High Temperature Phase Diagrams of the PMN – PT – PbO Systems

The phase diagram the (100-y)wt% PMNT65/35-ywt%PbO system shows that the pseudo-binary system exhibits a eutectic melting behaviour with the eutectic composition at 20wt%PMNT65/35-80wt%PbO. The eutectic temperature was determined at 846 °C. The established phase diagram of the (100-y)wt%PMNT65/35-ywt%PbO system has defined the eutectic point and the liquidus curves. It provides thermodynamic information on the melting and solidifying of the system, which is useful for improved growth of large and high-homogeneity PMN-PT crystals of MPB compositions by the flux, the solution Bridgman and other techniques.

On the other hand, the phase diagram of the (1-x)PMN - xPT solid solution system defines the liguidus and solidus lines, and shows that for the compositions near the MPB, a phase segregation coefficient $k = C_{SI}/C_{LI} \approx 0.64 < 1$ applies, which is the origin of the composition gradient in PMN-PT single crystals grown by the Bridgman method. This phase diagram provides useful quantitative information for crystal growers to minimize the composition fluctuation, and thereby to enhance the production of the large and high quality piezocrystals on a large scale and to reduce the costs.

Based on these two phase diagrams, a (partial) 3D phase diagram of the PMN-PT-PbO ternary system was established, as shown in Fig. 12.

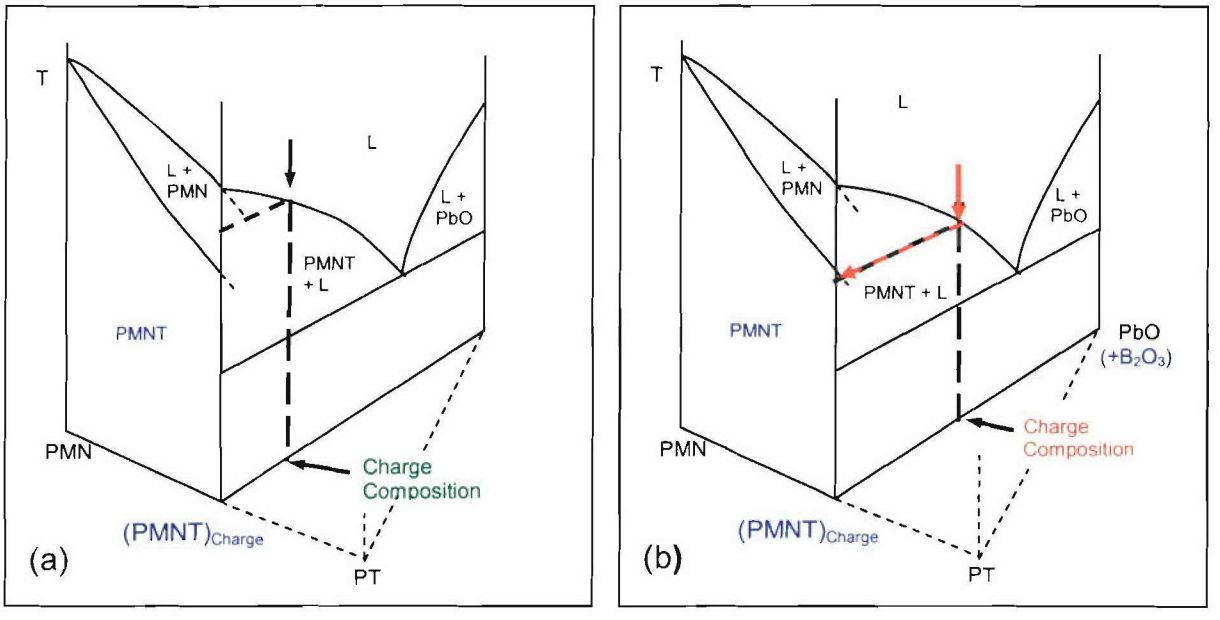

Figure 12. Partial 3D phase diagram of the PMN – PT – PbO ternary system showing different possible pathways for the growth of the PMN-PT single crystals: (a) with composition segregation; (b) without (or minimized) composition.

Careful inspection of this phase diagram indicates that different pathways are possible in the growth of PMN-PT single crystals, giving rise to very different results. In Fig. 12(a), the charge composition will necessarily lead to severe composition segregation, which had been the common growth route taken by most of crystal growers. However, by adjusting the charge composition and with the help of appropriate flux additives (such B_2O_3), it is possible to find an optimum growth path, as indicated by the red arrows in Fig. 12(b), which would lead to the crystallization of the PMN-PT crystals with much reduced or minimized composition segregation between PMN and PT. The analysis of the phase diagrams allowed us to originate the concept of improved flux growth technique, which has been successfully applied, in collaboration with Microfine Materials Technologies Pte Ltd (Singapore, c/o Dr. Leong-chew Lim), to the growth of high-homogeneity PMN-PT crystals and wafers, which have shown excellent electromechanical properties. This effort has led to a viable resource of piezocrystals available for a wide range of defense and civilian applications.

2.2) Materials Design, Synthesis and Characterization

In this Section, we report the technical rationale, approach and results in the design, synthesis and characterization of several piezo- and ferroelectric materials systems that we have investigated during the granting period of this award. The materials systems studied include:

i) Innovative PiezoCrystals of the PMN-PT and PZN-PT Solid Solution Systems;

ii) New High-T_C Piezoelectric Crystals of the PSN – PT Solid Solution;

iii) Single Crystals of the '$PbSnO_3$'–$PbTiO_3$ [PSn-PT] System: A New Family of PiezoCrystals;

iv) Piezo- and Ferroelectric Materials from the Ternary $Pb(Yb_{1/2}Nb_{1/2})O_3$-$PbTiO_3$-$PbZrO_3$ [PYN–PT–PZ] System;

v) Single crystals of $Pb(Zr_{1-x}Ti_x)O_3$ [PZT];

vi) Solid Solution System of $BiFeO_3$ – $PbTiO_3$.

2.2.1) Improved Growth of the PMN-PT and PZN-PT PiezoCrystals

2.2.1.1) Technical Rationale

Based on the data of thermodynamic analysis and phase diagrams mentioned above, the innovative relaxor-based piezocrystals PMN-PT and PZNT-PT were grown by various techniques with a view to optimizing the growth parameters and conditions and to develop new growth processes capable of providing crystal resources both for fundamental research and for applications.

2.2.1.2) Technical Approach

2.2.1.2.1) High Temperature Solution Growth

High temperature solution technique was used to grow the single crystals of (1-x)PMN-xPT (x= 0.10, 0.25, 0.35, 0.50), PZN, PZNT91/9 and PZNT95.5/4.5. The effects of chemical, thermodynamic and kinetic parameters on the growth results were systematically studied by varying the compositions and the concentration of the flux. Both PbO and the mixture of PbO and a small amount of B_2O_3 [PbO + δB_2O_3] were used as flux. PbO has been shown to be an effective solvent for many oxides, as well as for the complex perovskites. Moreover, as a starting component of PZNT, PbO can avoid the incorporation of foreign ions into the lattice of the grown crystals. The composite flux of B_2O_3 and PbO was expected to combine the advantage of both the borate and the PbO solvent. The starting chemicals were mixed to form various compositions of relaxor crystals PMNT65/35, PZN and PZNTT with various Ti-concentrations. The growth conditions were related to the growth results to find out the optimum flux concentration and compositions. A double crucible assembly consisting of a Pt crucible inside an alumina one was used to prevent the volatilization of PbO at high temperatures. A slowly accelerated cooling process (at 1 – 5 °C/h) was designed in order to create a constant supersaturation and thereby to reach a more stable growth.

2.2.1.2.2) Solution Bridgman Growth

A modified Bridgman method using excess of PbO as solvent was developed for the growth of PZNT91/9 crystals. The technical set-up is shown in Figure 13. The PZNT/PbO ratio was 55:45 (mol %). The maximum temperature was 1,120°C. A typical temperature gradient of 15 °C at 1,050 °C was built up. The size of Pt crucibles used was 40 mm (in diameter) x 200 mm (in length) with a wall thickness of 0.4 mm. A cooling rod of 3 mm x 100 mm was used to initiate nucleation. The crucible was descended at 0.3 mm/hr. An air flow was carefully controlled at 100 ml/min.

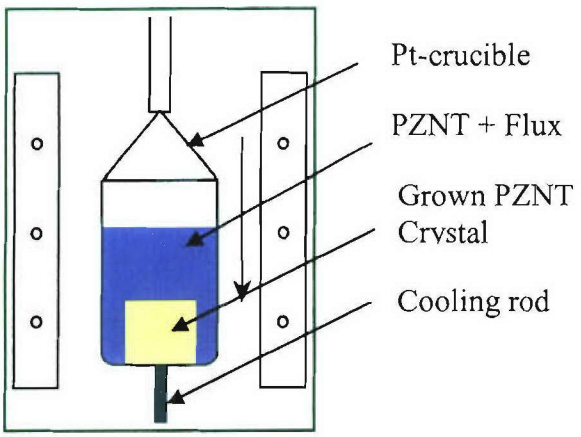

Figure 13. Experimental set-up for the solution Birdgman growth of PZNT91/9 single crystals.

2.2.1.2.3) Top-Cooled-Solution-Growth (TCSG)

The improved flux growth still present some inevitable drawbacks, one of which is the formation of a large number of nuclei resulting from spontaneous multiple nucleation. As a result, the size of the crystals is usually small. The modified Bridgman process developed can provide large crystal boules of large size. However, the Bridgman method has a major disadvantage, which is the high cost, because (i) it is difficult to separate the grown single crystals from crucibles, and thus the crucibles cannot be reused; (ii) the growth rate is very slow. Moreover, a non-uniformity in composition usually appears with a smaller Ti^{4+}-concentration on the bottom and a higher Ti^{4+}-rate on the top of the grown boules, resulting from a possible phase segregation.

In the framework of our continuous effort in the growth and characterization of relaxor-based piezocrystals, we have developed a new technique of top-cooled-solution-growth (TCSG) for the growth of PZNT95.5/4.5 crystals. This technique was aimed at overcoming the deficiencies of both the flux growth and the Bridgman growth, in order to grow piezocrystals of medium size and high quality by controlling the nucleation and growth via top cooling. Stoichiometric 95.5%PZN-4.5%PT powders were mixed with PbO flux at the optimum ratio PZNT : PbO = 1:1 (50 wt% flux). The mixtures were ground homogeneously in acetone. The dried mixture was put in a platinum crucible (100 ml), and the crucible was placed inside an alumina crucible with a platinum wire hanged on the top, as shown in Figure 14. The top cooling was ensured by the Pt wire, which triggers nucleation around it. The alumina crucible was then sealed to an alumina cover with refractory cement. The assembly was placed in a Muffle furnace with an open hole on the top. The grown crystals were separated from the solidified flux using dilute hot HNO_3 solution.

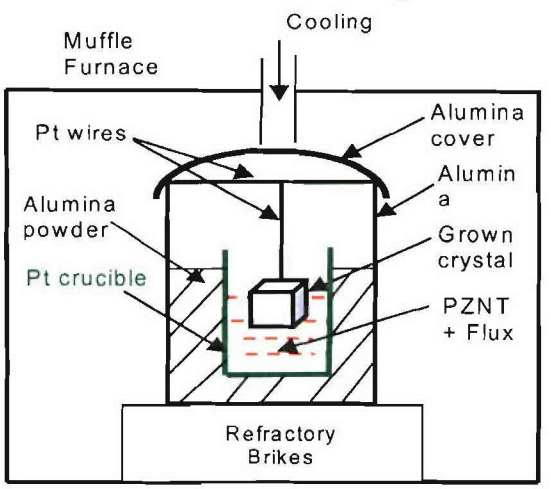

Figure 14. Experimental set-up for the Top-Cooled-Solution-Growth of PZNT95.5/4.5 crystals.

2.2.1.2.4) Top-Seeded-Solution-Growth (TSSG)

To meet the increasing need for piezocrystal resources in various applications, it was essential to develop effective techniques to grow large and high quality PZNT and PMNT crystals. Therefore, as our continuous effort in the growth of piezocrystals, we have developed a new technique of top-seeded-solution-growth (TSSG) for the growth of (1-x)PZN-xPT and (1-x)PMN-xPT single crystals.

A SiC-heating tubular furnace was specially designed and built for top-seeded-solution-growth. Figure 15(a) shows the schematic section view of the furnace and the growth setup. A 50 ml Pt crucible (ϕ=40 mm) was placed above a firebrick at 5 cm height. The PZNT or PMNT seed crystals (2 – 5 mm size) used were obtained from conventional flux growth by spontaneous nucleation. A seed crystal was attached to one end of an alumina rod *via* Pt wire. The temperature gradient is about 1 °C/cm near the surface of the molten. At the early stage of growth, the grown crystal can be rotated *via* the Al_2O_3 rod which was driven by a motor at a speed of 0 to 30 rmp. Figure 15(b) gives the vertical temperature distribution inside the furnace measured for a control temperature set at 1100 °C.

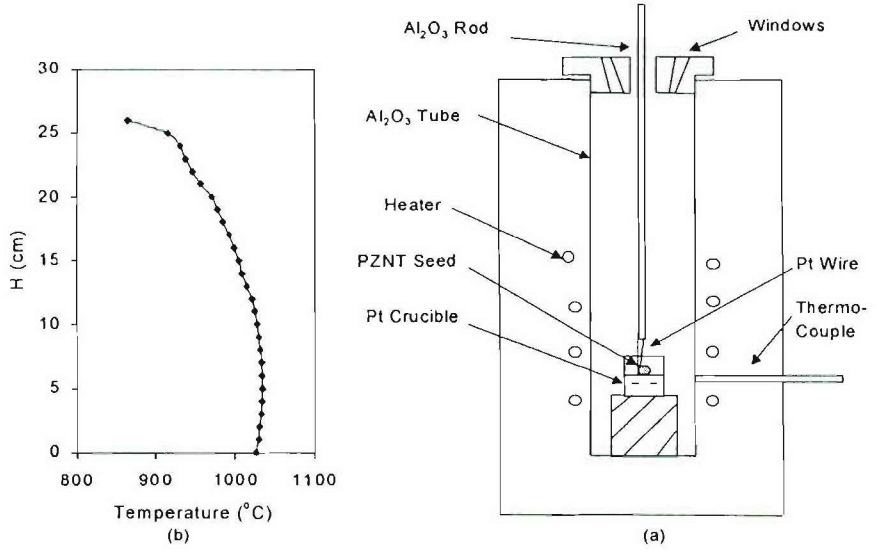

Figure 15. Schematic side section view of the tubular furnace and the setup for the top seeding solution growth (a), and Vertical temperature profile of the furnace for a control temperature set at 1100 °C (b).

For the growth of PMN-PT crystals, both PbO and (PbO + B_2O_3) were tried as flux, but the latter was found to be particular efficient for the growth of PMN-PT crystals. Therefore, most of our work on the TSSG was further performed using the complex flux, especially $Pb_4B_2O_7$ (= 4PbO + B_2O_3). Mixtures of various compositions corresponding to the general formula of yPMN - (1-y)$Pb_4B_2O_7$, y = 20 - 35 mol% were prepared to study the forming condition of the perovskite phase. PbO, Nb_2O_5, TiO_2, MgO (all 999.99%) and B_2O_3 (99%) powders were were ground homogeneously in acetone and then loaded in a Pt crucible and dried in an oven and then in the furnace described above. The $<111>_{cub}$ oriented PMN seed crystals were dipped into the solution at the saturation growth temperature T_{SGT} = 1130 - 1180° C. The solution was then cooled from T_{SGT} to 1000° C at 1° C/h. At that temperature, the grown crystals were pulled out of the solution and cooled at 50° C/h to room temperature.

2.2.1.3) Technical Progress and Results

2.2.1.3.1) Growth of PZNT91/9 Single Crystals by the Flux Method

The single crystals of (1-x)$Pb(Mg_{1/3}Nb_{2/3})O_3$-x$PbTiO_3$ [PMNT] (x = 0.10 – 0.5) and (1-x)$Pb(Zn_{1/3}Nb_{2/3})O_3$-x$PbTiO_3$ [PZNT] (x=0 and 0.09) were successfully grown from high temperature solutions, using PbO or (PbO + δB_2O_3) as flux. The optimum flux compositions and concentrations were found to be 50wt% PbO and (49wt% PbO + 1wt% B_2O_3). It has been shown that, for all the systems studied, addition of up to 1wt% B_2O_3 can stabilize the perovskite phase and improve the effectiveness of the flux by providing an optimum degree of complex formation and an adequate viscosity. The optimum thermal profile consists of a soaking temperature at 1180 °C for PMNT and 1100°C for PZNT and a gradually increasing cooling rate from 2 to 5°C/min. The spontaneous nucleation process could be significantly modified by top-seeding technique. The crystal morphology was studied and related to a layer growth mechanism controlled by two-dimensional growth, and to the formation of pyramidal growth sectors. The grown PMNT crystals exhibit small size of regular pseudo-cubic forms, ready to be used for transducer arrays (Fig. 16(a)). The PZN and PZNT91/9 crystals exhibit very good quality and a typical size of 10x8x5 mm^3, thus suitable for both physical characterization and device testing. Figure 16(b) shows an as-grown PZNT91/9 crystal.

Chemical analysis of the grown PMNT crystals by laser ablation ICP mass spectrometry reveals a significant fluctuation of the local composition for the B-site ions Mg^{2+}, Nb^{5+} and Ti^{4+}. In a PMNT65/35 crystal, the Ti^{4+} concentration may vary by ±5% from its nominal composition. This composition fluctuation could affect the domain structure, phase transition and electromechanical properties of the PMNT crystals.

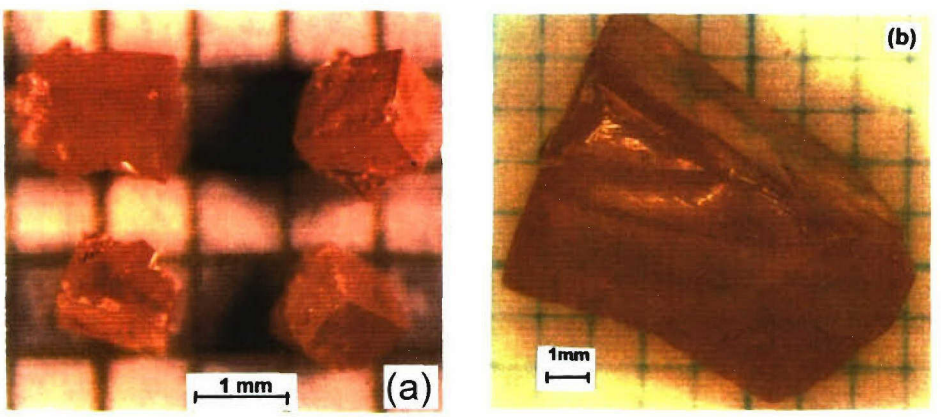

Figure 16. PMNT65/35 crystals (a) and PZNT91/9 crystal (b) grown by the improved flux method.

2.2.1.3.2) Top-Cooled-Solution-Growth of PZNT95.5/4.5 Crystals

The Top-Cooled-Solution-Growth (TCSG) has been developed to grow the piezo-/ferroelectric perovskite single crystals of 0.955$Pb(Zn_{1/3}Nb_{2/3})O_3$-0.045$PbTiO_3$ [PZNT95.5/4.5]. The flux composition and concentration, and the thermal parameters have been optimized, leading to the growth of high quality PZNT crystals with a size up to 20×15×10 mm^3 from a crucible of 100 ml. The perovskite crystals are found to form upon slow cooling down to 1020 °C, while the undesirable pyrochlore crystals of $Pb_{1.5}Nb_2O_{6.5}$-type start growing upon further cooling from 1020 °C to 950 °C. By controlling the growth pathway, the formation of the pyrochlore phase can be avoided. Compared with the Bridgman growth, the TCSG technique presents some advantages: (i) no seed crystals are needed; (ii) the grown crystals show more regular morphorlogy with principal facets oriented to

$\{001\}_{cub}$, hence are easier to be handled in transducer applications; (iii) it is expected that the grown crystals are less stressed, thus the residual internal strain could be minimized; (iv) it is easier to separate the primary grown crystals from the solidified flux, and (v) the Pt crucibles can be reusable. Therefore, the TCSG provides an alternative solution to the Bridgman method to grow medium size piezocrystals at lower cost, suitable for various kinds of device applications. Figure 11 shows the as-cooled crucible surface (a) and an as-grown PZNT95/5/4.5 crystal of very good quality (b).

The dielectric properties of the grown PZNT95.5/4.5 crystals have been measured as a function of temperature at various frequencies. The phase transition for the rhombohedral R3m to the tetragonal P4mm phase takes place at 132 °C, while the tetragonal to cubic phase transition occurs at 160 °C.

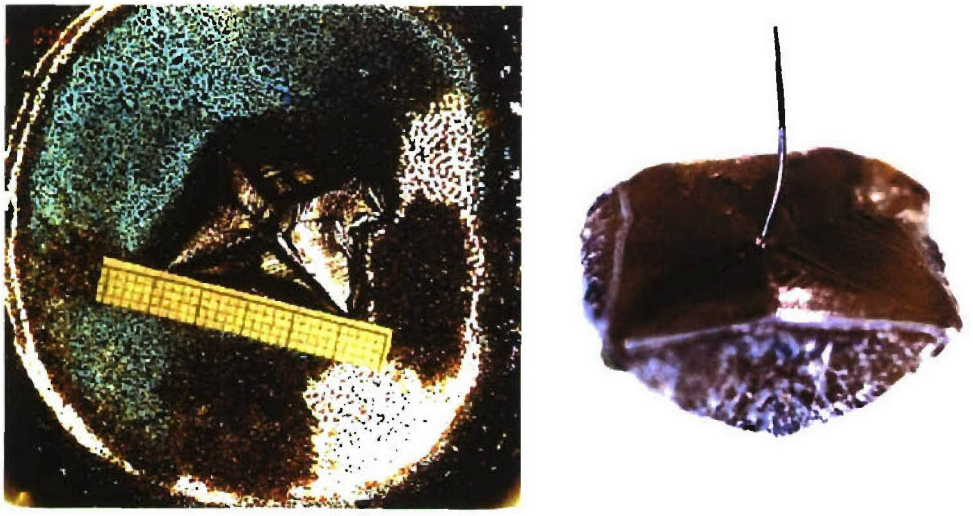

Figure 17. (a) Top view of an as-cooled crucible from top cooling solution growth of PZNT95.5/4.5 single crystals (scale in mm); (b) A single crystal grown from a primary single nucleation triggered by top-cooling (20x15x10 mm^3).

2.2.1.3.3) Top-Seeded-Solution-Growth (TSSG) of (1-x)PZN – xPT Crystals

Based on the above first success in TCSG, a new technique of top-seeded-solution-growth was then applied more systematically to grow the single crystals of (1-x)$Pb(Zn_{1/3}Nb_{2/3})O_3$-x$PbTiO_3$ (PZN-PT) with composition around the MPB (x=0.045, 0.06, 0.07, 0.09, 0.10, 0.12 and 0.15).

(i) Saturation-Growth Temperature of PZNT in PbO

For top seeding solution growth, it is very important to have an accurate knowledge of the saturated solubility, or the saturation-growth temperatures Ts, of the PZNT crystals in the PbO flux. At temperatures above Ts, the seed crystal will be completely dissolved in the flux, while at T < Ts, the spontaneous nucleation and growth will prevail over the top-seeding growth, resulting in numerous small crystals on the surface of the molten system. Thus, Ts indicates the appropriate temperature at which the seed crystal can retain and effectively grow from the solution, i.e. the onset of top-seeding growth.

The saturation-growth temperature Ts of PZNT crystals in PbO flux was determined prior to top-seeding growth experiments. A seed crystal was dipped onto the surface of the molten solution at a temperature slightly (a few degrees) above T_s, then the temperature was decreased to T_s at 15-20 °C/h and maintained there for 5 - 8 h. A pair of optical windows allowed us to observe the melting state. At the end of dwelling, the crystal seed was taken out to check if it had grown or dissolved. T_s is determined as the highest temperature at which the seed crystal remains undissolved, and the lowest temperature at which no spontaneous nucleation occurs. Several experiments were usually necessary to find out the exact

saturation-growth temperature for each composition of the (1-x)PZN - xPT crystals. The cooling rate for the crystal growth was set between 0.1 - 3 °C /h.

Figure 18 shows the variation of the saturation-growth temperature of PZNT95.5/4.5 crystals as a function of flux concentration in the (1-y)PZNT95.5/4.5 – yPbO system (in wt%). Ts decreases from 1100 °C for 40%PbO to 980 °C for 62.5% PbO. From Fig. 18 and the growth experimental that followed, it was identified that 50wt%PbO represents an optimum flux concentration for the growth of PZNT95.5/4.5 crystals. This is consistent with the previous growth results of PZNT91/9 crystals by spontaneous nucleation and of PZNT95.5/4.5 crystals by top cooling solution growth. Therefore, the saturation-growth temperatures of the (1-x)PZN – xPT crystals of other PT-contents were then determined in 50wt%PbO flux. Table 1 gives the results for x = 0.045, 0.06, 0.07, 0.10, 0.12 and 0.15. It is found that the Ts values vary only slightly from 1075 to 1080 °C for the various PZNT crystals.

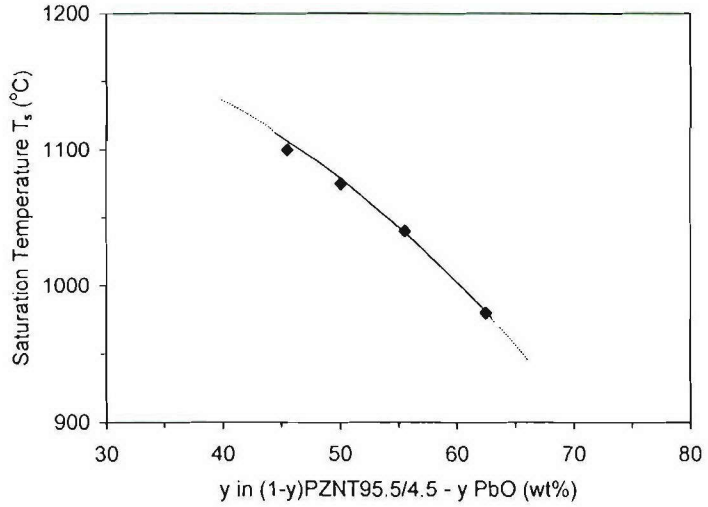

Figure 18. Variation of the saturation-growth temperature of PZNT95.5/4.5 crystals as a function of flux concentration in the (1-y)PZNT95.5/4.5 – yPbO system (in wt%).

It is expected that the variation of Ts as a function of PbO flux concentration for the (1-x)PZN – xPT crystals shows the same trend as that determined for PZNT95.5/4.5 in Fig. 18. This variation trend is consistent with the liquidus/solidus curve determined for the PZNT91/9 – PbO system by means of differential thermal analysis. However, the saturation-growth temperatures Ts determined here are systematically higher (by about 50 °C) than the liquidus/solidus points. Such a difference is mainly due to the fact that in an open setup such as the one in which the T_s was determined, the loss of PbO by evaporation during the dwelling process at high temperatures had significantly increased the effective saturation temperature of the system compared with the DTA data obtained from sealed samples. Also, when a PZNT-PbO solution is cooled down to the temperature of crystallization T_c, the spontaneous nucleation will not occur until the temperature is continuously decreased to a supersaturation temperature T_{ss}, which corresponds to the solidus points determined by DAT. The difference between T_c and T_{ss} may reach a few dozen degrees, especially at a fast cooling rate. When the seed crystal is introduced onto the solution the nucleation will be triggered at a temperature T_s higher than T_{ss}. This is another reason why T_s found here is higher than the liquidus/solidus points. These observations suggest that the saturation-growth temperature T_s has to be determined specifically for the TSSG process.

Table 4. Saturation-growth temperatures T_s of (1-x)PZN - xPT crystals in a molten system with 50wt% PbO flux.

x (mol%)	4.5	6	7	10	12	15
T_s (± 5 °C)	1075	1075	1075	1080	1080	1080

(ii) Growth of (1-x)PZN – xPT crystals

The growth of (1-x)PZN – xPT [PZNT(1-x)/x] crystals was thereafter performed with 50wt% PbO flux based on the saturation-growth temperatures determined above. Crystal boules with a upper diameter greater than 30 mm and a height (thickness) of larger than 10 mm were successfully grown for x = 0.045, 0.06, 0.07, 0.10, 0.12 and 0.15.

Figure 19(a) shows the photograph of a PZNT85/15 crystal boule grown from T_s = 1080 °C. The seed crystal was dipped into the molten system at 1085 °C. The temperature of the crucible was then decreased to T_s = 1080 °C at 15 °C/h. The gowth process took place upon cooling from T_s to 1070 °C at 0.5 °C/h, and then to 1000 °C at 1 °C/h. The grown crystal was pulled out of the molten at 1000 °C and kept in the furnace while the furnace temperature was cooled down to room temperature at 50 °C/h. The crystal boule (of conical form) shows an upper diameter of 35 mm and a height of 14 mm.

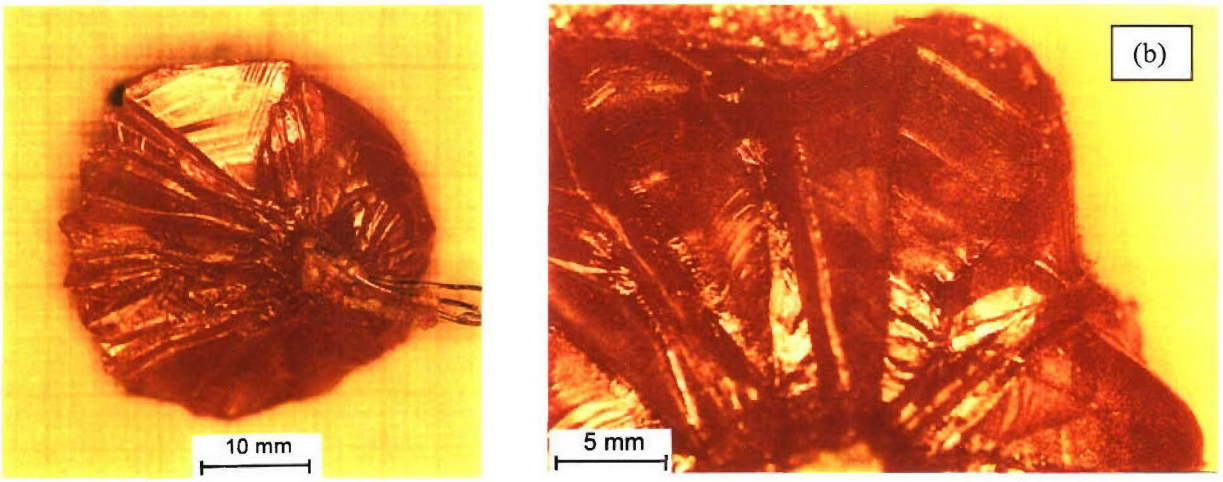

Figure 19. PZN-PT85/15 crystal boule wgrown by the

Figure 19(b) shows the photograph of part of a PZNT90/10 crystal boule grown from T_s = 1075 °C. The seed crystal was immersed into the solution at 1080 °C. The temperature of the crucible was then lowered to 1075 °C at 15 °C/h, to 1065 °C at 0.5 °C/h, and then to 975 °C at 1 °C/h. The crystal was pulled out from the flux at 975 °C and kept in the furnace during the final cooling to room temperature at 50 °C/h. The crystal boule shows an upper diameter of about 30 mm and a height of 12 mm.

The initial cooling from the saturation-growth temperature Ts was found to be a crucible stage for a successful top seeding growth, because after dipping into the solution, the seed crystal underwent a dissolution/crystallization equilibrium and hence required an appropriate supersaturation rate to trigger the epitaxial growth from the seed. Different cooling rates from T_s were tried out during the growth. A too slow cooling rate, for instance, 0.1 - 0.4 °C/h, could cause excessive vaporization of PbO, and hence seriously affected the solubility curve and increased the saturation-growth temperature Ts. As a result, only small crystals of poor quality were grown around the seed. A too fast cooling rate (> 3 °C/h) from Ts, on the other hand, could create excessive (spontaneous) multi-nucleation around the seed due to a high supersaturation rate. As a consequence, no top-seeding growth could take place. The optimum cooling rate from T_s for top-seeding growth was found to be 0.5 – 1 °C/h.

The grown crystal boules may contain more than one single crystal. Single crystals of larger size and better quality can be found in the part of boule further away from the center (seed). They were formed at mid and late stages of growth during which more room was available for individual nucleus to develop

into a single crystal along the radial sector. Due to the limit of the diameter of the crucibles used (ϕ=40 mm), the largest diameter of the grown crystal boules was usually confined to 35 mm. It is expected that larger PZNT single crystals would be grown using larger crucibles. Nevertheless, PZNT single crystals of respectable size (up to 15x12x10 mm^3) can be cut from the grown crystal boules, which are suitable for both fundamental studies and device applications.

The surface micrographs of the grown PZNT crystals reveal significant growth steps (Fig. 19), suggesting a dominant layer growth mechanism, i.e. the PZNT crystals are formed by two-dimensional growth starting from the primary nucleation or epitaxy around the seed crystal. Such a growth mechanism is common to the growth of complex perovskite relaxor crystals, as deduced from the flux growth of PZNT91/9 and PMNT65/35, and from the top-cooling growth of PZNT95.5/4.5, as previously reported.

The top-seeded-solution-growth technique developed in this work allows us to provide PZN-PT piezocrystal resources not only for academic research, such as neutron diffraction, but also for potential industrial applications.

2.2.1.3.4) Top-Seeded-Solution-Growth (TSSG) of (1-x)PMN – xPT Crystals

(i) Effects of Flux Compositions

With only PbO as flux, it was found that MgO could not be completely dissolved in the flux even at a temperature as high as 1300 °C at 1 atmosphere pressure. We observed from the experiment that when the temperature was above 1200 °C, the PbO evaporation becomes very severe and rapid. For the top-seeded-solution-growth (TSSG), the time remaining at high temperature may last a few days, which means the growth temperature must be brought down below 1200 °C. Therefore use of B_2O_3 as a flux additive is necessary for the growth of PMN-PT crystals from high temperature solutions.

By adding some B_2O_3 into the PbO flux, the complex flux has the power to dissolve MgO, Nb_2O_5 and TiO_2 completely at temperature lower than 1160 °C. At the same time, the melted B_2O_3 increased the viscosity of the solution. The lower growth temperature and higher viscosity effectively prevent the PbO from evaporating and significantly reduce the attack of molten PbO to the Pt crucibles. Thus, the PMN-PT crystals can be grown by TSSG method at 1 atmosphere pressure.

The PbO-B_2O_3 mixture has a melting point as low as 493 °C, with a reasonable viscosity, solubility and volatility, and its flux chemistry can be varied with ratio.

Although the actual role of the B_2O_3 on the growth of PMN-PT may be very complicated and needs to be studied more in detail, we believe that the melt complexing power of the boron oxide in liquid sate is the most important effect induced by B_2O_3. The reduced activity of the transition metals (Nb and Ti) in the melt occurs through the formation of metal–borate complexes. These complexes are inactive for nucleation, growth and thermodynamic equilibrium. The complexes are a reservoir of transition metal oxides. The thermodynamic equilibrium between the complexed species and free metal oxides:

$$(TiNb)_{1/3}BO_3 \leftrightarrow (TiNb)O_2 + BO$$

When the transition metal oxides are depleted as crystals grow, some complexes will break up to restore equilibrium.

Therefore, the addition of B_2O_3 reduces the saturation (liquidus) temperature and decreases the growth rates under similar conditions, providing a more stable growth, and expectedly a more homogeneous composition in the grown crystals.

(ii) TSSG of the PMN-PT Crystals

The technique of top-seeding-solution-growth developed in our laboratory in the last two years for the growth of PZN-xPT piezocrystals has been extended to the PMN-xPT system. One of the main

difficulties encountered here was the higher melting point of the PMN-PT system than that of PZN-PT, and therefore, it was more difficult to find the effective saturation temperature which is a key parameter for the TSSG process. Based on the pseudo-binary phase diagram that we established for the PMNT-PbO system, we were able to work out the optimum conditions for the growth of PMN-xPT, which have resulted in the formation of large and high quality single crystals (with x=0, 0.10 and 0.35). Figures 20(a) and (b) show the photographs of as-grown PMN and 0.65PMN-0.35PT single crystals, respectively.

Note that in the case of PMN crystal [Fig. 20(a)], by using an appropriate seeding direction along <111> direction, the as-grown crystals exhibit a naturally developed cubic morphology with {100} facets, which is very useful for applications since such a morphology eliminates the complicated crystal orientation process otherwise needed to identify the {100} faces. For PMNT65/35, crystal boules of dimensions 35x25x20 mm^3 have been consistently reproduced under the optimized conditions. The crystals grown by TSSG exhibit naturally grown (100) facets, and a pseudo-cubic morphology. Such a habit was developed thanks to the introduction of the seed crystal that favors the growth along the <111> direction, which is the fastest growth direction.

The largest PMNT35 single crystal was grown from y = 35% solution by TSSG method with a <111> PMN crystal as seed. The crystal, with dimensions of 33×25×10 mm^3 and a weight about 45 g, was grown from 1180 to 1170°C at 0.2° C/h then to 1040 °C at 0.5° C/h. The diameter of the crucible was 45 mm. The crystal was originally grown along <111> direction then developed to <100> direction. The growth steps can be clearly seen to along [100] direction.

The development of TSSG technique for the growth of PMN-PT and PZN-PT crystals has provides a crystal resource for these crystals not only for the fundamental research but also for device testing and applications. This technique has also been used to grow the single crystals of other new materials systems (see below).

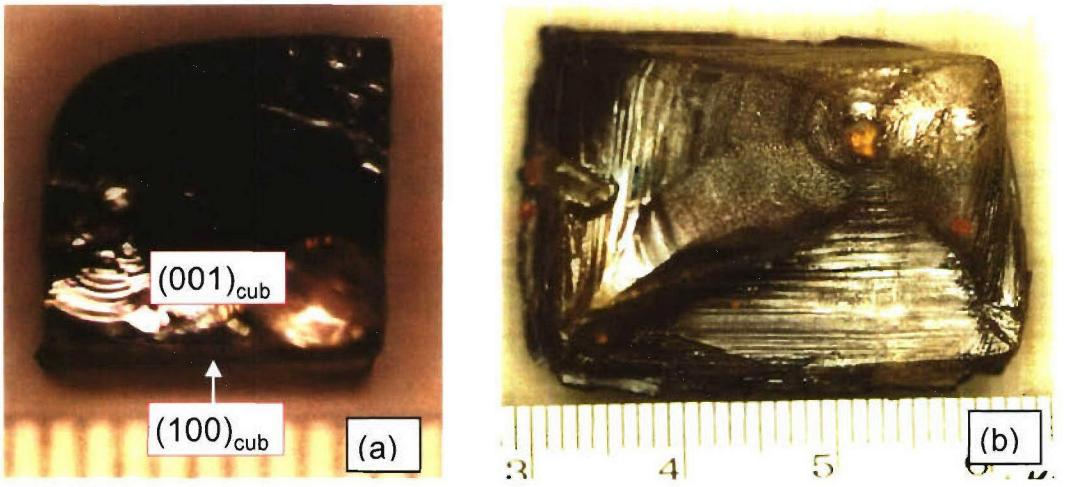

Figure 20. Morphology of PMN (a) and 0.65PMN-0.35PT (b) single crystals grown by the top-seeded-solution-growth technique.

2.2.2) High-T_C $Pb(Sc_{1/2}Nb_{1/2})O_3 - PbTiO_3$ (PSN-PT) Single Crystals

2.2.2.1) Technical Rationale

The solid solution relaxor ferroelectric $Pb(Sc_{1/2}Nb_{1/2})O_3$ and ferroelectric $PbTiO_3$, namely $(1-x)Pb(Sc_{1/2}Nb_{1/2})O_3 - xPbTiO_3$ [PSN-PT, or PSNT], emerged to be an interesting system, which had not been studied thoroughly. Single crystals of PSN-PT were expected to exhibit even higher piezoelectric performance. The advantages of PSN-PT over the PMN-PT and PZN-PT include its more stable perovskite phase and its higher T_C (=260°C) and high coupling factor k_{33}. High-T_C materials such as PSN-PT would allow medical transducers engineers to do high speed dicing which is absolutely necessary for array type transducers production. This is the reason why PZT5H (T_C=200°C) are used for medical transducers for time consuming job. PZN-PT and PMN-PT will easily be depoled by high speed dicing, therefore requiring very slow dicing speed. PSN-PT appears to be the most convenient for this purpose thanks to its high T_C. Another advantage of PSN-PT is its better mechanical properties, which are closely related to the Ti-contents of the MPB compositions, and can be ranked as:

PSN–PT (58/42) > PMN–PT (68/32) > PZN–PT (90/10) .

It can be seen that each of the three materials has its own unique properties and advantages for potential defense or civilian applications. However, in contrast to the remarkable progress recently made on PMN-PT and PZN-PT crystal systems, only some very preliminary work on PSN-PT crystal growth has been reported, and the grown crystals showed very poor quality with inclusions and fractures. The difficulties encountered in the growth of PSN-PT crystals can be attributed to its high melting point (T_m > 1425 °C). it is clearly the first system of choice when searching for high-T_C and high-performance piezocrystals.

Therefore, a considerable amount of effort has been made on the growth and characterization of the PSN-PT single crystals. We have investigated systematically the chemical and thermal parameters in order to optimize the growth of PSN-PT crystals by various techniques, and to fully characterize their properties.

2.2.2.2) Technical Approach

In order to fully explore the electromechanical properties and the device performance of the PSN-PT crystals, we have investigated the growth of PSN-PT single crystals and their piezo-/ferroelectric properties in detail. For a high melting point system such as PSN-PT, the choice of an effective high temperature solvent appeared to be particularly important. We used a mixture of PbO and B_2O_3 as flux. The addition of a small amount of B_2O_3 was expected to extend the metastable region (i.e. crystallization field), to increase the dissolving power of the melt, to decrease the melting point, and to create an optimum degree of complex formation. Due to its low melting point and high viscosity, B_2O_3 could also form an encapsulating layer, which prevented the flux from evaporation and the Pt crucibles from being attacked by the molten PbO at high temperatures. All these effects would lead to more stable growth. In addition, $(PbO+\delta B_2O_3)$ had been proven to be an effective mixed flux for the growth of PMN-PT and PZN-PT crystals, combining the advantages of both borate and PbO solvent.

The flux growth technique was first used to find out the optimum chemical and thermal conditions for the formation of the (1-x)PSN-xPT crystals. Because of the high melting point (>1420 °), it was quite a challenge to identify the right crystallization path. After many trials, we finally succeeded in the growth of PSN-PT crystals. As the research was advanced, progress has been continuously made and the size and quality of the PSN-PT crystals have been improved.

The PSNT57.5/42.5 crystals were grown using the high temperature solution. High purity (>99.99%) powders of PbO, Sc_2O_3, Nb_2O_5, and TiO_2 were used as starting materials of PSNT without pretreatment. The stoichiometric powders were mixed with a complex flux of $PbO-B_2O_3$ at various

ratios and loaded into a Pt crucible (35 ml). The Pt crucible was then placed in an alumina crucible that was sealed to an alumina lid with Al_2O_3 cements to prevent the evaporation of PbO. The loaded crucible was then put into a muffle furnace and heated to 1200 °C for PSNT crystals or 1300 °C for pure PSN crystals and soaked for 5 hrs. The crucible was then cooled down at a gradually increasing rate of 0.5 °C/h to 5 °C/h. Different lower limits of growth temperature (T_L), at which the slow cooling process was stopped, were used to study the effects on the phase formation and quality of the crystals. The solidified flux was leached out with hot HNO_3 (20%). X-ray powder diffraction was performed on ground single crystals using a Rigaku diffratometer to analyze the phase and symmetry of crystals.

The growth by a solution Bridgman method and the top-seeded solution growth were also tried.

The grown single crystals of PSN-PT solid solution were subject to a series of characterization to assess their dielectric, piezo- and ferroelectric properties.

2.2.2.3) Technical Progress and Results

2.2.2.3.1) Initial Flux Growth of the (1-x)$Pb(Sc_{1/2}Nb_{1/2})O_3$ –x$PbTiO_3$ Single Crystals

Compared with the $Pb(Zn_{1/3}Nb_{2/3})_{1-x}Ti_xO_3$ [PZNT] and $Pb(Mg_{1/3}Nb_{2/3})_{1-x}Ti_xO_3$ [PMNT] single crystals which have been intensively investigated and explored, $Pb(Sc_{1/2}Nb_{1/2})O_3$ [PSN], and its solid solution with PT were much less-well known. It was necessary in the first place to systematically study the growth and properties of PSNT single crystals with a composition near the MPB. The effects of the growth parameters on the morphology and quality of crystals have been investigated. The chemical compositions, such as the ratios of PSNT vs. flux and PbO vs. B_2O_3, have been varied to improve the quality of the grown crystals.

(a) Effects of Growth Parameters on the Formation of Perovskite Phase

Table 5 summarizes the various growth parameters and results of PSNT crystal growth. The crystals were grown on the bottom and walls of crucibles (Fig. 21) due to heat loss through the walls of the container. X-ray powder diffraction pattern shows that the majority of the crystals grown exhibit the pure perovskite phase without impurities, indicating that the growth was dominated by the formation of PSNT crystals. No distinguishable splits were found for the cubic (100) and (110) peaks, which indicates a rhombohedral symmetry for the grown crystals. The rhombohedral split of the (111) peak could not be observed by a conventional diffractometer due to the resolution limit, as in the case of PMNT and PZNT crystals, but has been confirmed by the results of high resolution synchrotron diffraction, which will be reported elsewhere.

Table 5 Summary of various growth parameters and results of (1-x)$Pb(Sc_{1/2}Nb_{1/2})$-x$PbTiO_3$ [PSN-PT] single crystals

Batch	Composition	Ratio of PSNT/Flux (mol%)	Ratio of PbO/B_2O_3 (mol%)	Lower limit temperature T_L for growth (°C)	Phases (wt %)
1	x = 0.425	15/85	75/25	1000	100%Perovskite
2	x = 0.425	15/85	70/30	980	80%Perovskite +20%Pyrochlore
3	x = 0.425	25/75	70/30	1030	100%Perovskite
4	x = 0.425	25/75	70/30	1000	98%Perovskite + 2%Pyrochlore
5	x = 0	25/75	70/30	1080	98%Perovskite+ 2%Pyrochlore

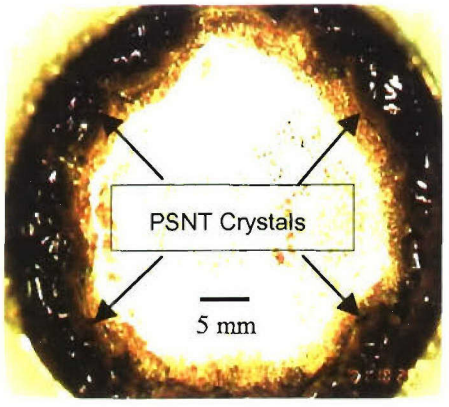

Figure 21. Top-view of an as-cooled crucible from Batch 4 of PSNT57.5/42.5 single crystals, showing the growth by spontaneous nucleation around the crucible walls.

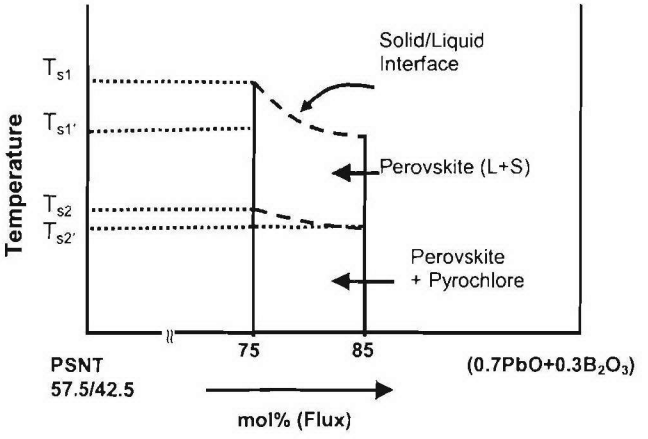

Figure 22. Schematic diagram showing the formation of the perovskite crystals in the pseudo-binary system of PSNT57.5/42.5 – $(0.7PbO+0.3B_2O_3)$.

From the above observation, if we consider PSNT57.5/42.5 – $(0.7PbO+0.3B_2O_3)$ as a pseudo-binary system, it can be concluded that the primary growth of the perovskite PSNT crystals takes place in the composition range of PSNT/Flux =15/85 – 25/75 (molar ratio) within a certain temperature interval, as sketched by the dashed area in Figure 22, where Ts_1 and $Ts_{1'}$ represent the upper limit of the solidification temperature range for the perovskite phase, and Ts_2 and $Ts_{2'}$ indicate the upper limit of the temperature range in which the pyrochlore phase starts to form.

(b) Effects of the PSNT/Flux and PbO/B_2O_3 Ratios on the Growth Thermodynamics

When we increased the ratio of PSNT/Flux in Batch 3 and 4, and kept the same ratio of PbO/B_2O_3 as in Batch 2, an increase in the yield of crystallized PSNT and hence in the slope of its temperature variation was observed. Therefore, by changing the chemical compositions, the slope of the variation of the yield of grown PSNT crystals as a function of temperature can be adjusted appropriately to achieve a more stable growth, as can be seen in the later discussion. When we considered Ti in PSNT compound as a substituent (dopant) element, the following factors are important parameters to ensure a stable growth: 1) the variation of the yield of the grown PSNT crystals as a function of temperature, which is related to the melting point of PSNT compositions in the flux (i.e. the solubility); 2) the temperature gradient of the furnace. Constitutional supercooling may occur when these two parameters do not fit properly, leading to cellular structure and facets, or dendrite growth.

(c) Effects of the PSNT/Flux and PbO/B_2O_3 Ratios on the Growth Kinetics

To study the kinetic factor affecting the growth of PSNT crystals, the morphology of PSNT crystals was carefully examined and the growth conditions in each batch were derived. The PSNT crystals show a pseudo-cubic form when grown on the crucible bottom, but a distorted form when grown on the walls. This suggests that the crystal was first developed from a single nucleus and grown under stable conditions at the beginning. Then, the "ribbons" structure appeared and spread. Such a structure is typical of the earlier stage of the so-called "cellular structure". The formation of the cellular structure implies that the growth was under severe constitutional supercooling conditions, in which the solid/liquid interface of growth could not adjust itself to keep in a planar surface shape, necessary for a stable growth. Upon this consideration, we increased the ratio of PSNT/Flux in Batches 3, 4, and 5, which has resulted in a significant improvement in both the morphology and the quality of the grown PSNT crystals. No cellular or dendrite growth phenomenon was observed in these

batches, as shown in Figure 23. The pseudo-cubic shape of crystals indicates that an appropriate saturation was achieved in the solid/liquid interface and kept almost constant during the growth.

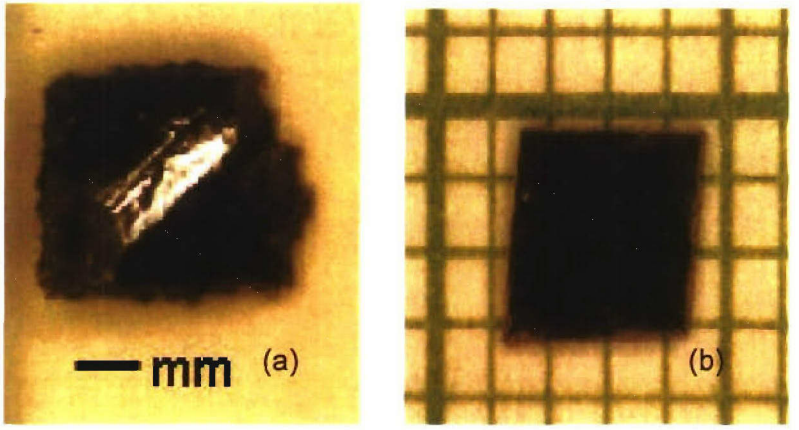

Figure 23. (a) A selected as-grown crystal of PSNT57.5/42.5 from Batch 4, showing a regular morphology; (b) A (001)-crystal plate cut from the bulk crystal.

2.2.2.3.2) Improved Flux Growth of the MPB (1-x)Pb($Sc_{1/2}Nb_{1/2}$)O_3 – x$PbTiO_3$ Crystals

Based on the above observation and reasoning of the results of initial growth, we kept optimizing and improving the growth of the (1-x)Pb($Sc_{1/2}Nb_{1/2}$)O_3 - x$PbTiO_3$ single crystals with compositions near or within the MPB region, using the mixtures of PbO and B_2O_3 as flux. More stable growth was achieved, leading to larger size and high quality PSN-PT single crystals, as shown in Figure 24. The crystal platelets and bar prepared from the as-grown crystal show high quality, suitable for subsequent characterization/applications.

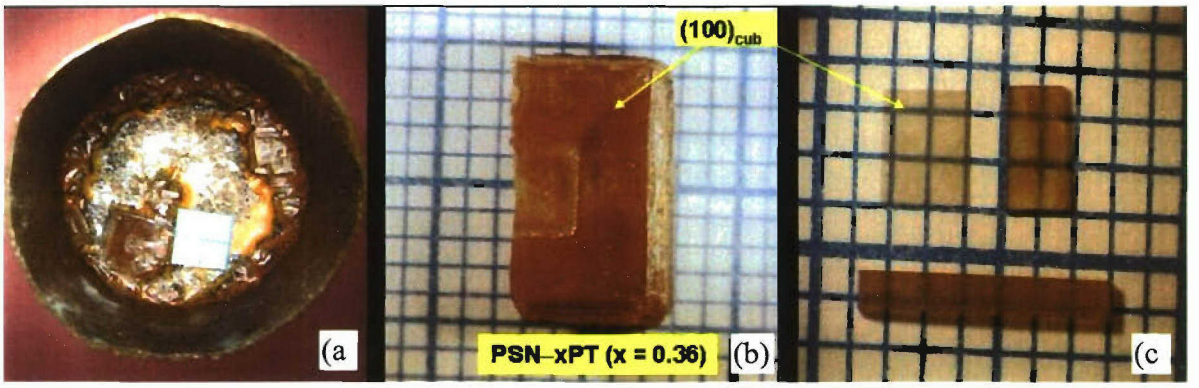

Figure 24. (a) As-cooled Pt crucible showing the growth of big PSN-PT single crystals around the walls; (b) An as-grown PSN-PT crystal after flux being leached out; (c) Two (100) platelets and a crystal bar (for k_{33} measurement) showing the good quality of the PSN-PT crystals.

Significant composition segregation is observed, giving rise to a Ti-concentration in the grown crystals lower than the nominal composition. Consequently, a composition shift towards the rhombohedral phase (i.e. lower PT) region occurs. By considering the phase segregation trend, the PSN–PT crystals of the MPB composition (PSN–0.37PT) have been grown from a nominal charge of PSN–0.51PT. The effective phase segregation coefficient for Ti is found to be k = 0.73 for the PSN–PT solid solution system of the MPB region.

2.2.2.3.3) Properties of the (1-x)Pb($Sc_{1/2}Nb_{1/2}$)O_3 – x$PbTiO_3$ Single Crystals

The grown PSN-PT single crystals with compositions close to the MPB region were found to exhibit very good dielectric, piezo- and ferroelectric properties. The PSN–0.37PT crystals exhibit a T_C = 250 °C and a T_{MPB} = 219 °C (Fig. 25) . The rhombohedral PSN–PT crystals show good dielectric and ferroelectric properties with a maximum dielectric constant of 60,000 (at 1 kHz) and a remnant polarization of 25 $\mu C/cm^2$ (Fig. 26). From the resonance and antiresonance frequencies (Fig. 27), the electromechanical coupling factor k_{33} was found to be 78%, which is slightly higher than that of the PZT ceramics. Although their piezoelectric performance is lower than that of the PMN–PT and PZN–PT crystals, the T_C (≈ 250 °C) and especially T_{MPB} (>200 °C) of the PSN–PT crystals are much higher than those of the PMN–PT and PZN–PT crystals.

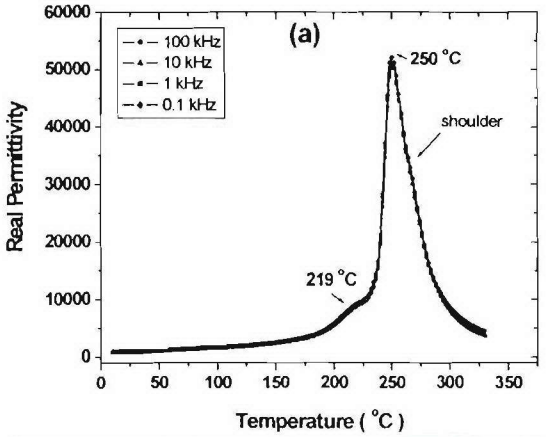

Fig. 25 Variation of the real part of dielectric permittivity as a function of temperature (upon cooling) for a $(001)_{cub}$-oriented PSN-37PT single crystal of MPB composition.

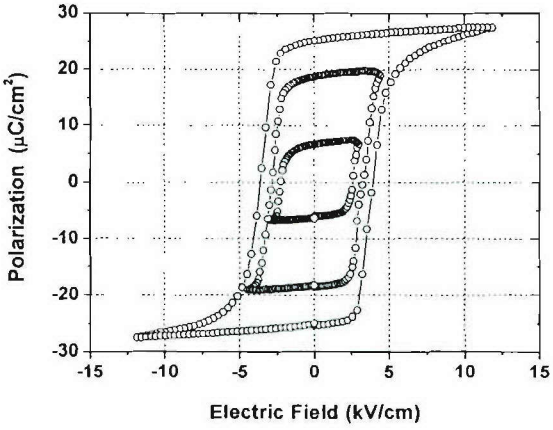

Fig. 26 Polarization *vs.* electric field (P–E) loops for the $(001)_{cub}$–oriented rhombohedral PSN–PT single crystal, displaying ferroelectricity.

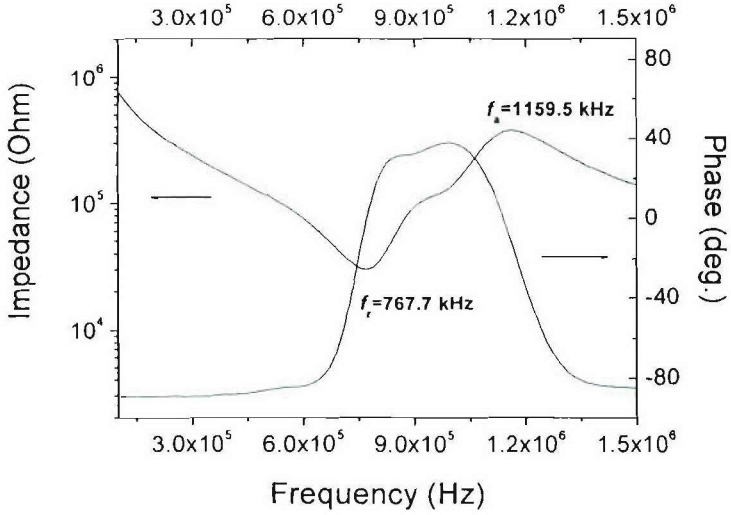

Fig. 27 Impedance and phase as a function of frequency for the $[001]_{cub}$–poled rhombohedral PSN–PT single crystal rod, with resonance and anti-resonance frequencies at 767.7 kHz and 1159.5 kHz, respectively, giving rise to an electromechanical coupling factor of k_{33}= 78 %.

These results demonstrate that, upon optimization of the MPB composition and the piezoelectric properties, the PSN–PT single crystals can constitute a new resource of high-T_C and high-performance piezocrystals potentially useful for a wide range of electromechanical transduction applications. High

T_C materials such as PSN-PT will allow medical transducers engineers to do high speed dicing which is absolutely necessary for array type transducers production. Another advantage of PSN-PT is its better mechanical properties, which are closely related to the Ti-contents of the MPB compositions.

2.2.3) Single Crystals of '$PbSnO_3$'–$PbTiO_3$ [PSn-PT]: A New Family of PiezoCrystals

2.2.3.1) Technical Rationale

In our continuous effort of researching for new high performance, high-T_C materials for electromechanical transducer devices, we have investigated the solid solution system between '$PbSnO_3$' and $PbTiO_3$, which had almost not been studied except from the original work by Jeffe *et al.* on the polycrystalline ceramic compounds in late 1950's. It was therefore much less-well known compared with PZT and the relaxor systems.

Although lead tin oxide '$PbSnO_3$' does not exist as a single-phase compound, the addition of 10 mol% PT helps stabilize the solid solution of (1-x)$PbSnO_3$ – x$PbTiO_3$ in the perovskite structure. The $PbSnO_3$-$PbTiO_3$ solid solutions share many of the features of the Pb(Zr,Ti)O_3 system. Solid solutions rich in PT are tetragonal with c/a ratio decreasing as Sn^{4+} concentration increases. Between x=40 and 45 mol%PT, a substantially morphotropic phase boundary occurs, with a rhombohedral ferroelectric phase replacing the tetragonal ferroelectric as in Pb(Zr,Ti)O_3. We believe that the solid solution of $PbSnO_3$–$PbTiO_3$ could be an alternative to the PZT and the relaxor-based systems. Single crystals of (1-x)$PbSnO_3$ – x$PbTiO_3$ system were expected to show excellent piezoelectric and electromechanical performance. However, no single crystals of this solid solution had been available. Therefore, we have systematically investigated this system, including synthesis of the solid solutions, growth of the single crystals and characterization of their structural and physical properties.

2.2.3.2) Technical Approach

As an initial approach, the flux method was used in the growth of (1-x)$PbSnO_3$ – x$PbTiO_3$ single crystals using PbO or (PbO + B_2O_3) as flux. This study has greatly benefited from our experience and expertise gained in the growth and characterization of the PMN-PT, PZN-PT and PSN-PT crystals, as described previously, since similar technical approach was used.

2.2.3.3) Technical Progress and Results

2.2.3.3.1) Growth of the (1-*x*)$PbSnO_3$ – *x*$PbTiO_3$ Single Crystals

Single crystals of the (1-*x*)$PbSnO_3$ – *x*$PbTiO_3$ (PSnT) solid solution system were successfully grown for the first time by a high temperature solution method using (PbO + δB_2O_3) as flux. Crystals of quite good quality with a length up to 8mm have been obtained, as shown in Fig. 28. X-ray diffraction confirmed the formation of pure perovskite structure.

2.2.3.3.2) Characterization of the Properties of the (1-*x*)$PbSnO_3$ – *x*$PbTiO_3$ Single Crystals

The dielectric, ferroelectric and piezoelectric properties of transparent (001) crystal platelets of 0.40$PbSnO_3$–0.60$PbTiO_3$ are characterized. The temperature dependence of the dielectric permittivity (upon cooling) reveals a Curie temperature of 206 °C, with a second anomaly at 190 °C associated with a phase transition between two ferroelectric phases, as shown in Figure 29, a typical behavior of the morphotropic phase boundary in many solid solution systems.

The room temperature ferroelectric and piezoelectric properties have been characterized and the following are parameters: a remnant polarization P_r = 23±1 μC/cm^2, a coercive electric field E_C = 2.8±0.2 kV/cm [Fig. 30], an electromechanical coupling factor k_{33} = 73±1% [Fig. 31], and a piezoelectric coefficient d_{33} = 370±10 pC/N [Fig. 32].

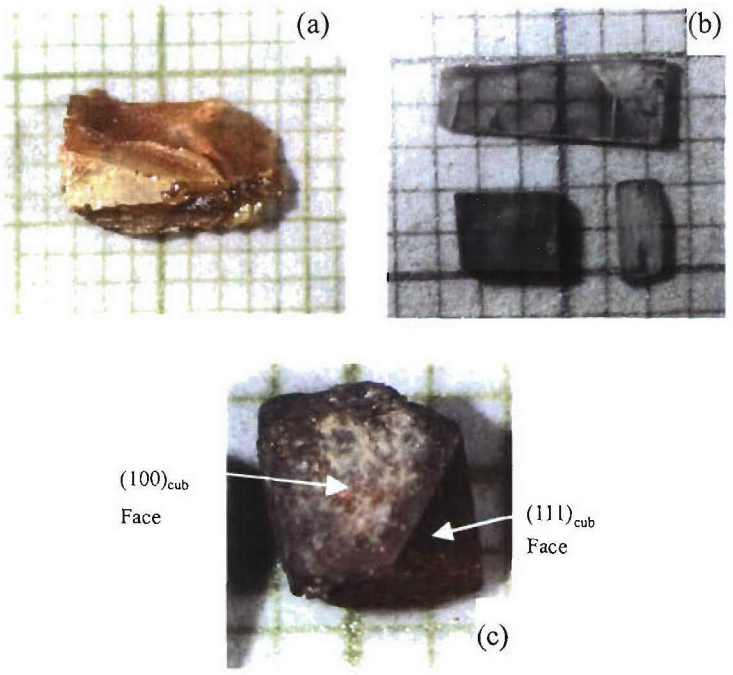

Fig. 28 Photographs of $0.40PbSnO_3$-$0.60PbTiO_3$ single crystals:
a) an as-grown crystal;
b) crystal platelets after polishing (scale = 1mm);
c) an as-grown crystal showing the growth facets.

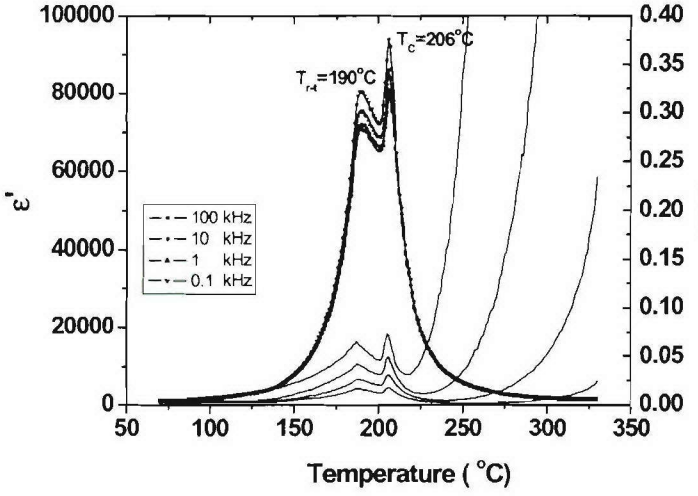

Fig. 29 Dielectric constant and losses of a <001>-oriented $0.40PbSnO_3$-$0.60PbTiO_3$ single crystal measured as a function of temperature at the frequencies of 0.1, 1, 10, 100 kHz.

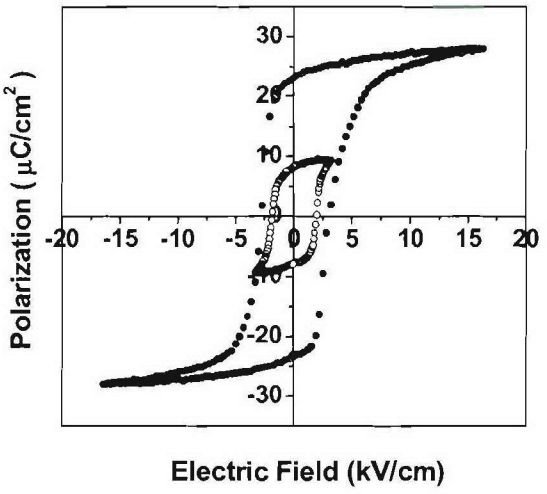

Fig. 30 Polarization vs. bipolar electric field (P-E) loops for a <001>-oriented $0.40PbSnO_3$-$0.60PbTiO_3$ single crystal, showing the ferroelectricity.

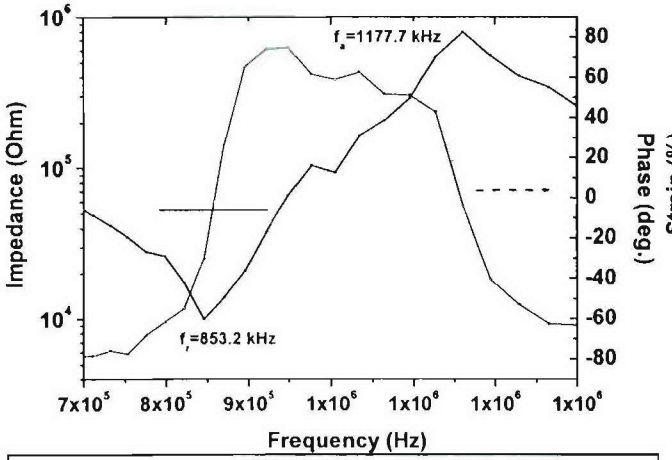

Fig. 31 Resonance and antiresonance frequencies measured from impedance and phase angle for a <001>-oriented $0.40PbSnO_3$-$0.60PbTiO_3$ single crystal.

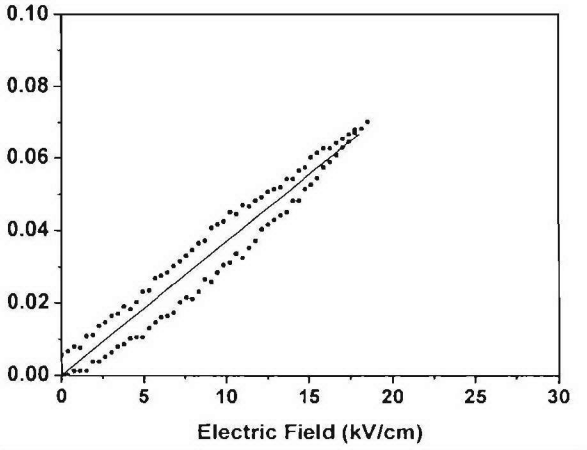

Fig. 32 Unipolar strain vs. electric field for a <001>-oriented $0.40PbSnO_3$ – $0.60PbTiO_3$ single crystal.

These results indicate that the dielectric (ε' and tanδ) and piezoelectric (k_{33}, d_{33}) properties of the PSnT40/60 crystals are comparable with the PZT ceramics. The properties are lower than in the 0.70PMN – 0.30PT and 0.93PZN – 0.07PT (MPB) crystals, but T_C, and especially T_{MPB}, of the PSnT crystals are much higher than those of the PMN–PT and PZN-PT single crystals.

Although preliminary, these original results indicate that the $PbSnO_3$-$PbTiO_3$ solid solution crystals form a new family of piezocrystals which exhibit a higher T_C and higher T_{MPB} than the PMN-PT and PZN-PT crystals. Other advantages of this piezocrystal system include its simpler composition (compared with the relaxor-based complex perovskite systems) and the lower melting points of its components (compared with the PZT system). Upon optimization of the MPB composition and piezoelectric properties, these crystals are a very promising alternative for new applications requiring high operation temperatures.

More elaborated investigations need to be performed on this new family of piezocrystals, both in the crystal growth and in the characterization and optimization of dielectric, piezo- and ferroelectric properties in order to make them a viable piezocrystal resource.

2.2.4) Piezo- and Ferroelectric Materials from the Ternary $Pb(Yb_{1/2}Nb_{1/2})O_3$-$PbTiO_3$-$PbZrO_3$ [PYN–PT–PZ] System

2.2.4.1) Technical Rationale

In our attempts of developing new materials systems that would yield single crystals with both relatively high T_C and high piezoelectricity, we have also studied novel ternary systems of perovskite compounds. In general, the ternary systems present some advantages over the binary ones: the MPB is a line at fixed temperature and pressure instead of a point, offering more MPB compositions for exploring optimum properties.

The $(1-x-y)Pb(Yb_{1/2}Nb_{1/2})O_3$-$xPbZrO_3$-$yPbTiO_3$ [PYN – PZ – PT] ternary system was identified to be a promising candidate. Compositionally ordered $Pb(Yb_{1/2}Nb_{1/2})O_3$ (PYN) is antiferroelectric with a monoclinic perovskite structure and has a T_C around 300 °C. It forms a solid solution with $PbTiO_3$, $(1-x)Pb(Yb_{1/2}Nb_{1/2})O_3$-$xPbTiO_3$ (PYN-PT), with a morphotropic

phase boundary (MPB) at x=0.46. The T_C for the MPB composition of this system is around 340 °C. It was reasonable to expect that an MPB would exist for the PYN-PZ-PT ternary system and the piezoelectricity and T_C of the MPB compositions would be high because of the similar perovskite structures for the three end members and the high T_C for both PYN-PT and PZT at the MPB compositions.

2.2.4.2) Technical Progress and Results

In the framework of the second program of this award, we have studied the ceramics of the ternary system and determined the low temperature phase diagram around the ternary morphotropic phase boundary (Fig. 33). The ceramics of the composition near the MPB, $0.33Pb(Yb_{1/2}Nb_{1/2})O_3$–$0.23PbZrO_3$–$0.44PbTiO_3$ (Point 8), were found to exhibit a high ferroelectric Curie temperature of T_C = 370 °C, a large bipolar strain of 0.4% (peak to peak) at 20 kV/cm, a large d_{33} value of 1247 pC/N (at E < 20 kV/cm) (Fig. 34), and a remnant polarization (P_r) of 28 μC/cm^2 (Fig. 35).

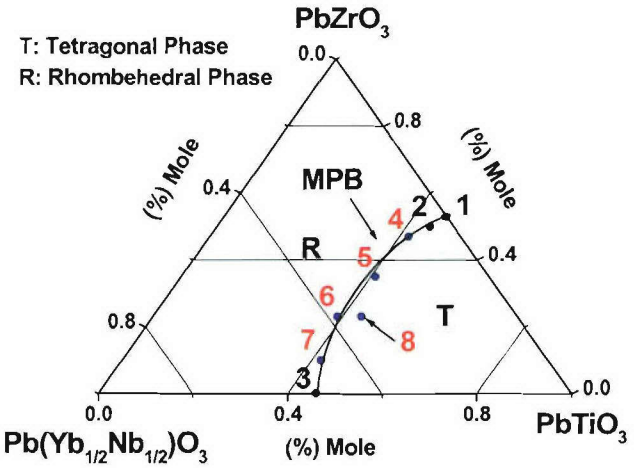

Point 4: 0.11PYN-0.47PZ-0.42PT; Point 5: 0.24PYN-0.35PZ-0.41PT
Point 6: 0.38PYN-0.23PZ-0.39PT; Point 7: 0.48PYN-0.10PZ-0.42PT
Point 8: 0.33PYN-0.23PZ-0.44PT

Figure 33. Updated morphotropic phase diagram for the (1-x)PYN-xPZ-yPT ternary system determined by X-ray diffraction and phase analysis.

Such a piezoelectric response is among the highest in ceramic compounds. In fact it places the $0.33Pb(Yb_{1/2}Nb_{1/2})O_3$–$0.44PbTiO_3$–$0.23PbZrO_3$ compound well above the d_{33}–T_C relation for most of the piezoelectric materials (Fig. 36). Therefore, the ternary system of $xPb(Yb_{1/2}Nb_{1/2})O_3$–$yPbTiO_3$–$zPbZrO_3$ [PYN – PT – PZ] forms a family of promising piezoelectric materials for high-temperature electromechanical transducer applications. However, no single crystals of the ternary system have been reported so far. In the present work, we propose to grow the single crystals of the same nominal composition by means of high-temperature solution method using ($PbO + B_2O_3$) and $LiBO_2$ as flux, and to characterize the dielectric properties, domains structures and phase transitions in the grown crystals, and compared the results with the ceramics data.

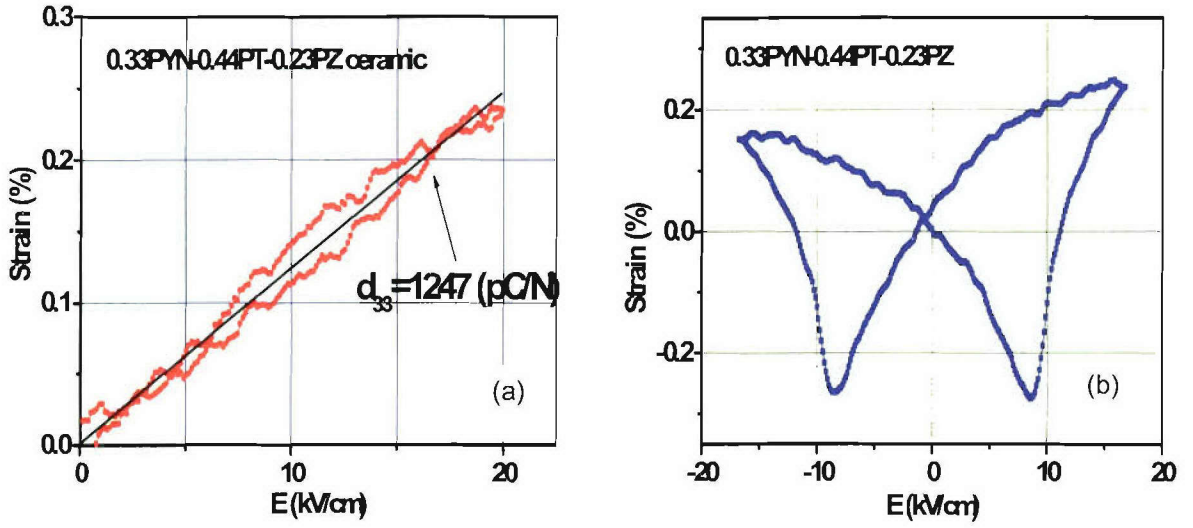

Figure 34. Piezoelectric responses of the PYN-PT-PZ ceramics: (a) Strain vs. unipolar electric field; (b) Strain vs. bipolar electric field.

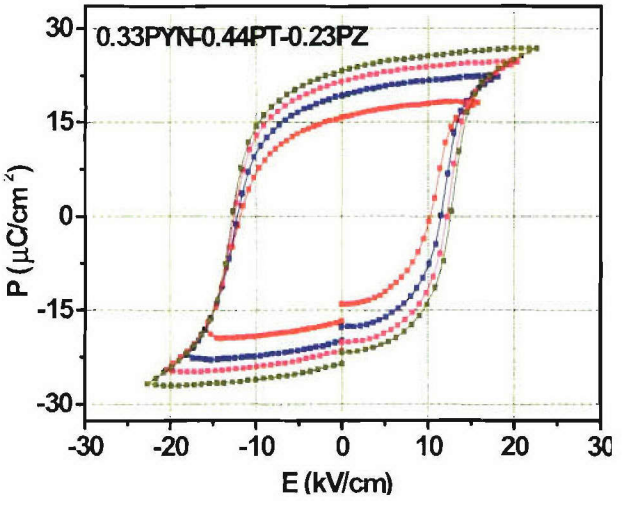

Figure 35. Ferroelectric hysteresis loops of the PYN-PT-PZ ceramics.

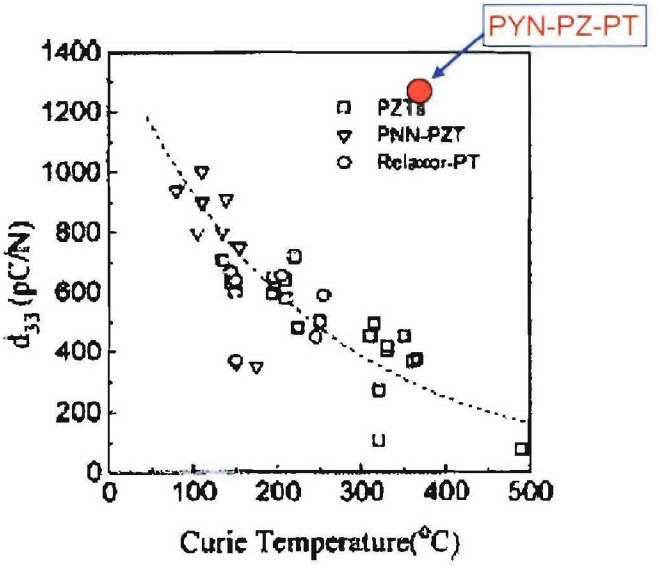

Figure 36. Inverse relation between d_{33} and T_C for most of the piezomaterials. The performance of the PYN-PT-PZ ceramics is placed well above the trend curve.

Given the extraordinary piezoelectric performance of the ceramics of this ternary system, it will be interesting to pursue the growth of the (1-x-y)$Pb(Yb_{1/2}Nb_{1/2})O_3$-x$PbTiO_3$-y$PbZrO_3$ single crystals, by the flux growth and the top-seeded solution growth techniques. Such a effort is in progress.

2.2.5) Single Crystals of $Pb(Zr_{1-x}Ti_x)O_3$ [PZT] - *Challenging the Impossible*

2.2.5.1) Technical Rationale

Lead zirconate-titanate solid solution, $Pb(Zr_{1-x}Ti_x)O_3$ [PZT], is undoubtedly the most important piezo-/ferroelectric and electroceramic material. The excellent piezo- and ferroelectric properties of the PZT ceramics appear in the composition range close to the morphotropic phase boundary (MPB) of the solid solution system which is located within the composition range of $x = 0.40 - 0.50$. Recent structural studies by Noheda *et al.* by means of synchrotron x-ray powder diffraction technique revealed by surprise a low temperature monoclinic *Cm* phase with a narrow composition range, $0.45 < x < 0.52$, lying in between the rhombohedral *R*3*m* ($x < 0.45$) and the tetragonal *P*4*mm* ($x > 0.52$) phases. The monoclinic phase serves as a structural bridge between the *R*3m and *P*4mm phases through the common symmetry element (the mirror or monoclinic plane *m*), which provides a new perspective to the understanding of the rhombohedral / tetragonal phase structure at MPB. The relatively ease rotation of the monoclinic polarization within the m plane can better explain the anomalously high piezoelectric response of PZT around the MPB, as supported by the theoretical calculations from first principles. On the other hand, the rhombohedral polarization rotation induced by an electric field applied along $<001>_{cub}$ is shown to generate very large distortion through a monoclinic phase.

Crystal chemistry consideration indicates that, the single crystals of PZT, if possible to grow, should be one of the best piezoelectric materials, with their dielectric, piezo- and ferroelectric performance comparable or superior to the relaxor-based piezocrystals, and a T_C definitely higher than that of the relaxor-base piezocrystals. However, the growth of PZT crystals, especially with composition around the MPB, had been a very difficult task because of the high melting point of the system on the one hand, and the strong phase segregation on the other hand. As a result, earlier attempts at crystal growth had only led to the small PZT crystals (< 2 mm) with compositions usually far away from the MPB ($x < 0.25$ or $x > 0.65$).

Therefore, in the second part of this program, we have taken on the challenge of growing the PZT single crystals and have been quite successful and achieved significant progress.

2.2.5.2) Technical Approach

We intended to develop an effective route to grow PZT single crystals. The choice of high temperature solvent was the most important task. The possible candidates include the combinations of ($PbO + B_2O_3$), ($PbO + PbF_2$), ($PbO + PbF_2 + B_2O_3$), etc, which are aimed at lowering the melting point of the system while providing a high enough dissolving power. The flux growth was first performed to grow PZT crystals. Single crystals with a size of several mm were grown via spontaneous nucleation. They appeared to be suitable as seed crystals to be used in the subsequent top-seeded solution growth (TSSG) process, as described in detail in Section 2.2.1.2. The electric, dielectric and piezoelectric properties of the grown PZT crystals were performed using the same approach as applied in the crystals of other materials systems.

2.2.5.3) Technical Progress and Results

In the past few years, after many trials and failures, we have finally succeeded in growing the PZT single crystals. We have found the appropriate growth conditions for improved flux method based on a complex high temperature solution of ($PbO + B_2O_3$) and developed an

effective top-seeded solution growth technique, which worked in a relatively low temperature range of 1150 – 800 °C. The TSSG-grown PZT crystal exhibit cubic or plate morphologies with a size ranging from a few mm up to 10 - 13 mm. Figure 37 shows the photograph of one of the PZT crystals of MPB composition with pseudo-cubic morphology.

The dielectric spectroscopic measurements show that the T_C of the PZT crystals varies from 350 to 405 °C, indicating that the corresponding crystal composition can be adjusted within the range of the MPB from x ≈ 0.45 to 0.52 (Fig. 38). The dielectric constant reaches 40,000 – 75,000 at peak value.

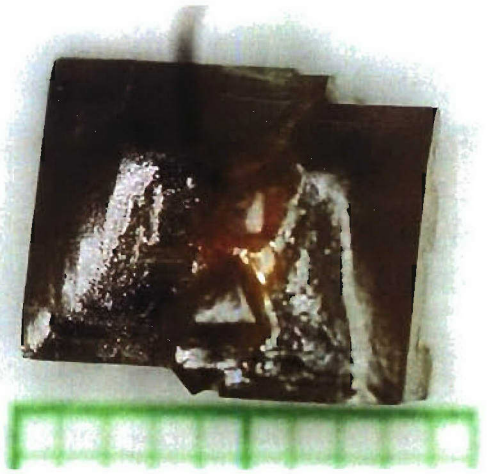

Figure 37. Photograph of a $Pb(Zr_{0.53}Ti_{0.47})O_3$ crystal grown by a TSSG technique.

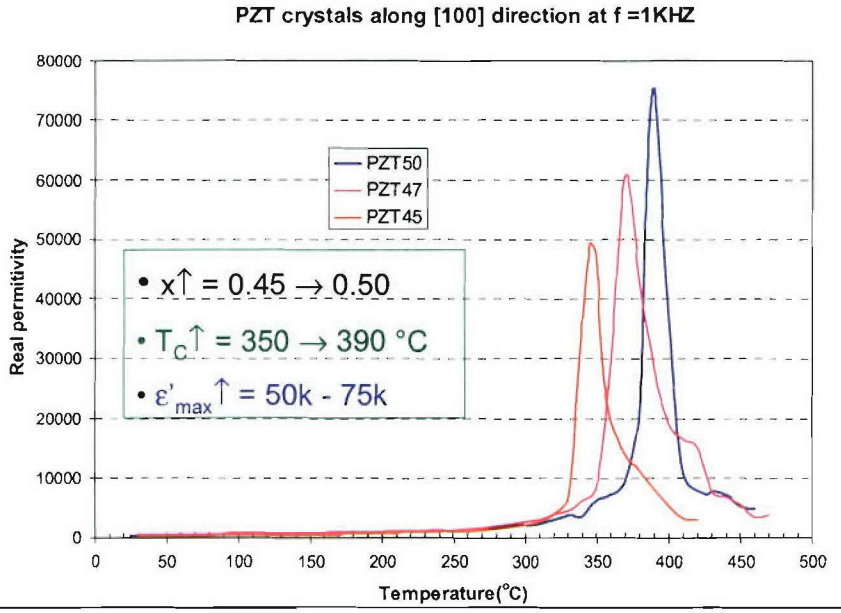

Figure 38. Dielectric permittivity as a function of temperature for the single crystals of $Pb(Zr_{1-x}Ti_x)O_3$ with compositions in the MPB region.

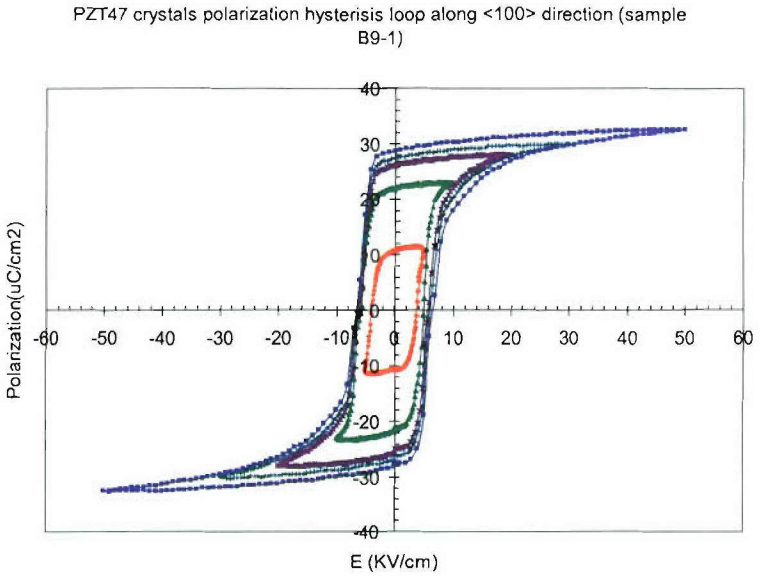

Figure 39. Dielectric hysteresis loops displayed in a $Pb(Zr_{0.53}Ti_{0.47})O_3$ crystal showing excellent ferroelectricity.

Figure 39 shows the dielectric hysteresis loops displayed in a $(001)_{cub}$ $Pb(Zr_{0.53}Ti_{0.47})O_3$ crystal at different field atrengthes. It can be seen that the grown PZT crystals exhibit excellent ferroelectric properties with a high remanent polarization of 32 $\mu C/cm^2$.

Bipolar strain measurement shows that the PZT crystals develop a very large peak to peak strain of 0.47% at a drive field of 15 kV/cm, i.e. more than 3 times higher than that of PZN-PT crystals, but unfortunately, with a strong hysteresis of "hard" appearance and a coercive field of 3-5 kV/cm (Figures 40 & 41). This unusual strain loop indicates a "hard-PZT" behavior which could be explained based on the domain reorientations.

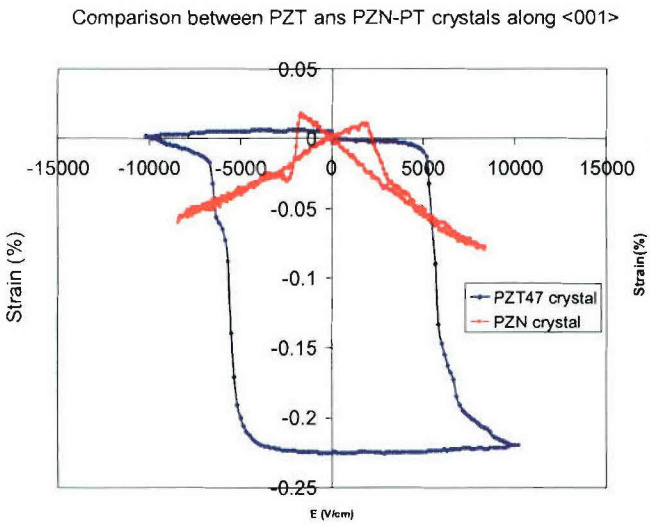

Figure 40. Strain as a function a bipolar drive field measured on a PZT50/50 crystal, in comparison with that of a PZN-PT crystal [(001) plates].

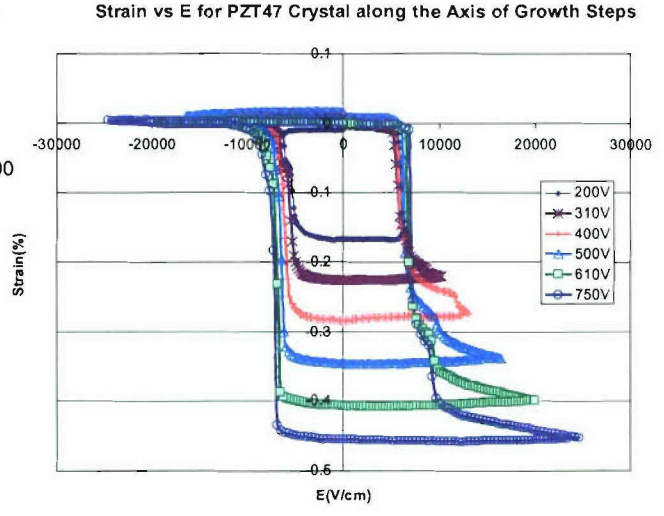

Figure 41. Strain as a function a bipolar drive field measured on a PZT53/47 crystal, measured at various filed strengths.

Our successful growth of the PZT single crystals of the MPB composition has been considered by many a breakthrough in the field of piezo- and ferroelectric materials research. However, there are several issues that need to be addressed. As in the case of PSN-PT system, difficulties are still encountered in the growth of PZT crystals because of the very high melting point and the severe phase segregation of the solid solution system. So far the growth results are not yet consistent, the success rate is still low and the production capacity is very limited because the problems that arise from the growth and the factors that affect the quality of the crystals have not been understood thoroughly. It is also crucial to be able adjust the composition and properties of PZT crystals by chemical method, so that the "soft-PZT" behavior can be obtained. The resolution of these issues will be crucial to turn the PZT crystals into a new resource of piezocrystals for advanced applications in electromechanical transduction. This subject is central to our ongoing research program which is aimed at the improved growth and complete characterization of the PZT single crystals.

2.2.6) Solid Solution System of $BiFeO_3$ – $PbTiO_3$: *High- T_C and Multiferroic*

2.2.6.1) Technical Rationale

In our continuous effort in developing other new materials with both high coupling coefficients and high T_C, the solid solution of $BiFeO_3$ – $PbTiO_3$ has become one of the obvious choices. PT is proved to be the most ideal ferroelectric with tetragonal symmetry, and it is also one of the components to form the MPB of all the developed and developing ultrahigh performance materials. $BiFeO_3$ seems to be an interesting compound to compose an MPB with PT, because $BiFeO_3$ exhibits a ferroelectric rhombohedral phase with a very high T_C = 850 °C. This system contains Bi^{3+} ions with lone electron pair as an 'active' A-site component. The solid solutions between $BiFeO_3$ and PT are expected to show high T_C and high electromechanical coupling factors. In addition, BF shows an antiferromagnetic ordering with the Neel temperature T_N = 370 °C, which could become weekly ferromagnetic at low temperature, giving thus rise to simultaneous ferroelectric and ferromagnetic orderings, i.e. *multiferroicity*.

Indeed, the (1-x)$BiFeO_3$-x$PbTiO_3$ solid solution of perovskite structure with compositions near the morphotropic phase boundary (MPB) (x=0.3 – 0.35) shows a huge tetragonality (lattice parameter ratio c/a) in its tetragonal phase, which theoretically predicts a large electric polarization. The ferroelectric Curie point of the MPB compositions derived from high temperature X-ray diffraction is around 700 °C, indicating the potential of this system for high temperature applications using piezo- and ferroelectric properties.

However, the ceramics of BF-PT solid solution exhibits high electric conductivity, which makes it very difficult to characterize the properties of the materials and to test their dielectric, piezo- and ferroelectric performance. Therefore, as the first stage of our studies in this project, we have performed the chemical modifications on the ceramics of BF-PT system in order to improve the dielectric performance of the materials.

2.2.6.2) Technical Approach and Results

Ceramics of 0.67$BiFeO_3$–0.33$PbTiO_3$, 0.67$BiFe_{0.98}Ti_{0.02}O_3$–0.33$PbTiO_3$ (*via* B site Ti^{4+} modification) and 0.67$BiFeO_3$–0.33$PbTiO_3$ sintered under O_2 flow were synthesized. The frequency-dependence of the impedance was measured at various temperatures and analyzed. It was found that the dielectric properties are improved by B site Ti^{4+} modification and by

sintering in O_2 flow. The temperature dependences of DC conductivity of the grains for the three ceramic samples are derived from impedance analysis by fitting their impedance data to an electric equivalent circuit of 3 RC components. The temperature dependences of both the DC conductivity of the grains and the measured AC conductivity (at high and low frequencies) show that the conductivity for O_2-sintered sample is the lowest, and the conductivity of $0.67BiFe_{0.98}Ti_{0.02}O_3$–$0.33PbTiO_3$ is lower than that of $0.67BiFeO_3$–$0.33PbTiO_3$ (Table 6). This result is consistent with the dielectric properties of the respective ceramics. The mechanism of the electric conduction is discussed in relation to the chemical modifications and the related defect chemistry.

Table 6. Dielectric constant (ε') and dissipation factor (tanδ) at room temperature for the BF-PT, BFT-PT and BF-PT(O) ceramics at different frequencies

		10^2 Hz	10^3 Hz	10^4 Hz	10^5 Hz	10^6 Hz
BF-PT	ε'	166	117	105	101	99
	tanδ	0.427	0.185	0.0557	0.0251	0.0398
BFT-PT	ε'	185	146	134	130	126
	tanδ	0.186	0.113	0.0375	0.0252	0.0349
BF-PT(O)	ε'	55	46	41	40	38
	tanδ	0.239	0.136	0.04	0.0155	0.0833

These results indicate that the electric conduction in the $BiFeO_3$–$PbTiO_3$ ceramics arises from the hopping of electrons from Fe^{2+} to Fe^{3+} through oxygen vacancies, which can be effectively decreased by aliovalent (higher oxidation state) ionic doping.

Therefore, in order to develop effective piezo- and ferroelectric materials of high-T_C, ceramic samples of $0.67BiFe_{(1-x)}Ti_xO_{3+x/2}$–$0.33PbTiO_3$ with different B site substitution amount of Ti^{4+} for Fe^{3+} were prepared in thto investigate the effect of Ti^{4+} doping amount on the electric and dielectric properties of $0.67BiFe_{(1-x)}Ti_xO_{3+x/2}$-$0.33PbTiO_3$ ceramics. Structural characterization by X-ray diffraction shows that the doping limit is 6 mol% (Fig. 42).

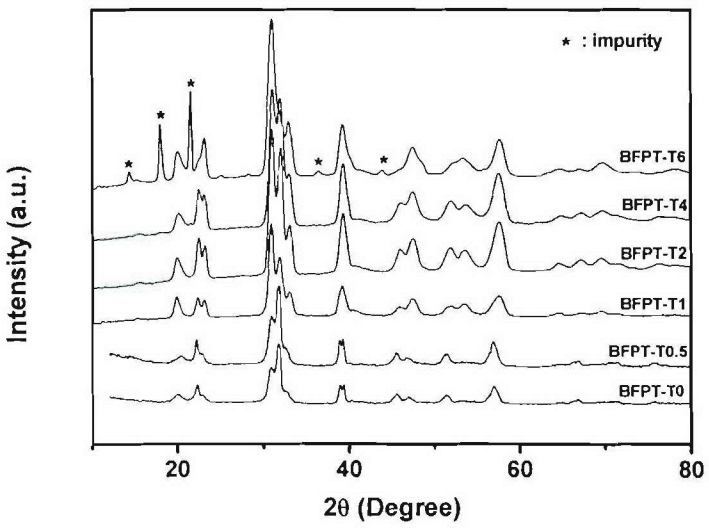

Figure 42. XRD patterns of sintered BFPT-T0, BFPT-T0.5, BFPT-T1, BFPT-T2, BFPT-T4, and BFPT-T6 ceramics (the number after T indicates the % of Ti^{4+} dopant).

The dielectric dissipation factor decreases significantly with increasing Ti^{4+} doping on the B site, so that the dielectric constant can be measured up to 450 °C (the upper temperature limit of the instrument) on all the Ti^{4+}-doped samples, which exhibit a T_C higher than 450 °C, as shown in Fig. 43.

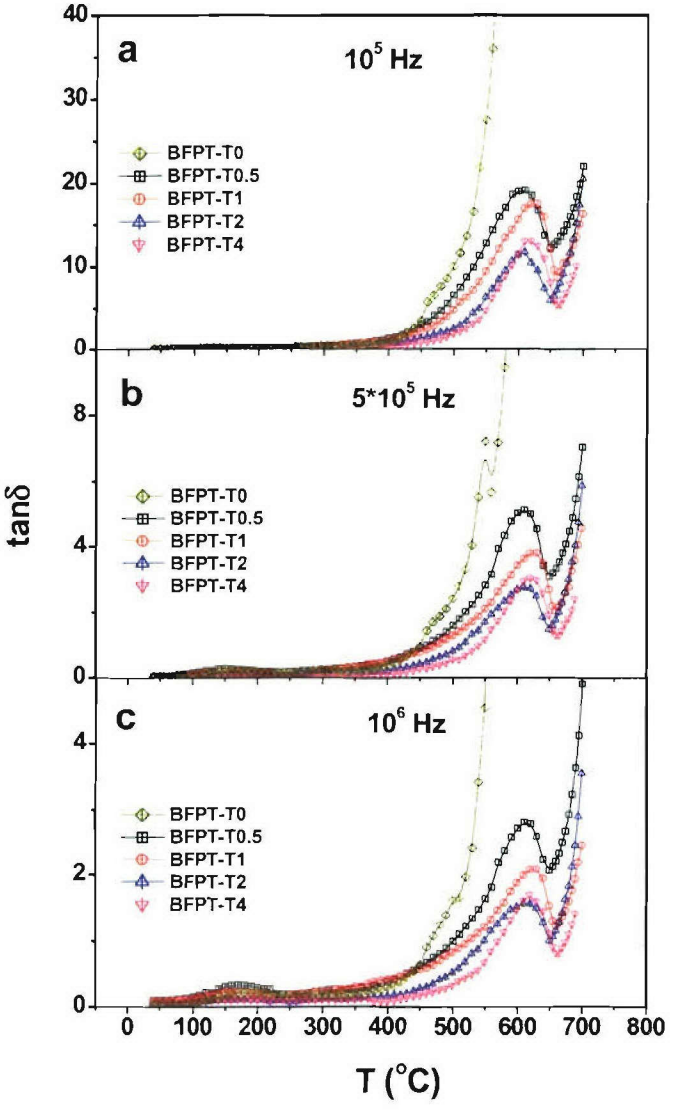

Figure 43. Temperature variation of dielectric dissipation factor (tan δ) of BFPT-T0, BFPT-T0.5, BFPT-T1, BFPT-T2, BFPT-T4, and BFPT-T6 (the number after T indicates the % of Ti^{4+} dopant).

Figure 44 shows that the dielectric hysteresis loop changes from a typical conductive type for undoped sample to a normal ferroelectric type for the Ti^{4+}-doped samples. A very high electric coercive field was observed from the hysteresis loops of the doped samples, which increases with the increase of the Ti^{4+} doping amount. A saturated dielectric hysteresis loop was obtained on a 0.5 mol% Ti^{4+} doped sample only, which shows a remnant polarization (P_r) of 8 $\mu C/cm^2$, and a coercive field (E_C) of 100 kV/cm. A much higher electric field is necessary to obtain saturated hysteresis loops for the samples with higher doping amount. A remnant polarization of 17 $\mu C/cm^2$ was obtained from the unsaturated hysteresis loop of a 2 mol% Ti^{4+} doped sample, which implies that P_r increase with the increase of doping amount and that a much higher P_r can be expected if the loop is saturated. This indicates that the

aliovalent ion-doped $BiFeO_3$-$PbTiO_3$ is a promising candidate for high temperature high performance piezoelectric, ferroelectric and multiferroic applications.

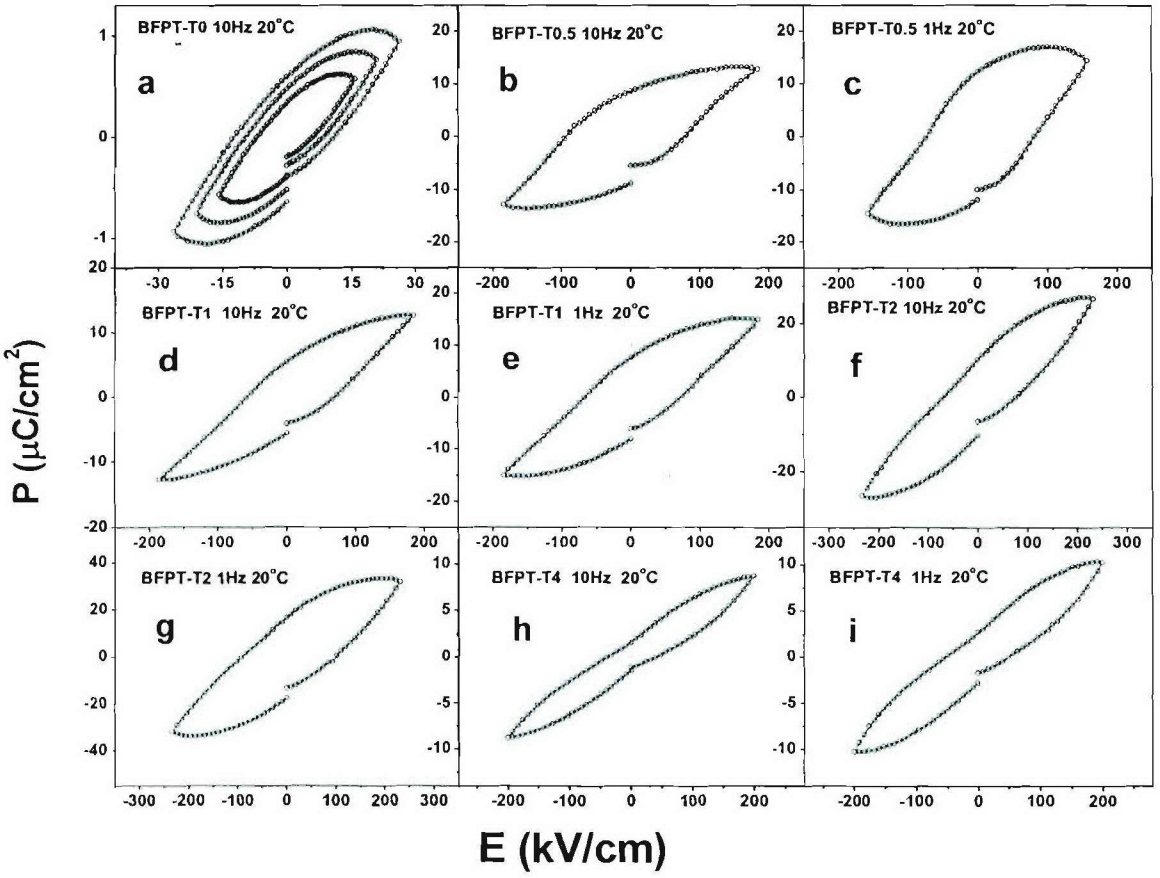

Figure 44. Room temperature dielectric hysteresis loops of BFPT-T0.5, BFPT-T1, BFPT-T2, and BFPT-T4 ceramics.

2.3) Fundamental Characterization and Understanding of Materials Properties

One of the most important features of our proposed effort was that, parallel to the original materials synthesis, crystal growth and measurements of their properties, more fundamental characterization of the structure and properties of the materials synthesized constituted an integrated part of our research programs. Based on our expertise in the field of crystal structure, ferroelectricity, relaxor ferroelectricity, ferroic domains and piezoelectricity and the research infrastructure that we have set up at Simon Fraser University, we have undertaken a variety of characterization in order to better understand the physical properties, the structure-property relationships of the piezo- and ferroelectric materials.

Our main results in materials characterization are presented in the following aspects:

(i) Structural Characterization of the *Morphortropic Phase Boundary;*

(ii) Complete Characterization of the Dielectric, Piezo- & Ferroelectric Properties;

(iii) Morphotropic Domain Structure, Phase Transitions and Polarization Switching;

(iv) Relaxor Ferroelectricity and Related Properties.

2.3.1) Structural Characterization of the *Morphotropic Phase Boundary*

2.3.1.1) Technical Rationale

The existence of morphortropic phase boundary (MPB) appears to the most characteristic feature of the relaxor-based and other solid solution systems from which the innovative piezoelectric singles are formed, such as the PZN-PT, PMN-PT, and PSN-PT systems. It has been commonly believed that the enhanced piezoelectric performance of the relaxor-based single crystals is closed related to the effects of morphotropic phase boundary (MPB). However, the initial knowledge on MPB, which was described as an almost temperature-independent concentration separating the rhombohedral phase of the relaxor side and the tetragonal phase of the PT side in the temperature (T) *v.s.* concentration (x) phase diagrams, appeared to be an oversimplified picture of the real feature of MPB. Therefore, it was necessary to revisit the MPB phase diagrams of the PMN-PT and PZN-PT systems and to determine the true symmetry of the MPB phases and the sequences of phase transitions, in order to provide a better understanding of the MPB nature and its effects on the piezoelectric properties, and to understand the microscopic mechanisms of the electromechanical properties.

2.3.1.2) Technical Approach

The complex structures of the morphotropic phase boundary were characterized by means of:

(a) Conventional X-ray Diffraction:

Conventional powder X-ray diffraction was used to verify the formation and purity of phases, and to study the phase components of the compounds, especially those with compositions close to or within the morphotropic phase boundary which usually exhibit multiple phases.

(b) Synchrotron X-ray Diffraction:

Synchrotron X-ray provides high intensity and high resolution diffraction technique which was exploited to investigate the delicate structural distortion and phase transitions occurring in some of the complex relaxor-based materials systems. These experiments were performed at the Brookhaven National Laboratory (NY) in very fruitful collaboration with Dr. B. Noheda, Dr. D. Cox, Dr. G. Xu and Dr. Gen Shirane.

For the PMN-xPT ($0.29 < x < 0.39$) system, synchrotron x-ray powder diffraction experiments were performed on unpoled ceramic samples prepared by solid state reaction using the columbite method. For the PZN-xPT, the diffraction was performed on single crystals of compositions x=0.07, 0.80, 0.85, 0.09 and 0.11, grown by the top-seed solution growth (TSSG) technique, as described in Section 2.2.1. The beamline X7A or X3B1 was used. A double-crystal channel-cut Si (111) monochromator was used in combination with a Ge (220) analyzer and a scintillating detector. The wavelength was set to $\lambda \approx 0.7$ Å and calibrated with a Si reference standard. The resulting instrumental resolution (full width at half maximum, FWHM) is about 0.005° on the 2θ scale, an order of magnitude better than that of a conventional laboratory instrument. At X7A, the data were collected directly from the ceramic pellets loaded on a symmetric "flat-plate" reflection (Bragg-Brentano) geometry with step-scans at 0.005° intervals over selected angular regions while the sample was rocking over 1 – 2° to obtain better powder averaging results. The measurements as a function of temperature were performed between 20 and 500 K. For low temperature measurements, the samples were loaded in a closed-cycle He cryostat, which has an accuracy of about ±2 K. The measurements above room temperature were carried out with the samples loaded inside a wire-wound BN tube furnace with an accuracy of ±3 K. At X3B1, the data were collected with rotating capillaries and Si powder was used as a standard at each temperature so that the accuracy in the calculated lattice parameters was within 0.0003 Å. In the most cases, the scans were carried out over narrow angular regions centred about the six pseudocubic reflections (100), (110), (111), (200), (220) and (222), in order to determine the crystal symmetry and related lattice parameters. For data analysis, the individual reflection profiles were fitted by least-

squares to a pseudo-Voigt function appropriately corrected for asymmetry, with intensity, peak position and peak-width (FWHM) as variables, to determine the lattice parameters.

2.3.1.3) Technical Progress and Results

2.3.1.3.1) New MPB Phase Diagram and Phase Transitions of the (1-x)PZN-xPT System

In this work, synchrotron x-ray measurements were performed to study the phase symmetry, phase component, and phase transitions in the piezo-/ ferroelectric system (1– x)$Pb(Zn_{1/3}Nb_{2/3})O_3$-x$PbTiO_3$ (PZN-xPT) with compositions (Ti-content x) around and beyond the MPB (x = 7 – 15%). The orthorhombic phase was observed for x = 10%, but, surprisingly, for x=11% only a tetragonal phase was found to exists down to 20 K. The orthorhombic phase thus exists only in a narrow concentration range with near-vertical phase boundaries on both sides. This orthorhombic symmetry (M_C type) is in contrast to the monoclinic M_A-type symmetry recently identified at low temperatures in the $Pb(Zr_{1-x}Ti_x)O_3$ (PZT) system over a triangle-shaped region of the phase diagram in the range x = 0.46–0.52. To further characterize this relaxor-type system, neutron inelastic scattering measurements have also been performed on a crystal of PZN-xPT with x = 15%. The anomalous soft-phonon behavior ("waterfall" effect) previously observed for x = 0% and 8% is clearly observed for the 15% crystal, which indicates that the presence of polar nanoregions extends to large values of x.

Figure 45 shows the new MPB phase diagram established of the PZN-PT system, where the low symmetry orthorhombic phase (O) was found to exits between the rhombohedral R3m phase on the relaxor side and the teragonal P4mm phase on the ferroelectric PT side. Figure 46 gives the variation of lattice parameters vs Ti-concentration at 20 K. It shows the structural evolution from the rhombohedral to the tetragonal phase *via* the orthorhombic phase. For x ≤ 8%, the crystals exhibit the expected rhombohedral symmetry. For x ≥ 11 %, the tetragonal symmetry is found with strain ratio c_t/a_t increasing from 1.0237 at x=11 % to 1.0331 at x=15%. The smooth variation in the tetragonal a and c parameters with composition is consistent with fairly precise compositional control during crystal growth. At 9% ≤ x ≤ 10%, the symmetry is found to be orthorhombic.

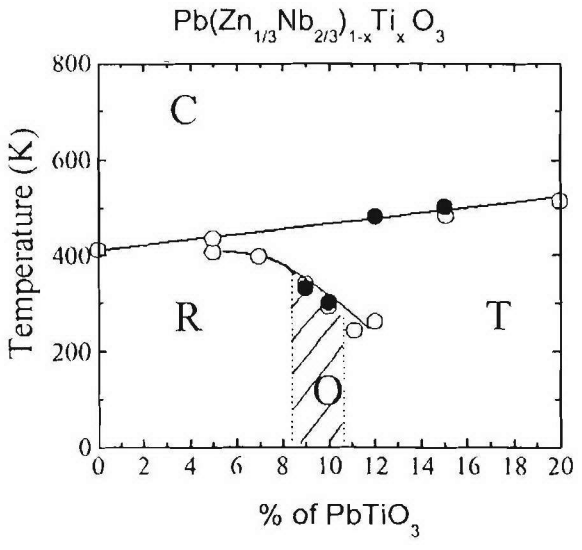

Figure 45. New MPB phase diagram established for the relaxor-based PZN-xPT system.

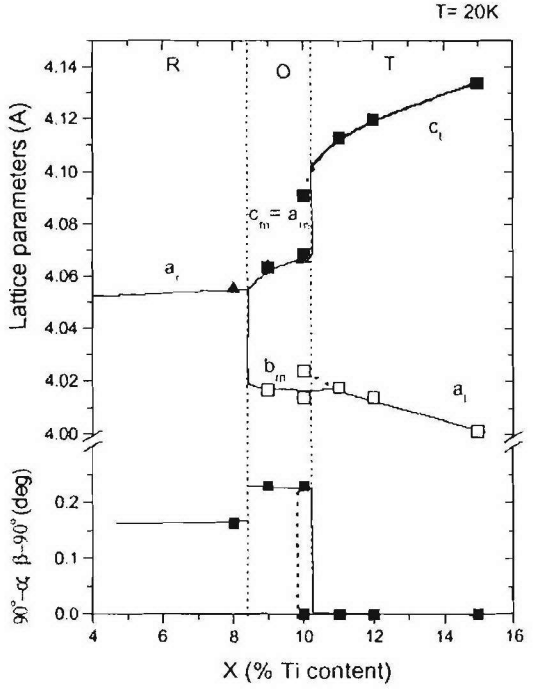

Figure 46. Variation of lattice parameters vs Ti-concentration at 20 K for the PZN-PT system.

2.3.1.3.2) New MPB Phase Diagram and Phase Transitions of the (1-x)PMN-xPT System

Synchrotron x-ray powder diffraction measurements were performed on unpoled ceramic samples of $(1-x)Pb(Mg_{1/3}Nb_{2/3})O_3–xPbTiO_3$ (PMN-xPT) with 30% - 39% as a function of temperature around the morphotropic phase boundary, which is the line separating the rhombohedral and tetragonal phases in the phase diagram. The experiments have revealed very interesting features previously unknown in this or related systems. The sharp and well-defined diffraction profiles observed at high and intermediate temperatures in the cubic and tetragonal phases, respectively, are in contrast to the broad features encountered at low temperatures. These peculiar characteristics, which are associated with the monoclinic phase of M_C-type previously reported by Kiat et al. [Phys. Rev. B 65, 064106 (2000)] and Singh and Pandey [J. Phys.: Condens Matter 13, L931 (2001)], can only be interpreted as multiple coexisting structures with M_C as the major component. An analysis of the diffraction profiles has allowed us to properly characterize the PMN-xPT phase diagram and to determine the stability region of the monoclinic phase, which extends from x = 31% to x = 37% at 20 K. The complex landscape of observed phases points to an energy balance between the different PMN-xPT phases which is intrinsically much more delicate than that of related systems such as $PbZr_{1-x}Ti_xO3$ or $(1–x)Pb(Zn_{1/3}Nb_{1/3})O_3–xPbTiO_3$. These observations are in good accord with an optical study of x = 33% by Xu et al. [Phys. Rev. B 64, 020102 (2001)], who observed monoclinic domains with several different polar directions coexisting with rhombohedral domains, in the same single crystal.

Figure 47 presents the updated phase diagram of (1-x)PMN-xPT around the MPB, where a low symmetry monoclinc M_C phase was found to exits between the rhombohedral R3m phase on the relaxor side and the teragonal P4mm phase on the ferroelectric PT side. At $x < 0.31$, the PMN-PT system shows a clean rhombohedral phase, and at $x > 0.37$, a clean tetragonal phase. But for the MPB compositions ($0.31 \leq x \leq 0.39$), the phase diagram is characterized by the *coexistence* of the rhombohedral R3m and monoclinic M_C phase on the one hand ($0.31 \leq x \leq 0.32$), and the *coexistence* of the M_C and the tetragonal P4mm phase on the other hand ($0.32 \leq x \leq 0.39$). Figure 48 gives the composition dependence of the lattice parameters of the major phases in PMN-xPT around the MPB at 300 K, showing the structural evolution from the rhomohedral to the tetragonal phase *via* the monoclinic M_C phase.

In a related study, a ferroelectric monoclinic phase of space group *Cm* (M_A type) was discovered in $0.65Pb(Mg_{1/3}Nb_{2/3})O_3–0.35PbTiO_3$ by means of high resolution synchrotron X-ray diffraction. It appears at room temperature in a single crystal previously poled under an electric field of 43 kV/cm applied along the pseudocubic [001] direction, in the region of the phase diagram around the morphotropic phase boundary between the rhombohedral (*R*3m) and the tetragonal (*P*4mm) phases. The monoclinic phase has lattice parameters a = 5.692 Å, b = 5.679 Å, c = 4.050 Å and $\beta = 90.15°$, with the b_m-axis oriented along the pseudo-cubic [110] direction . It is similar to the monoclinic phase observed in $PbZr_{1-x}Ti_xO_3$, but different from that recently found in $Pb(Zn_{1/3}Nb_{2/3})O_3$ - $PbTiO_3$, which is of space group *Pm* (M_C type). An updated phase diagram between PMN and PT has been proposed, as shown in Figure 12.

2.3.1.3.3) MPB Phase Diagram of the $Pb(Sc_{1/2}Nb_{1/2})O_3–PbTiO_3$ system

The complex morphotropic phase boundary (MPB) behaviour of the relaxor ferroelectric-based $(1-x)Pb(Sc_{1/2}Nb_{1/2})O_3$ - $xPbTiO_3$ (PSN-PT) solid solution system was investigated systematically by experiments with both ceramics and single crystals. The study of the PSN-PT ceramics with compositions within the MPB region by means of dielectric spectroscopy has revealed two phase transitions. A new phase diagram of PSN -PT solid solution with the MPB region and a curved upper boundary has been established. A morphotropic phase boundary region has been confirmed to exist and the composition range has been refined to be $x \approx 0.36 – 0.45$, as shown in Fig. 49. A new phase with monoclinic (M) symmetry has been found by X-ray phase analysis. It is believed to bridge the rhombohedral and tetragonal phases.

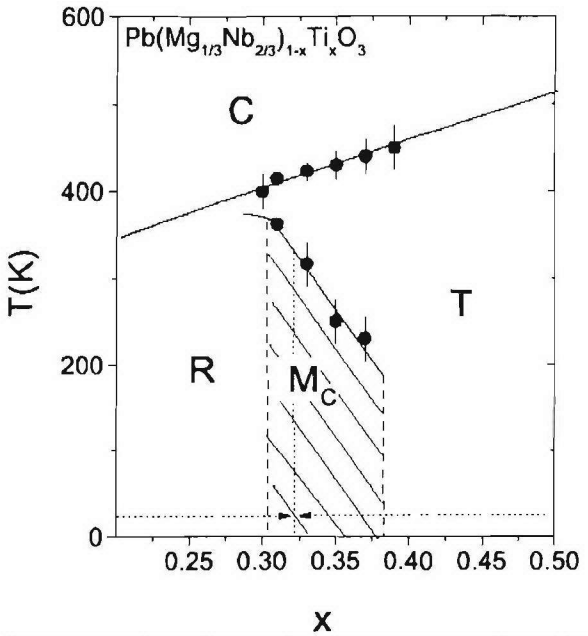

Figure 47. MPB phase diagram established for the relaxor-based PMN-xPT system.

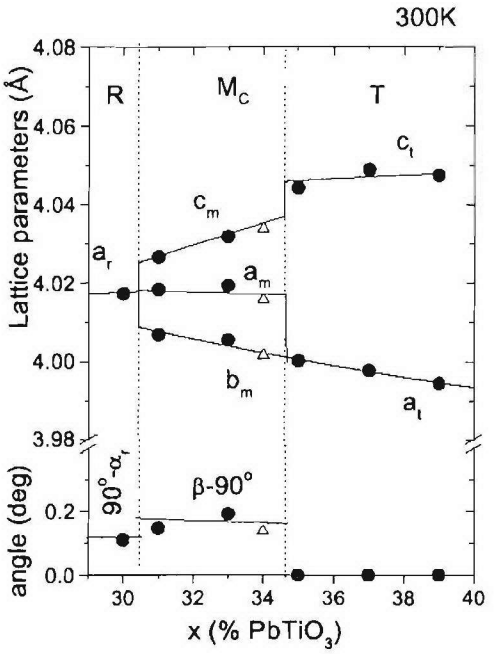

Figure 48. Lattice parameters of the major phases around MPB for the PMN-xPT system at 300 K.

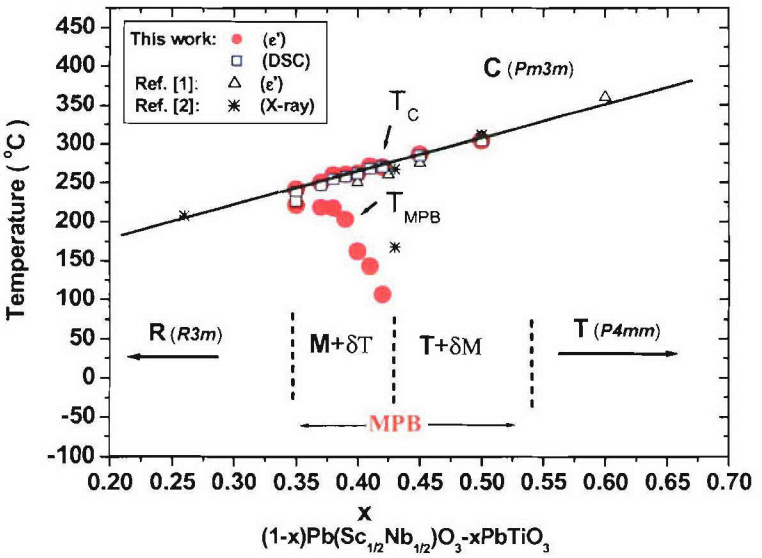

Figure 49. (Preliminary) MPB phase diagram established for the PSN-PT solid solution system.

2.3.2) Complete Characterization of the Optical, Dielectric, Piezo- & Ferroelectric Properties

2.3.2.1) Technical Rationale and Approach

In addition to the conventional characterization of the properties of the materials which was described in the previous Sections of materials synthesis, we have put special effort in investigating some peculiar properties, especially the properties of the newly discovered monoclinic phase, which could help reveal the mechanism(s) underlying the extraordinary properties of the innovative high performance piezo- and ferroelectric crystals.

With the discovery of the new monoclinic or orthorhombic phase as a bridging phase in the range of MPB in high-performance piezoelectric PMN-PT and PZN-PT materials (see Section 2.3.1), a natural presumption was that, it is the monoclinic phase that gives rise to the extraordinary piezoelectric properties. However, no direct measurements of the ferroelectric and electromechanical properties of that new phase have been reported so far. The purpose of this work was to investigate the electrical behavior of the monoclinic phase in PMN-PT crystals.

Because of the unavoidable macroscopic spatial variations of the cation ratio on the B-site, which occurs during the crystal growth, any meaningful studies of the relationship between the structure and properties of PMNT and similar solid solutions should be complemented by careful examinations of the crystal symmetry and phase components of the very same sample in which the measurements of properties are to be performed. Note that X-ray diffraction and related techniques, which are commonly used in practice, are not fully suitable for these purposes, because the lattice distortions in different phases differ only slightly from each other, and a small admixture of the secondary phase may not be detected, but may affect greatly the physical properties. That is why the measurements in this work are accompanied by simultaneous observation of the domain structures by polarization light microscopy. In this way, the tetragonal, rhombohedral and monoclinic phases, that are expected to exist for the compositions near the MPB, are unambiguously identified and distinguished from each other.

2.3.2.2) Technical Approach

2.3.2.2.1) Dielectric Spectroscopy

The dielectric spectroscopy is a useful technique not only for determining the phase transition temperatures (T_C and T_{MPB}) which are important for device applications, but also for studying dynamics of the polar nanoregions which is a key piece of information for the fundamental understanding of the relaxor mechanisms and thereby for the materials design. The complex dielectric permittivity ($\varepsilon = \varepsilon' - i\varepsilon''$) was measured as a function of frequency at different temperatures under isothermal conditions. A weak ac field (0.05-0.2 V/mm) was applied. The data were taken during the cooling or heating runs. A computer-controlled impedance analyzer (Solartron 1260) was used for measurements in conjunction with a dielectric interface (Solartron 1296), covering a wide frequency range from 10^{-2} to 10^{5} Hz.

2.3.2.2.2) Piezo- and Ferroelectric Measurements

The piezoelectric and ferroelectric properties of the piezo-/ferroelectric crystals were characterized by conventional dielectric, resonance, and ferroelectric measurements, according to the Standard for the Characterization of Piezocrystals (drafted under the ONR initiative, 2002 -). The polarization *v.s.* electric field was measured using a Radiant RT66A Test System at the frequency of 0.2 Hz to reveal the ferroelectric properties. The variations of polarization and strain versus electric field were measured using a Radiant RT66A Test System and a fiber-optic system MTI-2000, respectively. A drive voltage of triangular pulses was applied. The sample holder was designed to allow the crystal to deform without mechanical constraints. The electromechanical coupling factors were measured by resonance frequencies which were determined using a Solartron 1260 impedance analyzer and a Solartron 1296 dielectric interface.

2.3.2.2.3) Polarized Light Microscopy

The polarized light microscopy is a powerful tool for studying the optical properties of the pizeo-/ferroelectric crystals. It can reveal the domain patterns which result from the crystallographic symmetry elements of the materials. Therefore, the analysis of the complex domain structures helps us deduce the phase symmetry of the various components of the MPB crystals, and thereby understand the multiple phase coexistence, which is characteristic of the MPB crystals. The domain structures were studied by a polarizing microscope (Olympus BX60) in a wide temperature range (- 190 to 600 °C) thanks to a temperature stage (Linkam). The direction of the polarized light propagation and that of the applied electric field were parallel to each other, and to the [001] direction of the crystal. Domain structure was examined based on the principle of optical crystallography. For *in situ* study of the domain structure under a dc bias, semitransparent gold layers were sputtered as electrodes. Gold wires were attached to the electrodes by silver paste to connect the sample with a high voltage source.

2.3.2.3) Technical Progress and Results

2.3.2.3.1) Piezo- and Ferroelectric Properties of the *Monoclinic Phase* in PMN-xPT Crystals

(i) Overall Domain Structure and Phase Transitions

Preliminary examinations of large (~10 x 10 mm^2) crystal plates in polarizing microscope revealed the coexistence of macroscopic domains of different phases, namely, the rhombohedral and tetragonal phases, and another phase of lower symmetry. We successfully identified the part of the crystal containing the low-symmetry phase only, cut a few (001)–oriented monophase plates with an area of ~2 × 2 mm^2 and a thickness of 0.14 mm, and studied their properties. All regions of the platelets showed in crossed polarizers a clear extinction that is not parallel to <100> or <110>. Such an optical behavior is not compatible with either a tetragonal or a rhombohedral symmetry. More detailed analysis of the domain structure of these samples before and after poling revealed a monoclinic *Pm* symmetry, in agreement with the neutron and x-ray diffraction data). The temperature dependence of the real part of dielectric permittivity ε' showed a maximum at T_m = 162 °C. This temperature was used to estimate the average composition x_{av} of the sample by comparing it with the T_m values of the ceramics, where the composition is known exactly and $T_m(x)$ is a linear function. In this way, it was found that $x_{av} \approx 0.33$.

(ii) Ferroelectric Properties

The dielectric hysteresis loops at a drive voltage of different frequencies are shown in Fig. 50. The well-saturated and symmetrical loops indicate the ferroelectricity of the monoclinic phase. The remanent polarization P_r and the coercive field E_c depend on frequency when it is higher than about 1 Hz, but in the low-frequency range the variation becomes negligible, e.g., the same values of P_r = 23 μC/cm^2 and E_c = 2.7 kV/cm are obtained at 1 Hz and 0.2 Hz. This means that the process of domain switching are practically completed during the period. As the spontaneous polarization vector of the *Pm* phase lies somewhere in between [001] and [101], the magnitude of its spontaneous polarization P_s is estimated to be: $P_r < P_s < \sqrt{2}\, P_r$ = 33 μC/cm^2.

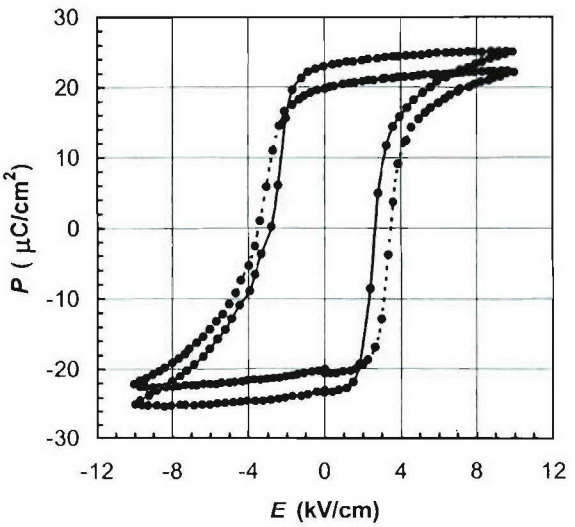

Figure 50. Hysteresis loops displayed in a monoclinic PMNT (001)-oriented crystal at 25 °C at frequencies of 1 Hz (solid line) and 100 Hz (dashed line).

(iii) Domain Structure of the Monoclinic Phase

Figure 51 gives the photograph of the domain structure of the crystal observed by polarizing microscope. It consists of laminar birefringent domains separated by straight dark boundaries, which are oriented along <110>. The width of the domain stripes is about 1-4 μm. As the spontaneous polarization vectors of all the domains in the poled monoclinic phase form the same angle to the [001] direction, the change of energy density caused by the electric field applied afterwards in that direction should be the same for all the domains. Consequently, such a field should not affect the domain walls. In agreement with this analysis, no any noticeable changes in the configurations of the domain walls are observed under the electric field [compare Figs. 49 (a) and (b) as an example].

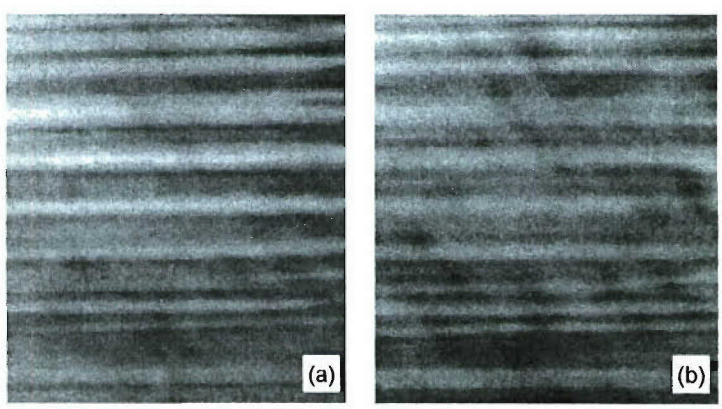

Figure 51. Domain structure of the monoclinic phase observed on the (001) PMNT platelet: (a) under an electric field of 10 kV/cm // [001] (i.e. perpendicular to the plane of the platelet); (b) after the removal of the field.

(iv) Dielectric Spectroscopy of the Monoclinic Phase

The dielectric spectra measured at room temperature under a small (3 V/cm) ac signal are shown in Fig. 52. A significant dispersion is evidenced in the whole measurement range of frequency, suggesting an extremely wide distribution of relaxation times. After poling, the dispersion is attenuated and the real part of permittivity diminishes dramatically. The stronger dielectric dispersion and the higher values of permittivity and tanδ in the unpoled state can be attributed to the motion of the domain walls, which is a usual phenomenon in multi-domain ferroelectrics. As observed above, a field does not affect the position of the domain walls of the poled crystal. As a result, they no longer contribute to the dielectric response. Another possible cause for the change of the dielectric properties after poling is the anisotropy of monoclinic phase. The losses at very low frequencies still remain significant after poling. They are probably arise from the polarization of mobile charge carriers, characteristic of many materials at low frequencies including PMNT.

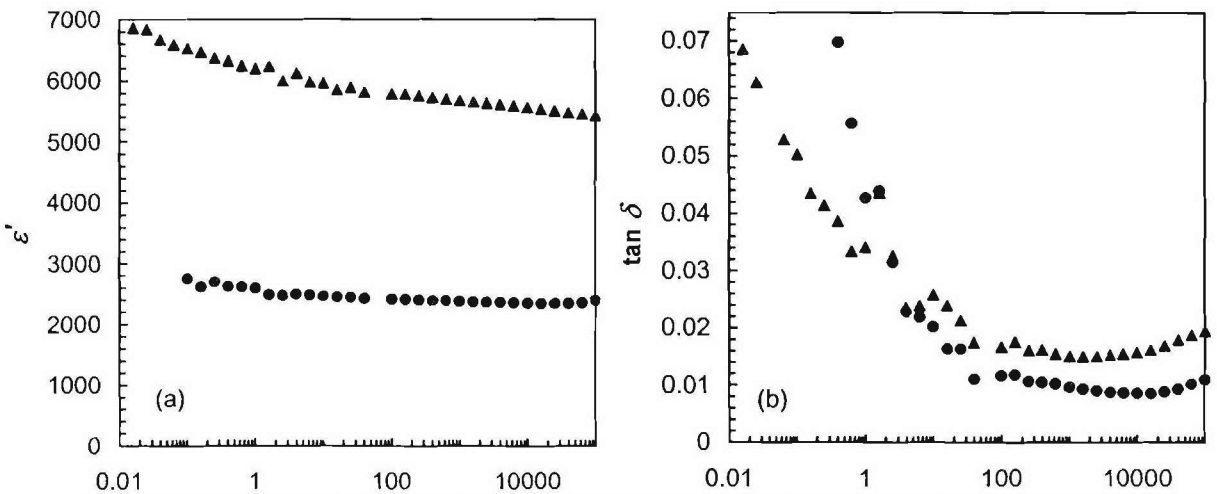

Figure 52. Frequency dependences of (a) the relative permittivity, and (b) tanδ of the (001)-oriented monoclinic PMNT crystal measured at 25 °C, before (triangles) and after (circles) poling.

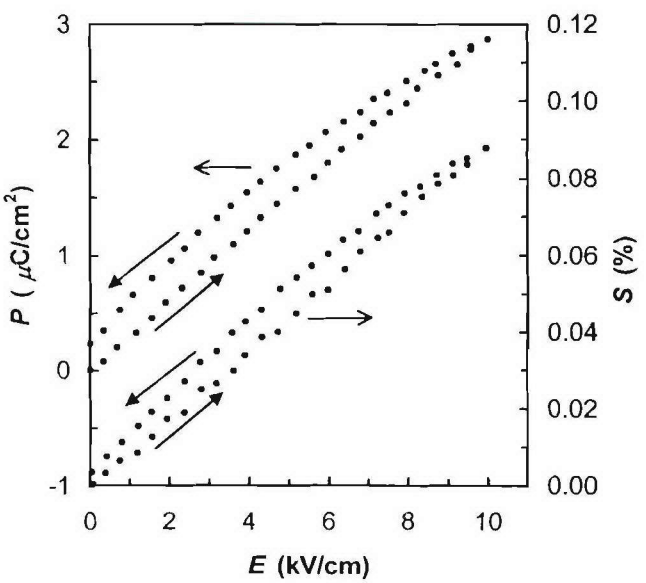

Figure 53. Polarization (upper curve) and longitudinal strain (lower curve) as a function of unipolar drive field (f = 1 Hz) measured in the (001)-oriented and poled monoclinic PMNT crystal.

(v) Electromechanical Properties of the Monoclinic PMN-PT Crystal

The electromechanical coupling of the poled crystal is measured by the IEEE resonance technique. The value of k_t is found to be 0.60, which is within the range of the values (0.54 – 0.62) reported for the PMNT crystals of MPB composition. The dependences of the polarization and the longitudinal strain S on the unipolar drive field in the poled crystal are shown in Fig. 53. Both of them are almost linear and nearly nonhysteretic. From these dependences, the piezoelectric constants, $d_{33} = S/E \approx 900$ pC/N and $g_{33} = S/P \approx 30\times 10^{-3}$ m^2/C, are found. This value of d_{33} falls into the interval of 340-2800 pC/N previously reported for different (001)- oriented PMNT crystals with the MPB composition and for different regions of the same crystal, but much smaller than the upper limit value of that interval. The same can be said regarding the relative permittivity. We find in the poled crystal the small-signal value of $\varepsilon'_{33}\approx 2500$ [see Fig. 52 (a)], while the reported values for different MPB compositions are about 3500-5500. The significantly different values of d_{33} (and ε'_{33}) measured in the crystals with the same or close nominal composition can be attributed to the presence of different phases near the MPB, i.e. the rhombohedral phase that has the highest piezoelectric constant, the monoclinic phase with a smaller constant, and probably the tetragonal phase. Shrout and co-workers [Ferroelectrics Lett. **12,** 63 (1990)] reported d_{33} values in the range of 900 – 1100 pC/N for the PMN-xPT crystals with x = 0.35, which agree well with our results. It seems that their crystal might inadvertently be composed (or mainly composed) of the monoclinic phase. In the other study of the PMNT crystals with MPB composition by Li et al. [Ferroelectrics **253,** 31 (2001)], the magnitude of the piezoelectric constant was related to the domain configuration. It was shown that the crystals with large (> 0.1 mm) domains had a higher d_{33} value (1700 – 2800 pC/N), while small laminar domains (resembling those observed in our work) had a smaller d_{33} value (340 – 1810 pC/N). It is possible that the large and small domain regions belong to the distinct rhombohedral and monoclinic phase, respectively, which would explain the difference in the d_{33} values measured.

2.3.3) Morphotropic Domain Structures, Phase Transitions and Polarization Switching

2.3.3.1) Technical Rationale and Approach

One of the most characteristic features of the relaxor-based piezocrystals (and other ferroic crystals) is the complexity of mesoscopic domain structures. By 'domains', we mean here the different crystallographic orientation states in the same crystal. They are formed as the result of loss of symmetry elements when a crystal is cooled down from high temperature (and high symmetry) phase to low (room) temperature phase. The presence of multi-domain states makes the materials electrically active as more polarization states will response (by re-orientation) to external electric field excitation, leading to high electromechanical effect. On the other hand, the piezoelectric properties of the crystals (which are anisotropic) and thereby the performance of the piezoelectric devices depend closely on domain structure. Therefore, the ability to control domain structures remains a challenge for the applications of piezocrystals in transducers, and the analysis of domain structures and establishment of the relationship between the mesocsopic domain structure and the macroscopic properties would not only provide useful information on the nature of MPB phase components, but also be of relevance to applications.

We were one of the first research groups in the area of piezoelectric crystals to become aware of, and to point out, the importance of understanding the domain structure. And we originally proposed to investigate the complex domain structures of the crystals of MPB compositions, with single or coexisting phases of rhombohedral, tetragonal and/or monoclinic symmetry.

The principle of optical crystallography and crystal symmetry species was applied to the analysis of domain structures of PMNT crystals. The complex perovskite exhibits a high temperature phase of

cubic prototype symmetry $Pm\bar{3}m$. The phase transitions from the cubic into a polar rhombohedral (or trigonal) R3m phase, and into a polar tetragonal P4mm phase, result in the (non-magnetic) ferroic species $m\bar{3}mF3m$ and $m\bar{3}mF4mm$, respectively. The loss of symmetry elements in the R3m phase gives rise to spontaneous deformations (strains) along $<111>_{cub}$. Two antiparallel spontaneous polarizations ($\pm\mathbf{P}_S$) can develop in each of the ferroelastic states, leading to eight fully ferroelectric / partially ferroelastic domains with $\mathbf{P}_S$ and the optical axes (OA) oriented along the $<111>_{cub}$ directions, as shown in Fig. 54(a). In the tetragonal 4mm phase, the spontaneous deformations appear along the equivalent $<001>_{cub}$ directions, giving rise to six fully ferroelectric / partially ferroelastic domain states with the spontaneous polarizations and the optical axes oriented parallel to $<001>_{cub}$.

When we observe the $(001)_{cub}$-platelets between crossed polarizers along the $<001>_{cub}$ direction, the cross-section of the optical indicatrix, coupled to the crystallographic axes, will exhibit extinction directions parallel to $<110>_{cub}$ for the trigonal domains (Fig. 54(b)), while the tetragonal phase will generate domains with extinctions parallel to $<100>_{cub}$. The extinction directions of different domains can be identified by the birefringence contrast created with a compensator applied in appropriate directions, and thereby the domain structures and the phase symmetry have been analyzed.

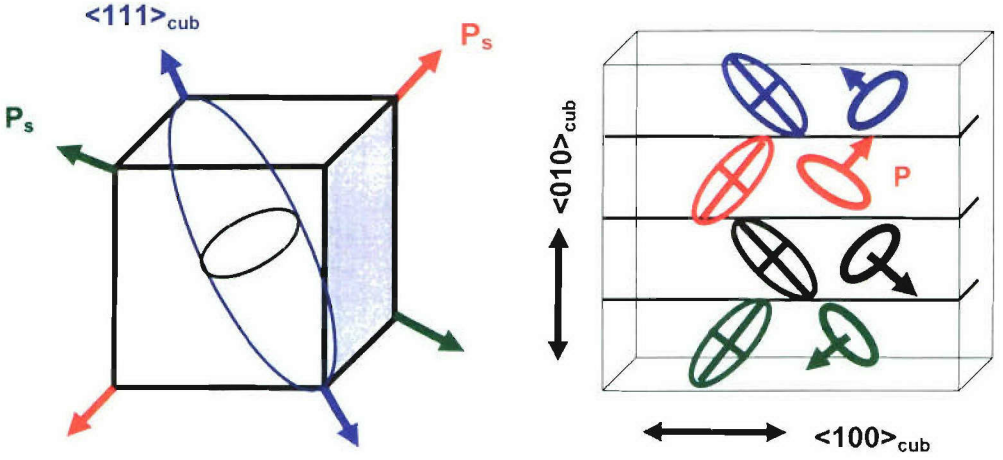

To analyze the domain structures of the monoclinic phase, we need to consider the possible domain configurations based on group/subgroup symmetry relationships. The high temperature prototype phase has $Pm\bar{3}m$ space group symmetry. The phase transition into a rhombohedral $R3m$ phase or a monoclinic m phase would normally result in eight or twenty-four (fully) ferroelectric / (partially) ferroelastic domain states (equivalent to the number of symmetry elements lost), respectively. The domain structures are therefore very complicated, especially for the monoclinic phase. However, a much-simplified situation can be produced by electric field poling ($E//[001]_{cub}$), which constrains the c-axis to lie along the pseudo-cubic [001] direction. The monoclinic domain configuration now consists of two b-domains related by a 90°-rotation around the c-axis, each of which contains two domains, as shown in Fig. 55.

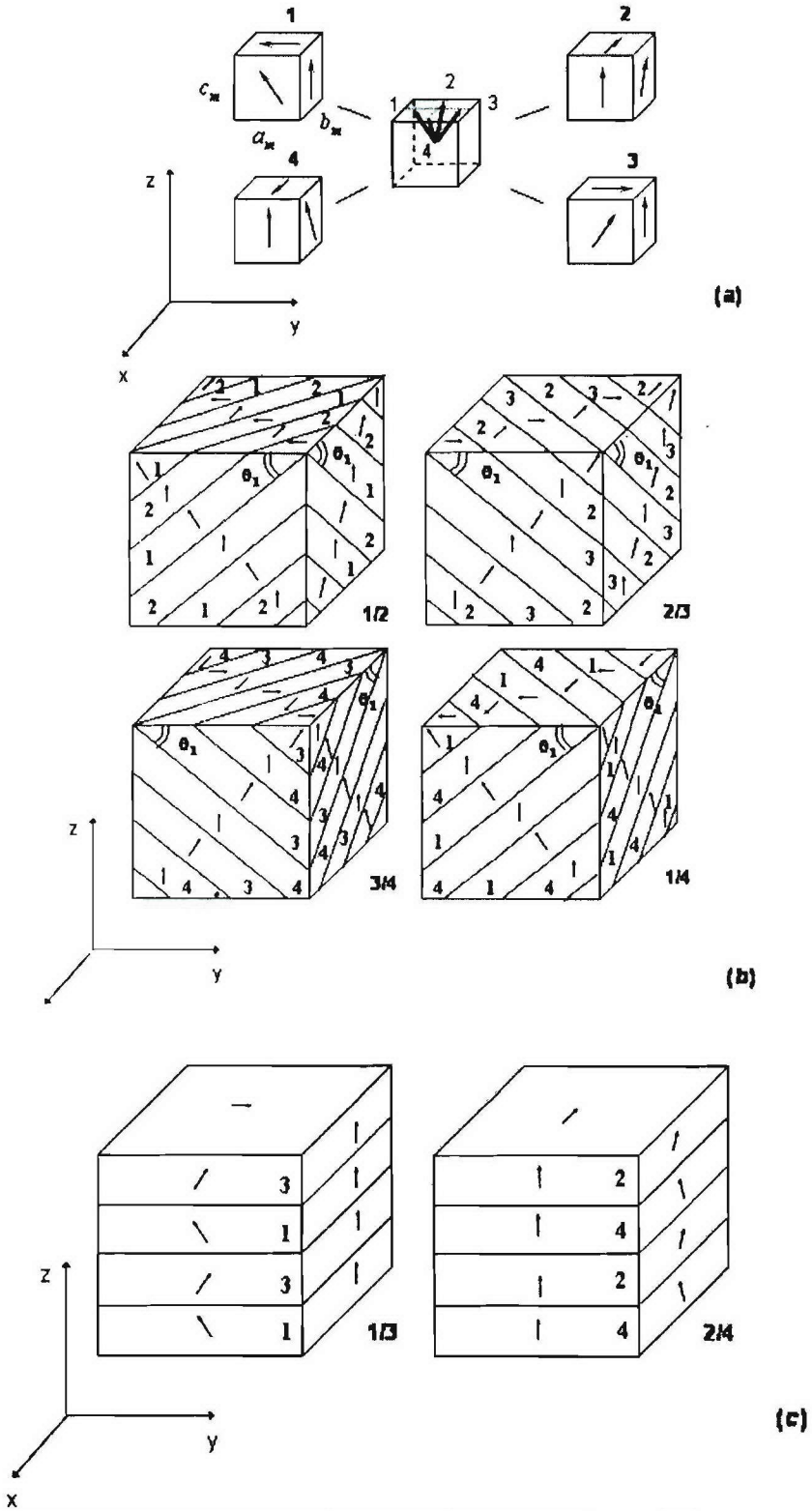

Figure 55. Possible domain structure of the PMN-PT crystals of monoclinic M_C symmetry after Poling along $[001]_c$: (a) 4 Possible polarization states and their "elementary" motifs; (b) & (c): Theoretically predicted "elementary" motifs of uncharged domain walls.

The domain structures of the PMN-xPT, PZN-xPt and PSN-xPTT single crystals of various compositions were studied by means of polarized light microscopy (Olympus BX60). A heating/cooling stage (Linkam HTMS600) was mounted on the microscope to study the domain structures and phase transitions as a function of temperature. The optical retardation and birefringence of the domains was measured using a tilting compensator (3λ) for λ=546.1 nm (e-line).

2.3.3.2) Technical Progress and Results

2.3.3.2.1) Domain Structures of (1-x)PMN – xPT Crystals (with x = 0.20 & 0.35)

The domain structures of PMNT crystals were found to depend close upon the Ti-concentration. Crystals of 0.80PMN-0.20PT [PMNT80/20] show birefringent domains at room temperature. On a $(001)_{cub}$ platelet, domains with perpendicular indicatrix sections are separated by unsharp walls (Fig. 56). The extinction directions of the domains are parallel to $<110>_{cub}$, indicating a trigonal R3m symmetry with a weak birefringence, $\Delta n=n_E'-n_O=5.3\times10^{-3}$ at 25 °C. The trigonal symmetry with observable birefringent domains suggests that a long-range ferroelectric order has been triggered by the substitution of 20% Ti^{4+} for the B-site complex ions $(Mg_{1/3}Nb_{2/3})^{4+}$. It is suggested that the introduction of Ti^{4+} into the B-site of the perovskite PMN increases the size of local polar domains by strengthening the off-center displacement, and thereby enhances the interactions between dipolar moments, leading to a macroscopic symmetry breaking of the pseudo-cubic phase. The weak birefringence and the irregular domain walls suggest that the trigonal distortion induced by 20% Ti^{4+} is relatively weak, corresponding to a primitive long-range ferroelectric phase.

Increasing the concentration of Ti^{4+} on the B-site was found to further enhance the long-range ferroelectric ordering. Single crystals with 50% Ti^{4+}, 0.50PMN-0.50PT [PMNT50/50], exhibit birefringent domains with extinctions oriented parallel to $<001>_{cub}$ directions on a $(001)_{cub}$ platelet (Fig. 56(b). This indicates that PMNT50/50 crystallizes in a tetragonal P4mm symmetry, which results from the room temperature phase of $PbTiO_3$. In addition to large single domain areas, mutually perpendicular domain bands were also observed with $(110)_{cub}$ domain walls appearing as stripes along $<110>_{cub}$ directions. Those domains correspond to the so-called *a*-domains in the tetragonal $PbTiO_3$ with polarization lying in the $(001)_{cub}$ plane of the platelet. The principal birefringence for the tetragonal phase was found to be $\Delta n = n_E - n_O = 3.5\times10^{-2}$ at room temperature, much higher than the trigonal birefringence of the PMNT80/20 crystal. Therefore a long-range tetragonal ferroelectric phase is well established in PMNT50/50 crystals with a strong anisotropy.

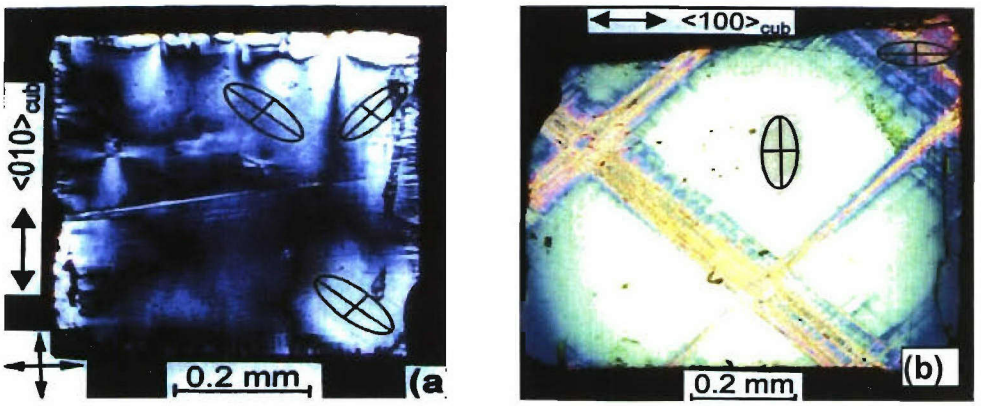

Figure 56. (a) Domain structures of a $(001)_{cub}$ PMNT80/20 platelet (58 μm thick) with weakly birefringent areas and extinction directions along $<110>_{cub}$, indicating a trigonal distortion; (b) Domain structures of a $(001)_{cub}$ PMNT50/50 (thickness = 38 μm) with strongly birefringent domains with extinction directions along $<100>_{cub}$, indicating a tetragonal P4mm symmetry (T=25 °C).

2.3.3.2.2) Morphotropic Domain Structures of the PMNT65/35 Crystals

The domain structures of morphotropic PMNT65.35 crystals were found to be very complex, as shown in Fig. 57 for a $(001)_{cub}$ platelet at 25 °C. Detailed analysis of the orientation states indicates that the crystal presents two types of domains, one with indicatrix sections having extinctions parallel to $<110>_{cub}$ directions (noted as representative Domains 1-4), another with extinctions along $<100>_{cub}$ with stripe walls parallel to $<110>_{cub}$ (noted as Domains 5 & 6). The former indicates a rhombohedral phase, while the latter corresponds to a tetragonal symmetry. Although a phase boundary separating the tetragonal from the trigonal domains can be observed at room temperature, and some areas are dominated by the presence of one domain type, these two phases are actually intimately mixed with each other in the whole crystal. Therefore, the PMNT crystals of MPB composition show the presence of both the trigonal and the tetragonal phase, incarnating the crystallographic features of both the relaxor PMN and the ferroelectric PT.

Upon heating, the tetragonal domains grow and the phase boundary propagates through the crystal in reverse. Fig. 58 shows some selected domain patterns for the sequence of the trigonal to tetragonal phase transition, which takes place in a large temperature interval from -190 °C to 90 °C. Above T_{C1}=95 °C, the whole crystal plate transforms into the tetragonal phase, which is characterized by superimposed lamellar domains with mutually perpendicular stripes oriented along $<110>_{cub}$. Upon further heating, a second phase transition of 1st order takes place from the tetragonal phase into the cubic phase, with the phase boundary crossing the crystal. The birefringence measurements confirm the phase transitions observed by domain structures.

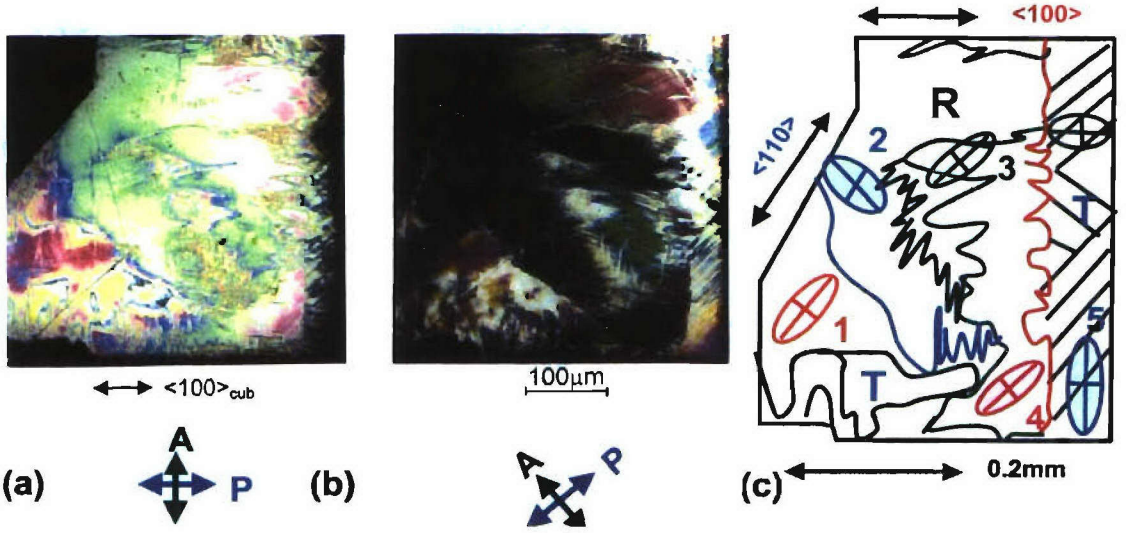

Figure 57. Morphotropic domain structures of a $(001)_{cub}$ PMNT65/35 platelet (thickness=34 μm) at 25 °C: (a) Domain pattern revealed with crossed polarizers parallel to $<100>_{cub}$; (b) Domain pattern with crossed polarizers parallel to $<110>_{cub}$; (c) Schematic presentation of the domain structures with the rhombohedral domains (R) having extinctions parallel to $<110>_{cub}$ directions (Domains 1-4 with interference color in (a)), and the tetragonal domains (T) having extinctions along $<100>_{cub}$ (Domains 5 & 6, and the areas in diagonal position in (b)).

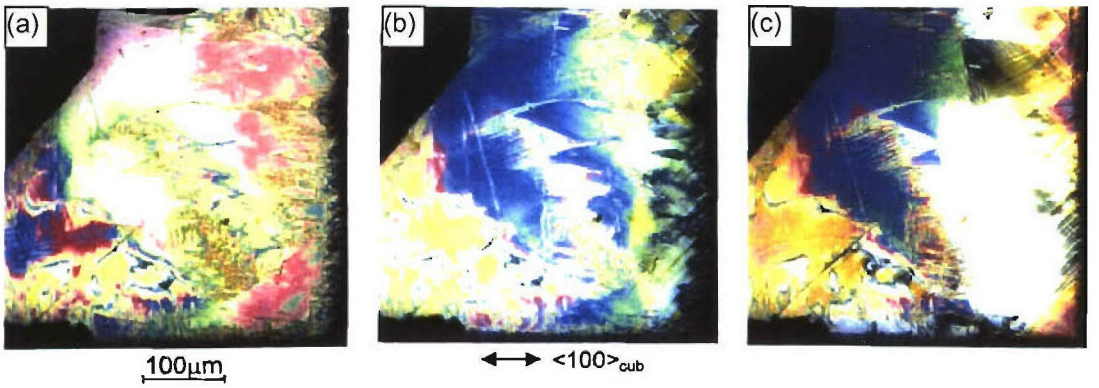

Figure 58. Sequence of the morphotropic transition from the trigonal into the tetragonal phase: (a) T= - 40 °C with a dominant trigonal phase; (b) T=65 °C with the tetragonal phase growing at the expense of the rhombohedral phase, and the R/T phase boundary moving across the crystal; (c) T=80 °C with further increase of the tetragonal areas.

2.3.3.2.3) Morphotropic Domain Structures of the PZNT91/9 Crystals

The domain structures and phase transitions of PZNT91/9 crystals were analyzed as a function of temperature. Figure 59(a) shows the domain structure of a $(001)_{cub}$ PZNT91/9 crystal at room temperature. It is composed of two distinct orientation states, one with extinction directions along $<110>_{cub}$ (R), another with extinction directions parallel to $<100>_{cub}$ (T). The former indicates a rhombohedral (or trigonal) symmetry, while the latter corresponds to a tetragonal phase. This domain structure reveals that both the rhombohedral R3m and the tetragonal P4mm phases are intimately mixed up in the morphotropic PZNT91/9 crystals. Upon heating, the trigonal phase transforms into the tetragonal phase, with an increase in the volume of the tetragonal domains at the expense of the trigonal ones [Fig. 59(b)], indicating a first-order phase transition. The rhombohedral to tetragonal phase transition takes place in a temperature interval between T_{RT} = 50 and 85°C. Above 85°C, the whole crystal is in the tetragonal phase with mutually perpendicular striped domains oriented along $<110>_{cub}$. Upon further heating, the tetragonal phase transforms into the cubic phase with emergence and growth of the isotropic area starting from T_C = 170°C.

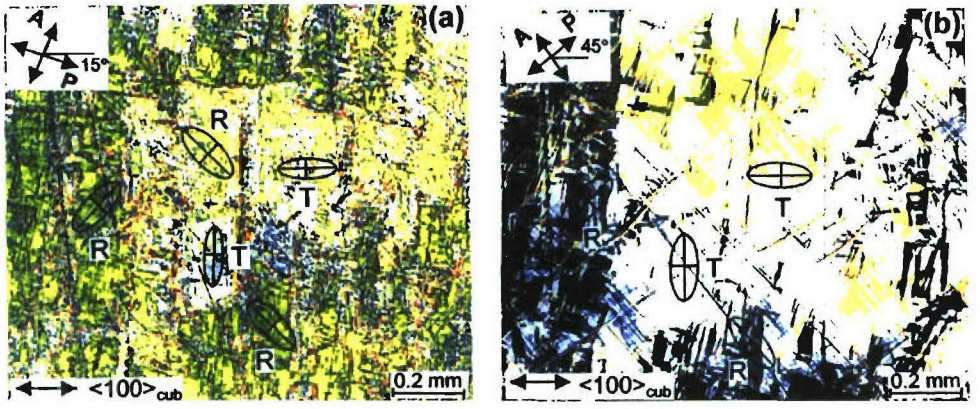

Figure 59. Domain structures and phase transition of a $(001)_{cub}$ PZNT91/9 crystal platelet (48μm thick): (a) Coexistence of the rhombohedral domains (R, with extinction // $<110>_{cub}$) and the tetragonal domains (T, with extinction // $<100>_{cub}$) at 25°C; (b) Morphotropic phase transition from the rhombohedral (in extinction) to the tetragonal phase at 70°C.

2.3.3.2.4) Domain Structure of the Monoclinic Phase in PMN-PT Crystals near MPB

The complex domain structure of the monoclinic phase in the PMN-x%PT crystals with composition near MPB (x=32%) was investigated. As predicted in Session 2.3.3.1), the domain structure of the monoclinic phase of an unpoled crystal appeared to be very complex, as shown in Fig. 60(a). After poling, the domain structure was modified with more recognizable orientations. It consists of laminar birefringent domains (width = 1-4 μm). Interestingly, the intersections of domain walls // [110] or [1-10], which is consistent with the domain patterns theoretically predicted for a monoclinic phase of *Mc* symmetry, thus confirming the phase symmetry experimentally established based on synchrotron x-ray diffraction. The domain pattern is formed by alternating opaque interdomain stripes with birefringent domains.

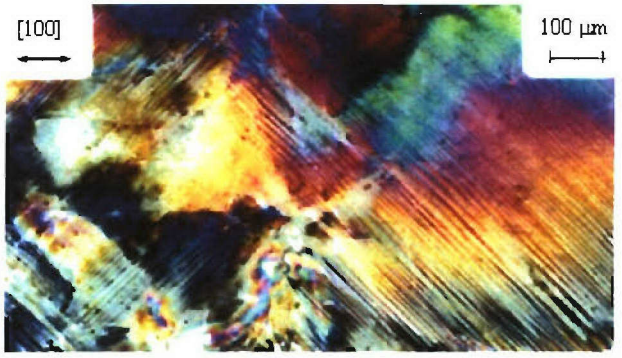

(*a*)

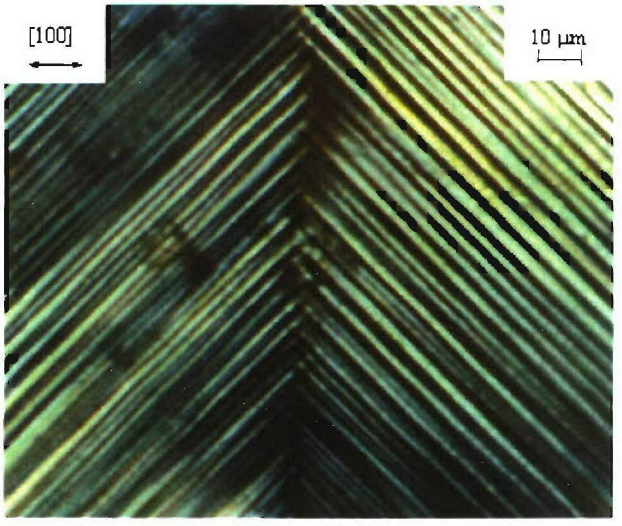

(*b*)

Figure 60. Domain structures of the monoclinic phase experimentally observed on a (001)–PMN-31%PT crystal by means of polarized light microscopy: (a) Unpoled crystal; (b) After poling along <001> direction (perpendicular to the surface of the platelet.

2.3.3.2.5) Significance of the Understanding of the Morphotropic Domain Structures

It was shown for the first time that the complex morphotropic domain structures of both PMNT65/35 and PZNT91/9 crystals are composed of the rhombohedral R3m and the tetragonal P4mm phases intimately mixed with multiple orientation states. The observation and analysis of the domain structure of the monoclinic phase in a PMN-32PT crystal has enriched our view on the complex domain structure of the MPB compositions. The sequence and temperature of the phase transitions closely depend on the types of local domains and the Ti^{4+} concentration, indicating the characteristic features of the MPB behavior of the relaxor-based piezocrystals.

In situ optical analysis of domain structures and phase transitions can be used as a non-destructive analytic tool for evaluating the local MPB composition in the PMNT and PZNT crystals. It is more sensitive than other characterization techniques, such as dielectric spectroscopy or X-ray diffraction, for studying the morphotropic phase symmetry, phase transitions and other properties, which closely depend upon the MPB composition.

The examination of the morphotropic domain structures has confirmed the assumption that the enhanced piezoelectric properties of the PMNT-PT and PZN-PT crystals result, to a large extent, from the multi-domain states with the presence of both the trigonal and the tetragonal polarizations, making the materials more electrically active. Since the piezo-/ ferroelectric properties closely depend on the crystallographic orientation states, it is important in the further studies to clarify the relationship between the domain structures and the electromechanical performance of piezocrystals.

2.3.3.2.6) Electric Field-Induced Domain Switching in PZNT91/9 Crystals

A zero field, the crystals of PZNT91/9 exhibit MPB domain features with coexistence of the rhombohedral R3m and tetragonal P4mm phases at room temperature, as shown in Fig. 61(a). It was found that application of an electric field along $<001>_{cub}$ enhanced the tetragonal domains at the expense of the R3m phase, leading to an electric field-induced phase transition and domain switching from the R3m to the P4mm phase. With increasing field strength, the tetragonal domains grow and the domain wall density decreases. A large single domain of P4mm phase was induced on a (001) platelet upon field heating at E=10 kV/cm up to $T > T_C = 170$ °C, followed by a field cooling down to room temperature, as revealed in Figure 61(b). Once induced, the P4mm single domain remains stable at room temperature after the electric field is removed. It is shown that the nucleation and growth of the tetragonal domains is triggered by the presence of the P4mm in the PZNT91/9 crystals of MPB-composition. The induced polarization indicates hysterestic effect, which can explain the origin of the hyesterestic behavior of the PZNT91/9 crystals.

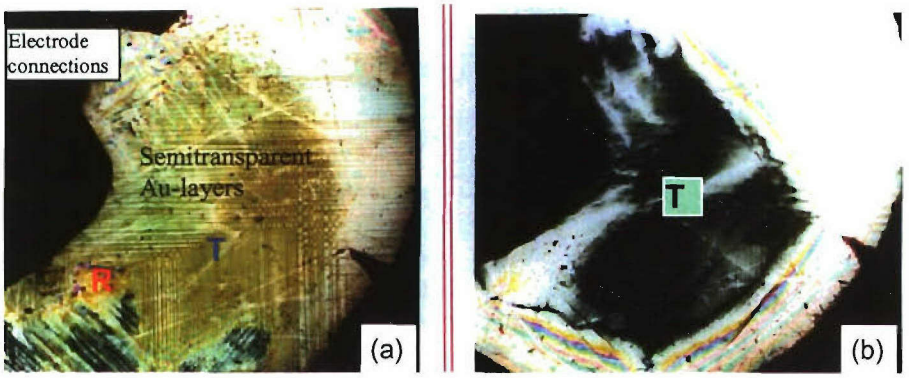

Figure 61. (a) MPB domain structure of a (001) PZNT91/9 crystal at zero electric field; (b) Electric field-induced ($//<001>_{cub}$) domain switching from R3m (R) to P4mm (T).

2.3.3.2.7) Electric Field-Induced Polarization Rotation in PZNT95.5/4.5 Crystals

To study the *intrinsic* polarization rotation induced by electric field, and to illustrate the possible mechanism of the related piezoelectric properties, it was necessary to examine the PZNT95.5/4.5 crystals of R3m symmetry. A special (110)/(001) crystal bar was shaped and polished, which allowed us to apply an electric field along <001> while observing on (110)-plate, since the R3m polarization rotation would be observable on (110). Figure 61 illustrates some selected domain patterns at various E-fields. At zero-field, the PZNT crystal shows very complex rhombohedral domains (Fig. 62(a)). Increasing field up to 4 kV/cm results in domain reorientations and significant domain wall motions (Fig. 62(b)), which is a time-dependent kinetic process (Fig. 62(c)). The density of domain wall decreases further with E increasing to 10 kV/cm (Fig. 62 (d)). At that field, some single domain areas appear with the extinction direction deriving from $<111>_{cub}$ (Fig. 62(e)). At higher field, the extinction direction of the optical indicatrix rotates with increasing E (Fig. 62(e-f)). At the same time, the domain pattern seems to remain stable until about E=35 kV/cm. At E > 35 kV/cm, some domain areas undergo major reorientations, while the induced polarization continues to rotate from $<111>_{cub}$ toward $<001>_{cub}$ (Fig. 62 (g)). When the electric field is removed, dense lamella domains reappear (Fig. 62(h)).

Since the polarization is coupled to the crystallographic axes, and thereby the optical indicatix, the rotation of the extinction directions necessary indicate a rotation of polarization from $<111>_{cub}$ toward $<001>_{cub}$, which is induced by the electric field applied along $<001>_{cub}$. A rotation angle α = 32° was observed at E=40 kV/cm, which is consistent with the thermodynamic calculations undertaken by Prof. E. Cross *et al.* The E-induced process is illustrated in Fig. 63. This work provides the first evidence of the electric field-induced polarization rotation process, which could be at the origin of the enhanced piezoelectric and electromechanical performance of the piezocrystals.

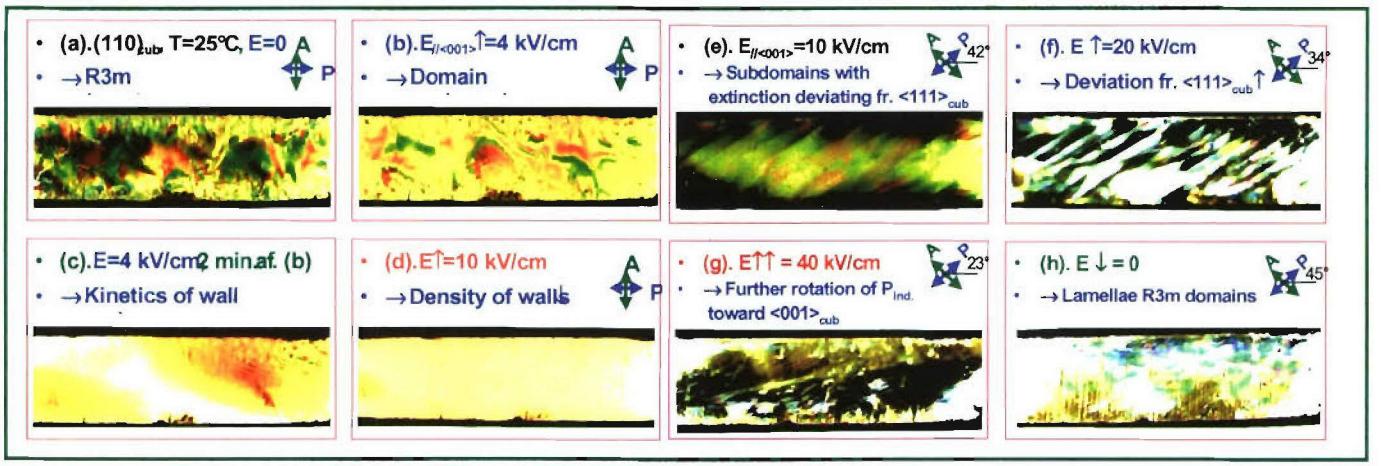

Figure 62. Electric field-induced domain switching and polarization rotation in a (110)/(001) PZNT95.5/4.5 crystal.

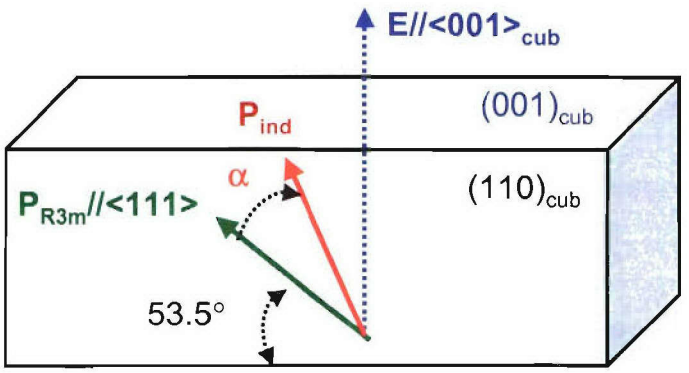

Figure 63. Schematic presentation and main features of the electric field-induced polarization rotation from <111>cub toward <001>cub, as evidenced by domain switching.

2.3.4) Understanding of the Relaxor Ferroelectricity and Related Properties

2.3.4.1) Phase Transitions in $Pb(Sc_{1/2}Nb_{1/2})O_3$ and $Pb(Zn_{1/3}Nb_{2/3})O_3$ Single Crystals

With a view to providing a better understanding of the phase transition and the transformation of polar nanoregions in the typical relaxors $Pb(Sc_{1/2}Nb_{1/2})O_3$ (PSN) and $Pb(Zn_{1/3}Nb_{2/3})O_3$ (PZN) single crystals, we have synthesized the PSN and PZN crystals by the flux method, and carried out the structural studies by means of high resolution synchrotron x-ray diffraction. We have also studied the dielectric properties of the materials with the application of electric field to reveal the effect of the electric field on the phase symmetry and phase transition.

The spontaneous phase transitions from the paraelectric to a relaxor, then to a normal ferroelectric state upon cooling have been disclosed in the disordered $Pb(Sc_{1/2}Nb_{1/2})O_3$ and single crystals, with the existence of macro domain state with a possible rhombohedral symmetry at room temperature. Figure 64 shows the domain structure of PSN crystal observed by means of polarized light microscopy.

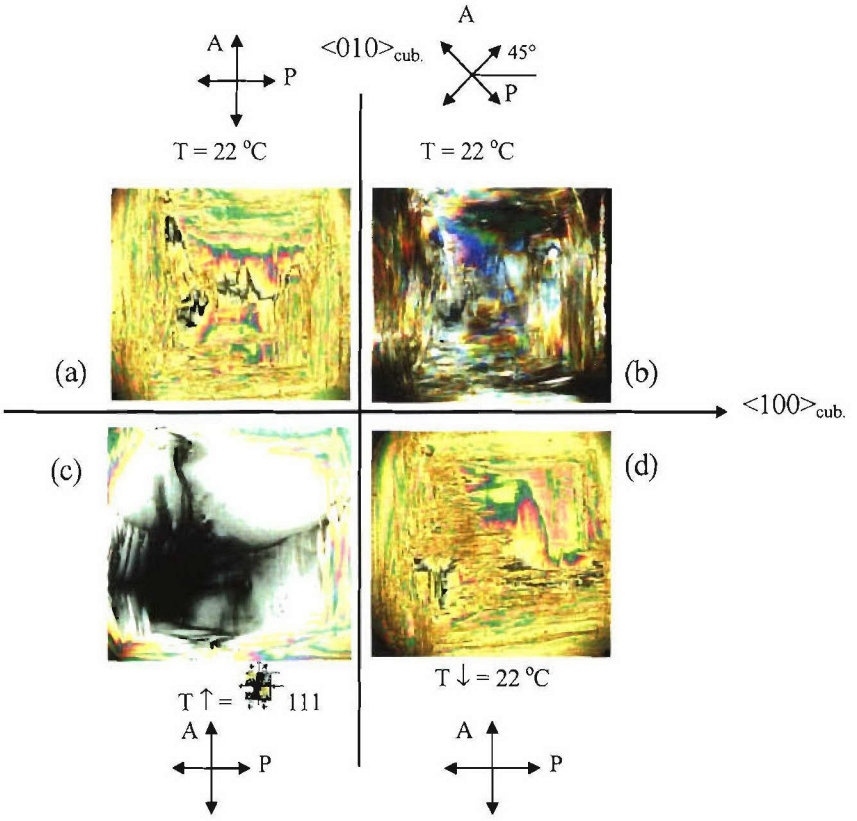

Figure 64. Domain structure and phase transition of the $(001)_{cub.}$ PSN–A single crystals under polarization light microscopy. (a) and (b): at room temperature before heating; (c) at phase transition temperature upon heating; (d) at room temperature upon cooling [1].

In comparison, the structure and the dielectric properties of $Pb(Zn_{1/3}Nb_{2/3})O_3$ (PZN) crystal have been investigated by means of high-resolution synchrotron x-ray diffraction (with an x-ray energy of 32 keV) and dielectric spectroscopy (in the frequency range of 100 Hz – 1 MHz). At high temperatures, the PZN crystal exhibits a cubic symmetry and polar nanoregions inherent to relaxor ferroelectrics are present, as evidenced by the single (222) Bragg peak and by the noticeable tails at the basis of the peak. At low temperatures, in addition to the well-known rhombohedral phase, another low-symmetry, probably ferroelectric, phase is found. The two phases coexist in the form of mesoscopic domains. The para- to

ferroelectric phase transition is diffused and observed between 325 and 390 K, where the concentration of the low-temperature phases gradually increases and the cubic phase disappears upon cooling. However, no dielectric anomalies can be detected in the temperature range of diffuse phase transition. The temperature dependence of the dielectric constant show the maximum at higher temperature (T_m = 417 – 429 K, depending on frequency) with the typical relaxor dispersion at $T < T_m$ and the frequency dependence of T_m fitted to the Vogel-Fulcher relation. Application of an electric field upon cooling from the cubic phase or poling the crystal in the ferroelectric phase gives rise to a sharp anomaly of the dielectric constant at $T \approx 390$ K and diminishes greatly the dispersion at lower temperatures [Figure 65], but the dielectric relaxation process around T_m remains qualitatively unchanged. The results are discussed in the framework of the present models of relaxors and in comparison with the prototypical relaxor ferroelectric $Pb(Mg_{1/3}Nb_{2/3})O_3$.

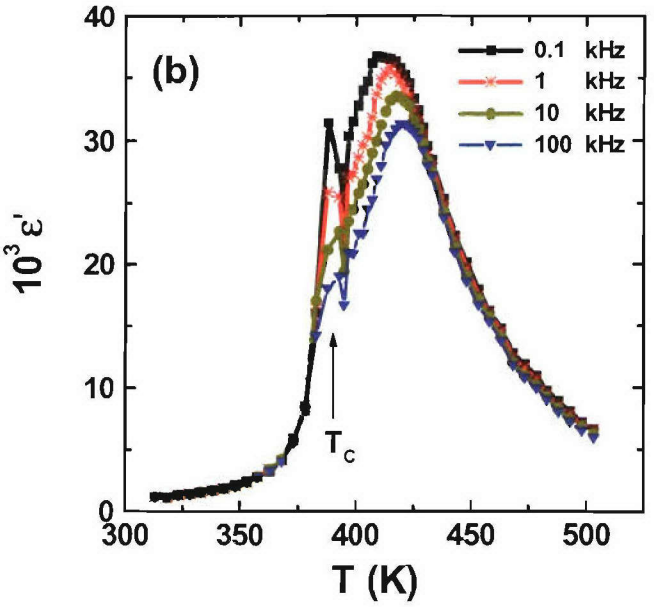

Figure 65. Variation of the real part of dielectric permittivity measured at different frequencies as a function of temperature for PZN crystal upon heating after poling at room temperature.

2.3.4.2) (Stretched Exponential) Electromechanical Relaxation in 0.65PMN – 0.35PT Crystals

The relaxation of electromechanical parameters is indicative of extrinsic response and its investigation will provide essential information. In general, relaxation patterns in disordered systems of different nature are remarkably universal. In the majority of cases they can be described in terms of one of the general forms: stretched exponential (Kohlrausch-Williams-Watts, KWW) decay function, $\exp[-(t/\tau)^{\beta}]$, or Curie–von Schweidler decay function, $(t/\tau)^{-n}$. Electromechanical relaxation is one of the areas which have not been investigated thoroughly. It was mainly studied in frequency domain and the information concerning the applicability of the above mentioned decay forms to this type of relaxation is still lacking. In this study, we have found that the relaxation pattern characteristic of electromechanical strain was determined to be of the KWW-type stretched exponential relaxation.

Under the action of a step electric field, the strain response to a step voltage was time-dependent and became apparently constant only after a certain period. Upon removal of the voltage, the residual strain was observed to decayto zero with time. The typical dependence of S on time (t) at constant voltage is shown in Fig. 66. To reduce random noise in the signal, several sequential experimental points were averaged together in this figure. A step field applied at $t = 0$ generated significant

electromechanical vibrations, which attenuated during several milliseconds. After that period, the strain was found to follow the KWW function,

$$S = S_\infty - S_{in} \exp[-(t/\tau)^\beta], \quad (1)$$

where S_∞ is the steady-state value measured in a long period after the step voltage was applied, τ is the relaxation time, S_{in} and β are the parameters. Solid line in Fig. 65 represents the fit to this equation with the least squares fitting parameters, $S_\infty = 0.0665$; $S_{in} = 0.0233$; $\tau = 9.4\ 10^{-3}$ s and $\beta = 0.123$.

If Eq. (1) is also valid down to the very beginning of time, the difference $S_{ex} = S_\infty - S_{in}$ (i.e. S at $t = 0$) gives the extrinsic (non-relaxational) part of the strain and thus S_{in} is the steady-state value of the extrinsic part. The possibility of such extrapolation to time zero is not evident, therefore the values of S_{ex} and S_{in} can only be used as an estimate of the extrinsic and intrinsic contributions. Using the typical values of parameters reported above, one can find that at 5 kV/cm not less than 20% of strain come from the extrinsic contribution.

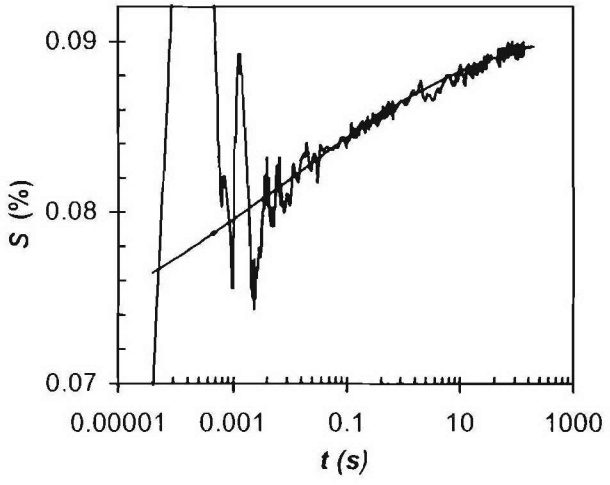

Figure 66. Strain as a function of time after an electric drive field was applied, indicating the stretched exponential relaxation.

2.3.4.3) Giant Electrostrictive Effect in 0.65PMN – 0.35PT Crystals

The field-induced strain $S(E)$ dependence was found to be linear for the fields lower than about 0.2 kV/cm, but a strong deviation from linearity was observed at higher fields (see Fig. 67 as an example). There are two possible reasons for such deviation: (i) nonlinear relation between the electric field E and the induced polarization P (which is often the case in ferroelectrics) and (ii) nonlinear coupling between strain and polarization. To ascertain which mechanism is valid, we studied the $P(E)$ dependence, which appeared linear with increasing field. Thus the nonlinear electromechanical coupling is responsible for the observed bending of $S(E)$ curve. In the whole measurement range, the $S(E)$ relation can be described as:

$$S = d_{33} E + M_{11} E^2 \quad (2)$$

with d_{33} = 400 - 1000 pC/N and M_{11} = (2-4) 10^{-15} m^2/V^2 (solid line in Fig. 67). This implies the existence of two contributions to the electromechanical coupling, i.e. (i) piezoelectric (linear) effect, which is described by the first term of Eq. (2) and the electrostrictive (quadratic) contribution (second term of Eq. (2)). The value of M_{11} is close to that observed in the best relaxor electrostrictors. It is surprisingly high in view of the fact that PMNT65/35 crystals are considered to be piezoelectric.

Therefore, the characteristic ultrahigh strain can be attributed not only to the piezoelectric effect, but also to a considerable electrostrictive contribution. The comparison of the estimate of S_{ex} with the piezoelectric contribution calculated using the first term of Eq. (2) suggests that a significant portion of electrostrictive strain must be intrinsic. The intrinsic electrostrictive effect can be related to the macro-domain structure of PMNT65/35.

In this work we examined the domain structure of the poled PMNT65/35 crystal. After unipolar strain measurements, the electrodes were removed and the crystal was observed in crossed polarizers. Two different types of large domain areas with extinction positions directed at 45° to each other were clearly observed. The first type of extinction which is parallel to $<100>_{cub}$ can be attributed to the *a*-domains of tetragonal symmetry and the second one, parallel to $<110>_{cub}$, indicates the domains of an average rhombohedral (or a possible monoclinic) symmetry. This phase inhomogeneity is believed to cause the variation of local electromechanical properties as observed in our experiments.

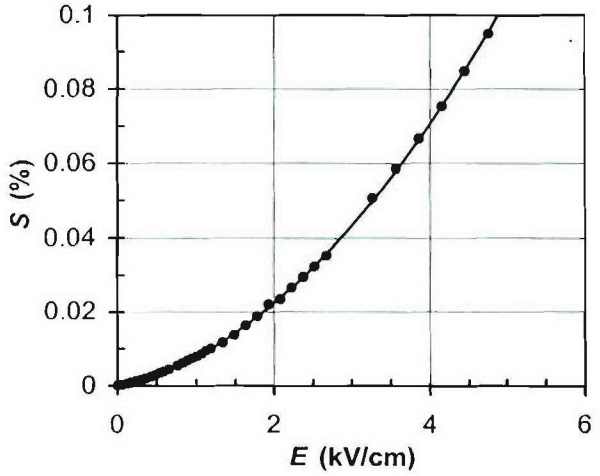

Figure 67. Stain as a function of electric field measured on a PMN-35PT crystal, showing strong non-linear relationship.

2.3.4.4) New Relaxation Process in Relaxor PMN and PMN-xPT

A complete analysis of dielectric spectroscopy was undertaken on 0.75PMN- 0.25 PT. It was found that in the temperature range of diffused $\varepsilon(T)$ peak (Fig. 68), the dielectric permittivity is determined by the contributions from two different polarization mechanisms, i.e.,

$$\varepsilon(f,T)=\chi_U(f,T) + \varepsilon_R(f,T).$$

The first part called "universal" (with susceptibility χ_U) is suggested to be the result of reversal of the nanometer size polar regions inherent in relaxor materials. The second "conventional relaxor" permittivity (ε_R) arises from the motion of boundaries of these regions. We managed to separate the overlapping dielectric responses related to these two polarization mechanisms and to study each of them individually.

Universal response is characterized by the susceptibility continuously (without any loss peak) growing with decreasing frequency according to the universal relaxation law $\chi_U \propto f^{n-1}$ with the exponent n which is close to unity at $T>T_m$. Unlike all other known (non-relaxor) materials in which the universal relaxation law was observed, the value of n in PMNT tends to become zero at $T_f< T_m$ in accordance with Vogel-Fulcher-like law (Figure 68):

$$n = n_0 \exp\left[-N/(T-T_f)\right] \qquad (3)$$

which indicates (as we have shown) freezing into the nonergodic glassy phase. Probably it is the same freezing process that was observed by other authors using different methods such as NMR and neutron scattering.

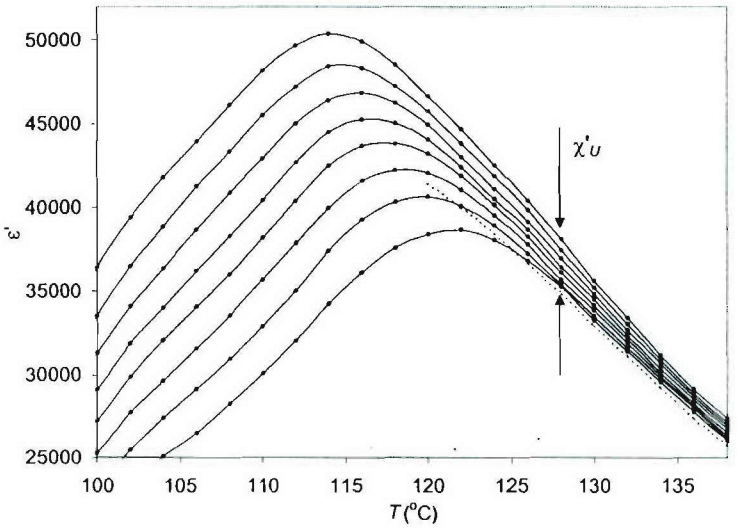

Figure 68. Temperature dependences of the real part of dielectric permittivity (ε') of 0.75PMN-0.25PT near ε'-maximum at frequencies f=100, 10, 1 kHz, 100, 10, 1, 0.1, 0.01 Hz (from upper curve). Broken line is the calculated static permittivity of the "conventional relaxor polarization", $\varepsilon_R(0)$. The susceptibility (χ'_U) associated with the "universal" polarization mechanism, which is the difference between ε' and $\varepsilon_R(0)$, is shown by arrows.

The first part called "universal" (with susceptibility χ_U) is suggested to be the result of reversal of the nanometer size polar regions inherent in relaxor materials. The second "conventional relaxor" permittivity (ε_R) arises from the motion of boundaries of these regions. We managed to separate the overlapping dielectric responses related to these two polarization mechanisms and to study each of them individually.

Universal response is characterized by the susceptibility continuously (without any loss peak) growing with decreasing frequency according to the universal relaxation law $\chi_U \propto f^{n-1}$ with the exponent n which is close to unity at $T>T_m$. Unlike all other known (non-relaxor) materials in which the universal relaxation law was observed, the value of n in PMNT tends to become zero at $T_f< T_m$ in accordance with Vogel-Fulcher-like law (Figure 69):

$$n = n_0 \exp\left[-N/(T - T_f)\right] \qquad (4)$$

which indicates (as we have shown) freezing into the nonergodic glassy phase. Probably it is the same freezing process that was observed by other authors using different methods such as NMR and neutron scattering.

It is shown that Vogel-Fulcher frequency shift of the temperature of T_m is related predominantly to the conventional relaxor dispersion at high frequencies ($f > f_c \approx 100$ Hz) while at low frequencies it is due to the universal dispersion solely. At $f < f_c$ the $\varepsilon'(f,T)$ data set for temperatures around and above T_m can be scaled using scaling parameters related to frequency by the fractional power relation. For $f > f_c$ this scaling holds only for temperatures above T_m.

Analyzing the data on PMNT and some other materials we found that at the diffuse phase transition in relaxor ferroelectrics, the dielectric permittivity ε obeys the relation

$$\varepsilon_A/\varepsilon = 1+0.5(T-T_A)^2/\delta_A^2$$

in a wide temperature range above the temperature of permittivity maximum T_m ($T_m>T_A$). The parameter δ_A remains invariant with the variation of measurement frequency and characterizes the

diffuseness of the transition. This finding draws the conclusion to years of discussion concerning phenomenological description of dielectric permittivity peak in relaxor ferroelectrics

The new critical behavior of the dielectric response discovered in 0.75PMN-0.25PT will help us understand the microstructural mechanisms of the enhanced electro-mechanical properties of relaxor-based piezocrystals.

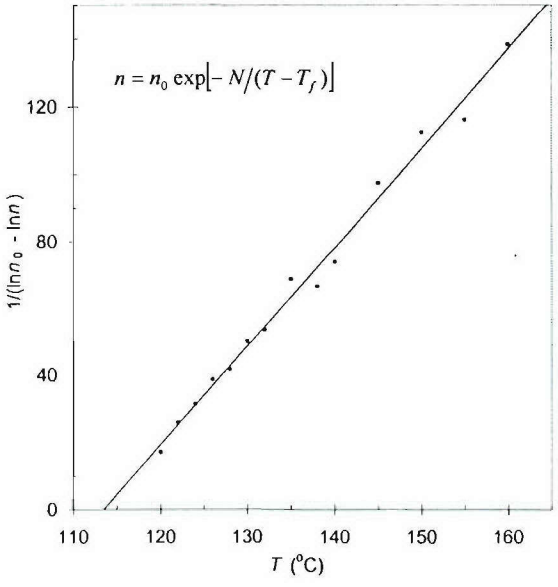

Figure 69. Temperature dependence of the universal relaxation exponent n in 0.75PMN-0.25PT. Solid line represents the least-squares fitting to equation (1).

2.3.4.5) Electric Field-Induced Redistribution of Polar Nano-Regions in a Relaxor

The competition and coexistence of local short-range and long-range polar order underlie the behaviour of relaxor ferroelectrics, materials of considerable technological importance. The conventional picture is that the polar nano-regions (PNR) that appear at high temperature form nuclei for the field-induced long-range order at low temperature.

In this work, we performed high-energy-x-ray diffuse scattering measurements on the relaxor $Pb(Zn_{1/3}Nb_{2/3})O_3$ (PZN) to study the short-range polar order under an electric field applied along the [111] direction. The sample being studied is a triangular plate of single crystal PZN with dimensions of $3 \times 3 \times 1$ mm^3, grown from high temperature solution. Top and bottom surfaces of the platelet are pseudocubic {111} planes, and covered with gold electrodes. Previous study has shown that the bulk of the crystal can be "poled" into a rhombohedral phase with applying a electric field along the [111] direction at room temperature. The crystal has been annealed (or "depoled") by heating to 800 K and cooling in zero field. The x-ray diffraction measurements were performed at beamline X17B1 of the National Synchrotron Light Source (NSLS), in collaboration with Dr. G. Xu.

It is known that diffuse scattering is very sensitive to local inhomogeneities and is among the few techniques that can be used to directly probe these local structures. PZN is one of the most extensively studied relaxor systems, with a maximum of the dielectric permittivity T_m around 410 K. Upon cooling, PZN undergoes a diffusive phase transition with a Curie temperature T_C slightly below T_m. The low temperature phase has ⟨111⟩ type polarizations, and a rhombohedral phase is easily stabilized with electric field poling along the [111] direction. The diffuse scattering in zero field has been recently mapped out to consist of six diffuse intensity rods.

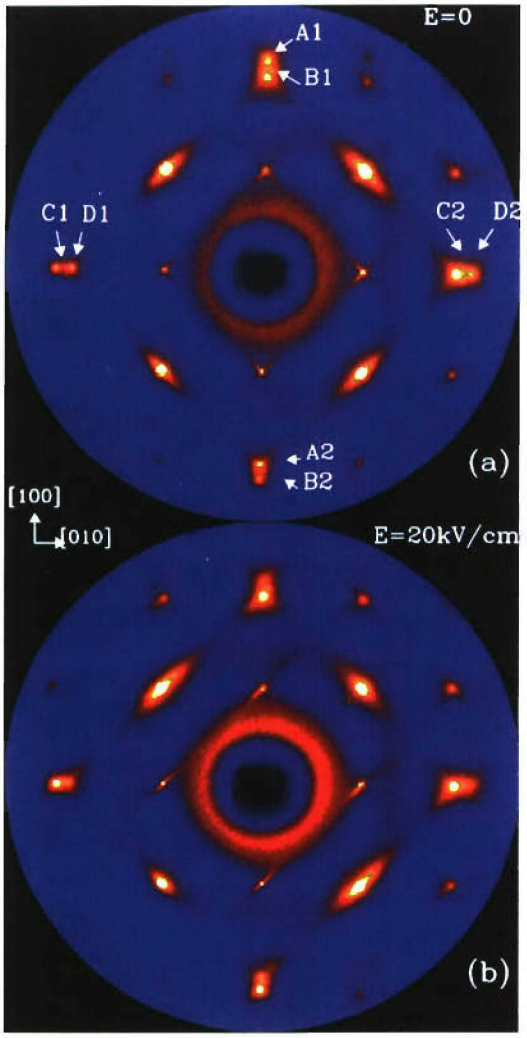

Figure 70. X-ray diffraction images from PZN taken by the CCD detector at room temperature (T = 300 K). (a) E=0, and (b) E=20 kV/cm along [111]. The incident x-ray beam is along the [001] direction.

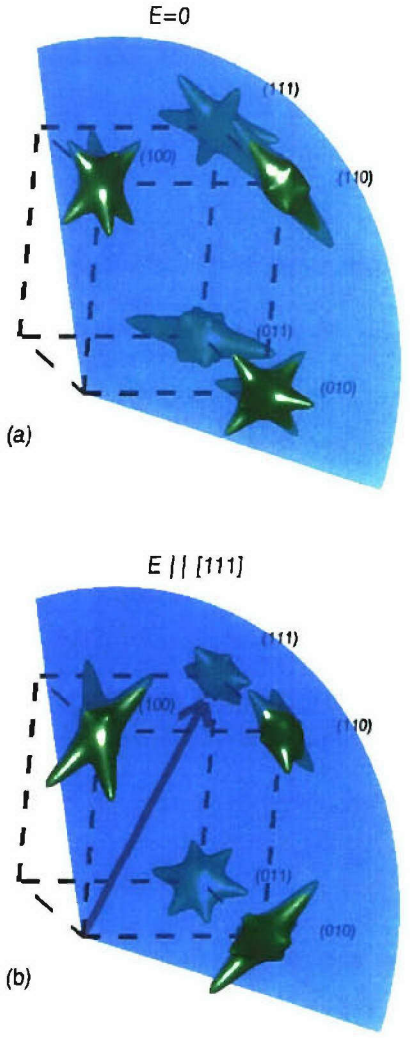

Figure 71. Sketch of the three-dimensional diffuse scattering distribution from PZN. They are plotted in the 3-D reciprocal space around (100), (110), (111), (010), and (011) reciprocal lattice points for (a) E=0, and (b) E along [111]. In (b) the diffuse rods along the [110], [101], and [011] directions are enhanced, while the diffuse rods along the $[1\bar{1}0]$, $[10\bar{1}]$, and $[01\bar{1}]$ are suppressed. The blue semi-transparent surfaces denote a portion of the Ewald sphere of scattering.

Figure 70 shows the X-ray diffraction images from PZN taken by the CCD detector at room temperature (T = 300 K). (a) E=0, and (b) E=20 kV/cm along [111]. The incident x-ray beam is along the [001] direction. Contrary to conventional expectations, the overall diffuse scattering intensity is not suppressed, even in a field as high as 40 kV/cm. On the other hand, the field induces a dramatic change on the shape of the three-dimensional diffuse scattering intensity pattern in reciprocal space, corresponding to a redistribution of PNR in real space, as shown in Fig. 71.

Figure 72 shows the hysteresis curve of diffuse scattering intensities vs. field. They are measured at different points (a) A1+A2 vs. B1+B2, (b) C1+C2 vs. D1+D2 (see Fig. 70), when changing the field strength. The data on the red curve were taken while increasing the field along [111] direction. The data on the blue curve were taken while decreasing the field and then reversing the polarity and continuing on increasing the field along the $[\bar{1}\,\bar{1}\,\bar{1}]$ direction.

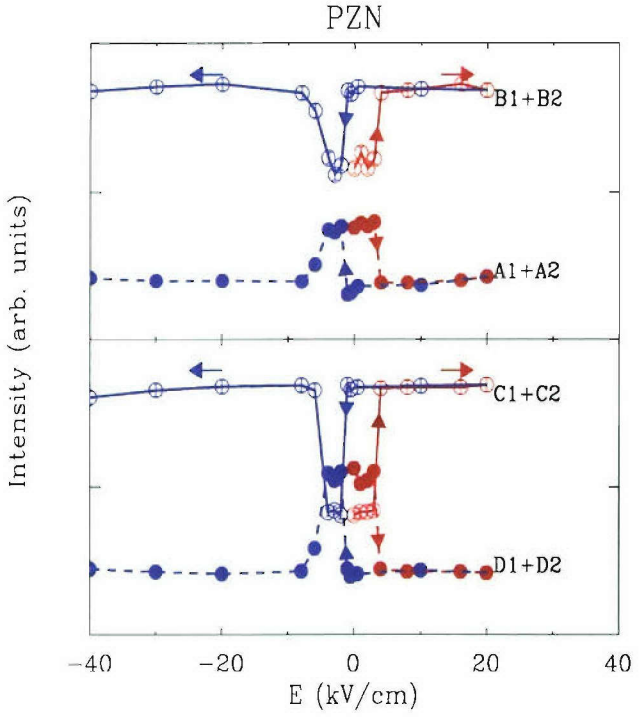

Figure 72. Hysteresis curve of diffuse scattering intensities vs. field.

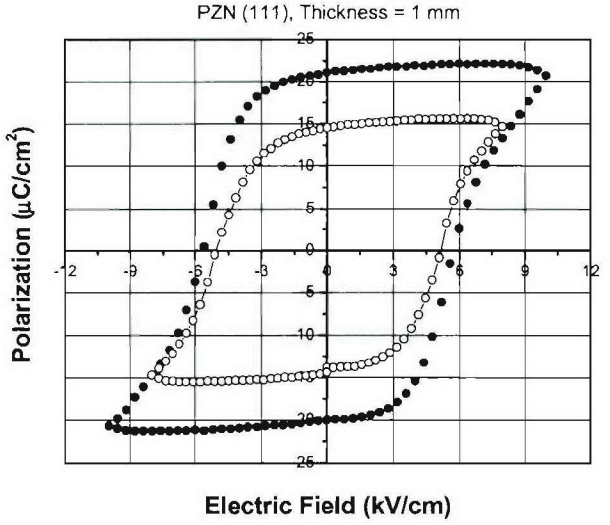

Figure 73. Polarization – electric field hysteresis from the PZN (111) single crystal platelet. The data were measured under different maximum drive field strengths of ±8 (open circles) and ±10 kV/cm (solid circles). The coercive field for the polarization switching is about ±5 kV/cm in both cases.

Figure 73 shows the polarization – electric field hysteresis from the PZN (111) single crystal platelet, confirming the induced macroscopic ferroelectric state in the crystal. The data were measured under different maximum drive field strengths of ±8 (open circles) and ±10 kV/cm (solid circles). The coercive field for the polarization switching is about ±5 kV/cm in both cases.

Our results, on one hand, suggest that the PNR in PZN are really robust entities that cannot be easily affected with an external [111] field. We have applied a field up to 40 kV/cm along the [111] direction, and no additional change or any overall suppression of diffuse scattering has been observed. Poling the sample directly in the low temperature phase does not result in a cross-over from relaxor behavior into a normal ferroelectric phase in PZN. On the other hand, by creating a single domain or almost single domain state with the [111] electric field, we have been able to probe directly how the PNR reside in the ferroelectric phase in PZN. Our findings show that the PNR prefer to have polarizations orthogonal to that of the lattice environment they reside in, which may be a key factor that prevents them from dissolving into the ferroelectric phase. This is an extremely interesting and rare situation where a stable short-range (polar) order persists in a long-range ferroelectric order with the polarizations of the two orders being perpendicular to each other; and this situation may be general in all perovskite relaxor systems.

This work has been published in *Nature Materials*.

2.3.4.6) New Insight into Dipolar Dynamics in Relaxors

Relaxor ferroelectrics form a class of disordered nanopolar crystals with an extremely high dielectric permittivity peak which shifts to higher temperatures with increasing frequency, following the characteristic Vogel-Fulcher law. Research on relaxors and related materials has undergone an accelerated growth in the last few years. This is to a large extent motivated by the excellent piezoelectric properties discovered in the relaxor-based single crystals which outperform the conventional electroceramics, pointing to promising applications in the next generation of the electromechanical transducers. On the other hand, the complex local structure and intriguing physics of relaxors remain a fascinating puzzle.

In order in understand the mechanism of the fascinating relaxor behavior and its role in high piezoelectricity, we have studied the complex dielectric permittivity of the crystals and ceramics of PMN–PT with $x = 0 - 0.35$ in wide frequency ($10^{-4} - 10^{5}$ Hz) and temperature (110- 460 K) ranges, and found that the temperature evolution of the dipole dynamics related to both the universal and conventional relaxations is very different in the canonical relaxors (i.e. compositions with small x) and in the solid solutions with large x in which a spontaneous transition into the ferroelectric phase takes place. Figure 74 gives the temperature dependences of the real part of dielectric permittivity at various frequencies for (a) PMN and (b) PMN-31%PT crystals.

In the classical relaxor $Pb(Mg_{1/3}Nb_{2/3})O_3$ [PMN] crystal, it is found that, in a wide frequency range of 10^{-4}—10^{5} Hz, the dielectric relaxation consists of two processes: the conventional relaxation (CR) obeying the Kohlrausch-Williams-Watts law, $\exp[-(t/\tau)^{\beta}]$ and the "universal" relaxation (UR) obeying the Curie–von Schweidler law, t^{-n}, respectively. Figure 75 shows the frequency dependences of the (a) real and (b) imaginary part of permittivity in PMN crystal at selected temperatures. Experimental data are shown by dots and solid lines represent fitting to the CR and UR relaxations. The UR and CR components used for fitting at 269 K are shown by dashed lines.

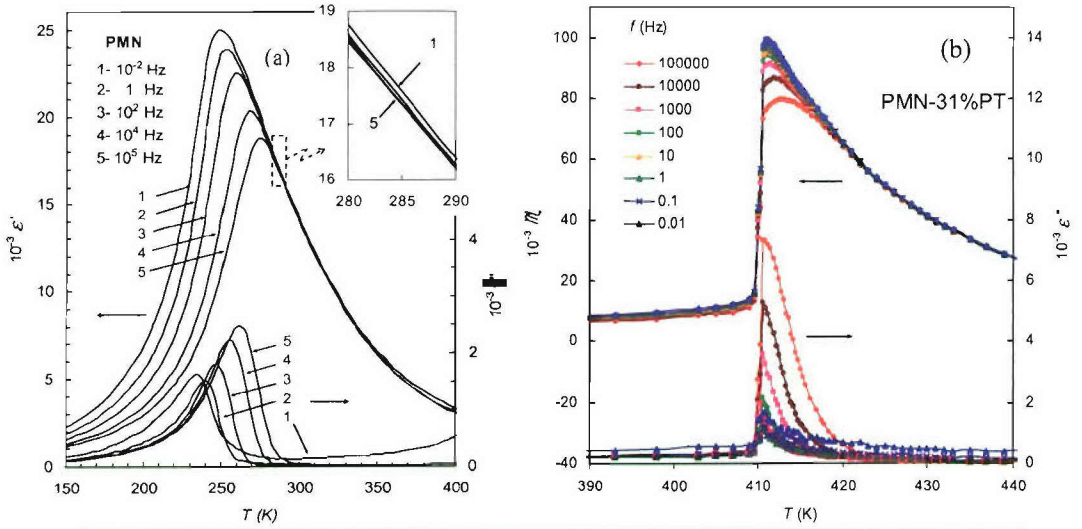

Figure 74. Temperature dependences of the real part of dielectric permittivity at various frequencies for (a) PMN and (b) PMN-31%PT crystals.

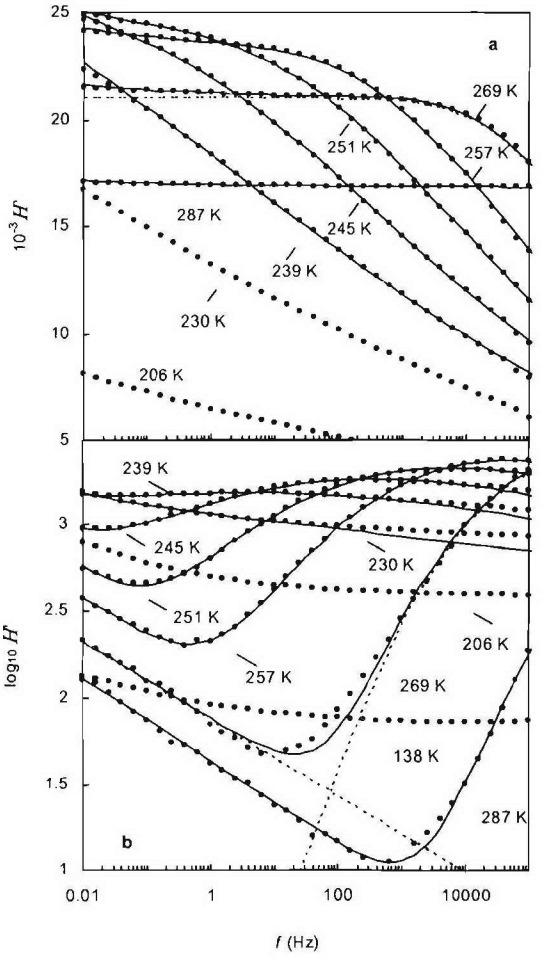

Figure 75. Frequency dependences of the (a) real and (b) imaginary part of permittivity of PMN at selected temperatures.

The slowing-down of dipole dynamics upon cooling into nonergodic relaxor phase has revealed a new phenomenon that is not present in other known systems undergoing ergodic-nonergodic transitions: the two overlapping relaxation processes tend to freeze out at the same temperature T_f (= 213 K). The freezing of the KWW and the CS relaxations is evidenced by the Vogel-Fulcher (VF) temperature dependences of the characteristic relaxation time τ and the exponent n, as shown in Fig. 76. It is accompanied by the widening of the KWW relaxation spectrum so that the parameter β describing the width tends to zero at T_f following the VF-like law (this behaviour also has not been reported previously). We suggest that both the KWW and CS contributions are associated with the PNRs, the number of which is known to vary considerably with temperature. The KWW relaxation can be due to the flipping of the PNR dipole moments between the allowed <111> directions. The CS dispersion is believed to originate from the reorientation of the specific moments of individual unit cells inside PNRs. Such kind of double freezing is not known in other systems undergoing ergodic-nonergodic transitions (e.g. in spin, dipole or structural glasses) where only one relaxation process is typically becomes frozen.

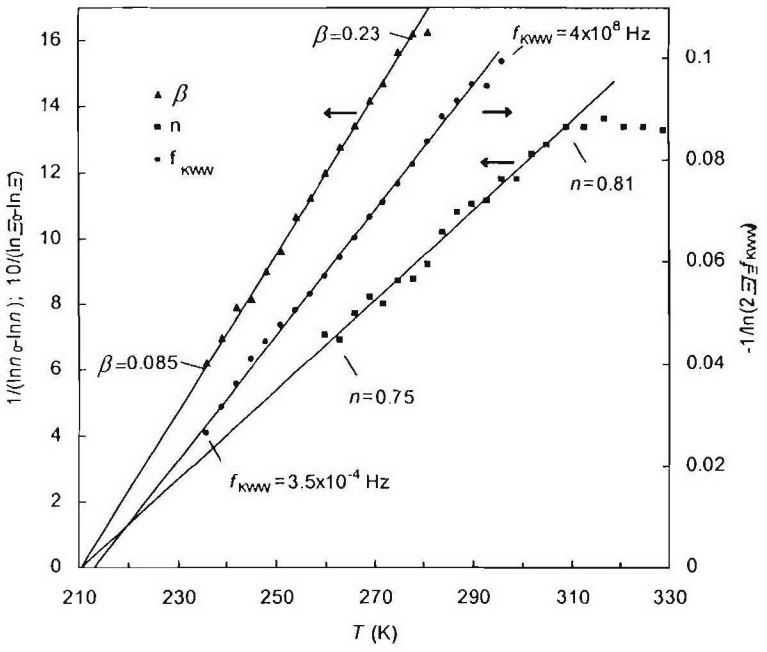

Figure 76. Temperature dependences of the CS exponent n and the KWW relaxation parameters β and $f_{KWW}=(2\pi\tau)^{-1}$. Solid lines are the fits to the respective relaxation process.

As the PT content increases to 31%, the Vogel-Fulcher freezing of both CS and KWW relaxations disappears, and the CS susceptibility undergoes a quadratic divergence associated with the long-range order ferroelectric phase transition. The PMN-25%PT crystal exhibits an intermediate situation: the Vogel-Fulcher type freezing of the CS relaxation is still present, while its susceptibility undergoes a quadratic divergence. Such a phenomenon of crossover from the double freezing in PMN to the quadratic divergence in PMN-31%PT is shown in Table 7.

Table 7. Comparison of Different Polar Dynamics in PMN - xPT

	(1-x)PMN-xPT	*x*=0	*x*=0.25	*x*=0.31
KWW relaxation	Scaling of susceptibility as a function of *T* *Fig. 3*	Lorenz	Lorenz	Lorenz
	Vogel-Fulcher-type freezing *Fig. 5*	Yes	No	No
	Vogel-Fulcher-type widening of spectrum *Fig. 7*	Yes	No	No
CS relaxation	Scaling of susceptibility as a function of *T* *Fig. 4*	Lorenz	Quadratic divergence	Quadratic divergence
	Vogel-Fulcher type freezing *Fig. 6*	Yes	Yes	No

2.3.4.7) Effects of Pressure & Biasing Electric Field on the Ferroelectric and Relaxor Properties of $Pb(Sc_{1/2}Nb_{1/2})O_3$ Crystal

While PMN is the prototypical classic relaxor that retains its high-T cubic phase down to the lowest temperatures, $Pb(Sc_{1/2}Nb_{1/2})O_3$ (PSN) and the isomorphous compound $Pb(Sc_{1/2}Ta_{1/2})O_3$ (or PST) exhibit more complex behavior that derives from the ability to control their degree of B site chemical order. Earlier work showed that pressure induces a FE-to-R crossover making the relaxor state the ground state of mixed, compositionally disordered perovskites at high pressure (or reduced volume). This background and the availability of a single crystal of PSN of suitable dimensions suggested that a high pressure study of this material could be fruitful. This work was undertaken in collaboration with Dr. G. Samara at Sandia National Laboratories (NM).

Single crystals of $Pb(Sc_{1/2}Nb_{1/2})O_3$ were grown by a high-temperature solution method using the mixture of PbO (80 mol.%) and B_2O_3 (20 mol.%). The crystals were formed upon slow cooling from 1180 °C to 1100 °C. The as-grown crystals exhibited cubic morphology. X-ray powder diffraction patterns of crashed crystals showed no superlattice peaks, indicating a disordered structure. The sample used in this study was a pseudocubic (001)-oriented platelet (with a thickness of 0.025 cm and an area of 0.034 cm^2) which was mirror polished with diamond pastes down to 3 μm. The (001) faces were vapor deposited with Cr followed by Au thin films for electrical contacts. The crystal was studied by dielectric spectroscopy as function of temperature (300-600 K), frequency (10^2-10^6 Hz), pressure (0-15 kbar) and electric field (0-5 kV/cm). The results provided a detailed view of the dielectric response and phase behavior. Two pressure apparatus were used. One is capable of pressure of up to ~10 kbar and temperature up to 450 K using He as the pressure transmitting medium. The other is capable of pressures >20 kbar and temperature from 300-700 K using a mixture of normal-and-iso-pentanes as the pressure transmitting medium.

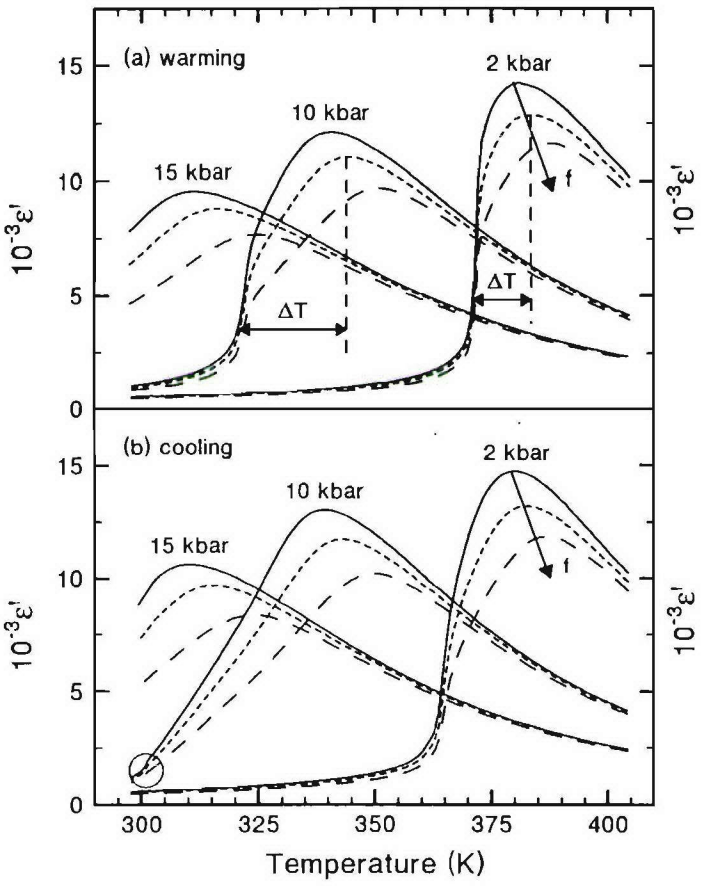

Figure 77. Heating and cooling isobars of ε′(T) revealing the influence of hydrostatic pressure on the dielectric response and phase behavior of PSN.

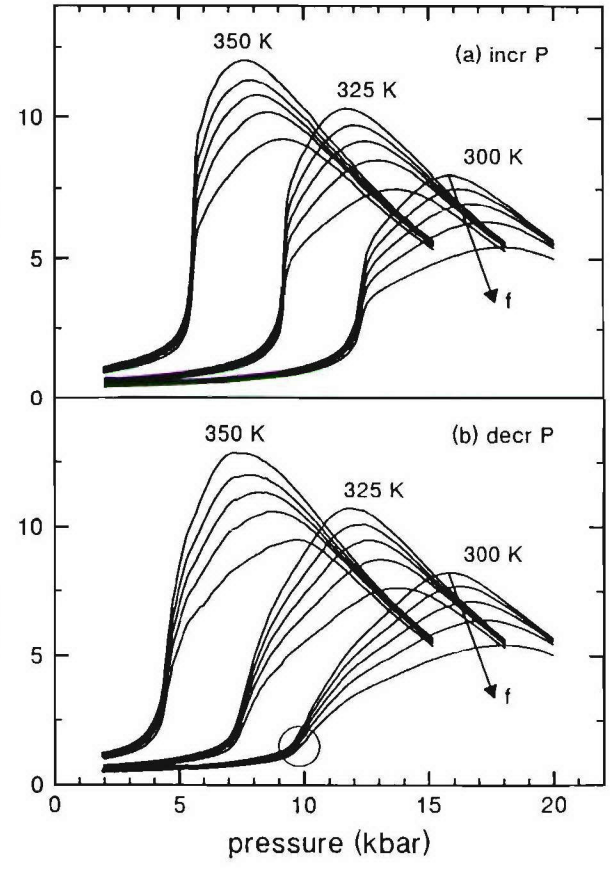

Figure 78. Isotherms of ε′ vs. pressure showing the influence on pressure on the dielectric response and phase behavior of PSN.

Figure 77 shows the heating and cooling isobars of ε′(T) revealing the influence of hydrostatic pressure on the dielectric response and phase behavior of PSN: as the pressure increases, the first-order phase transition becomes more diffuse and the relaxational dielectric maxima shifts to lower temperature. Figure 78 indicates the isotherms of ε′ vs. pressure showing the influence on pressure on the dielectric response and phase behavior of PSN.

Based on these results, a Temperature-Pressure phase diagram for the PSN crystal has been established, as shown in Fig. 79. An unusual feature is the expected termination of the $T_c(P)$ phase boundaries (for both increasing and decreasing T and P) at specific temperatures and pressures as denoted by the stars. The dashed curve defines a path for going from the FE to the R state continuously without crossing a phase boundary.

This work has been accepted for publication in *Phys. Rev. B.* (in press).

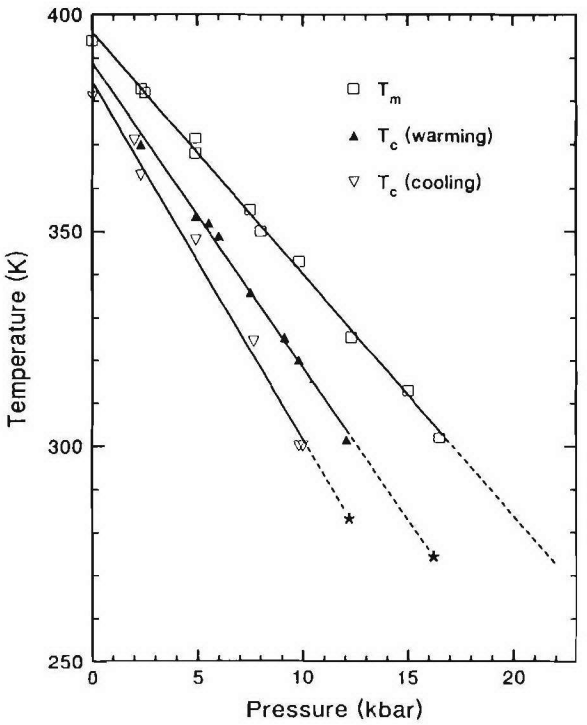

Figure 79. Temperature – pressure phase diagram for disordered PSN crystal.

3) Summary of Technical Contributions

Through the implementation of this research program funded by the ONR, we have made significant progress in the design, synthesis and characterization of innovative piezo- and ferroelectric materials, especially in the form of single crystals, with a view to developing new materials resources for the next generation of electromechanical transducers in a wide range of Navy and civilian applications. In particular, our contributions have covered the following main areas:

(a) Thermodynamic Analysis and Phase Diagrams

We have systematically studied the thermodynamic behavior of the PZN–PT & PbO, and PMN–PT & PbO systems, and established the relevant phase diagrams which provide information on the solubility and saturation rate, crucial for the growth of large and high quality piezocrystals. We have also determined the phase segregation rate for the solid solution system, PMN – PT, which is important for achieving composition homogeneity of single crystals. Based on the useful thermodynamic information we have obtained, huge progress has recently been achieved by industrial crystal growers, making the PMN-PT and PZN-PT crystals viable piezocrystal resources.

(b) Design, Synthesis and Growth of PiezoCrystals

We have developed various techniques, for the growth of relaxor single crystals: high temperature flux growth, top-cooled solution growth, top-seeded solution growth and a modified Bridgman growth, and have been successful in growing PMN-PT and PZN-PT single crystals of high quality, which have not only been used in academic research, but also in Navy and industrial device testing. More

importantly, we have made significant progress in developing several new piezo-material systems, including PSN-PT, PSn-PT, PYN-PT-PZ, BFe-PT and PZT, and successfully grown the single crystals of PSN-PT, PSn-PT and PZT of medium size and good quality. These material systems are demonstrated to exhibit good piezoelectric performance with T_C, and especially Trt, higher than the PMN-PT and PZN-PT crystals, thus they are very interesting as potential high T_C and high performance piezocrystal resources. More effort is being investigated in further investigation of these and other new materials systems.

(c) Morphotropic Phase Boundary, Domain Structures and Phase Transitions

Particular effort has been made to investigate the complex structures and phase components of the PMN-PT, PZN-PT and PSN-PT solid solution systems of MPB compositions, by means of synchrotron X-ray diffraction and neutron and Raman scattering. We have established the MPB phase diagrams of these important systems, and discovered the presence of low-symmetry (monoclinic or orthorhombic) intermediate phases in the MPB region. By polarized light microscopy, we have investigated the mesoscopic domain structures and phase components of the PMN-PT, PZN-PT and PSN-PT crystals, and showed the coexistence of the rhombohedral *R3m* and the tetragonal *P4mm* phases near the MPB. We have further identified and analyzed the domain structure and crystallographic features of the monoclinic phase in the PMN-PT crystals. We have also demonstrated the rotation of the rhombohedral polarization from $<111>_{cub}$ to $[001]_{cub}$, induced by application of an electric field, providing a piece of evidence for the intrinsic mechanism of the high strain behavior in these materials. The information obtained on the MPB phase diagram, domain structures and phase transitions provides not only a better understanding of the microscopic mechanisms underlying the extraordinary piezo- and ferroelectric properties, but also a useful guidance for designing new materials with higher performance.

(d) Complex Structures, Dynamics and Relaxation in Relaxor Ferroelectrics

From a more fundamental viewpoint, we have studied a broad spectrum of materials properties, including dielectric, piezoelectric, ferroelectric, and so on. Particular effort has been made to investigate the puzzling structure, dynamics and relaxation of polar nanoregions in relaxors and related materials, which constitute the basis of the PMN-PT, PZN-PT and PSN-PT piezocrystal systems. By means of broad band dielectric spectroscopy, especially down to very low frequency end (10^{-4} Hz), we have found that the complex permittivity is determined by the contributions from two different polarization mechanisms, the 'universal' relaxation which results from the reversal of nano-polar regions (PNRs) inherent in relaxor materials, and the 'conventional relaxation' arising from the motion of boundaries of these regions. Further analysis has allowed us to discover a new phenomenon: the two overlapping relaxation processes tend to freeze out at the same temperature T_f (= 213 K). Such kind of double freezing is not known in other systems undergoing ergodic-nonergodic transitions (e.g. in spin, dipole or structural glasses) where only one relaxation process is typically becomes frozen. It is therefore characteristic of relaxor ferroelectrics. On the other hand, synchrotron X-ray scattering has revealed an unusual behavior of redistribution of PNRs induced by an electric field, which may help illustrate the role of PNRs in the extraordinary piezoelectric response of the relaxo-based piezocrystals.

In conclusion, the impact of our research contributions and achievements has been very positive and significant. Thanks to the ONR funding, our laboratory has, during this granting period, become an internationally recognized ferroic materials research center and a world leader in the design, synthesis and development of new piezo- and ferroelectric materials, especially in the form of single crystals. We look forward to making further contributions to the ONR's Materials Research Program.

4) Research Achievements and Dissemination

The research achievements and dissemination undertaken in the framework of this research program can be summarized as follows:

- ✓ **53** Refereed research papers published or accepted for publication in international scientific journals (Section 4.1.1);
- ✓ **6** Invited reviews / Book chapters (Section 4.1.2);
- ✓ **39** Invited talks at national or international conferences, and at research institutions (Section 4.2);
- ✓ **90** Contributed oral & poster presentations and technical reports at national or international conferences (Section 4.3).

4.1) List of Publications (supported by ONR in the framework of this grant)

4.1.1) List of Research Publications in Peer-Reviewed Scientific Journals

[1] M. Dong and Z.-G. Ye, "High temperature solution growth and characterization of the piezo- / ferroelectric (1-x)$Pb(Mg_{1/3}Nb_{2/3})O_3$-x$PbTiO_3$ [PMNT] single crystals", *J. Crystal Growth*, **209**, 81-90 (2000).

[2] Z.-G. Ye and M. Dong, "Morphotropic domain structures and phase transitions in relaxor-based piezo-/ ferroelectric (1-x)$Pb(Mg_{1/3}Nb_{2/3})O_3$-x$PbTiO_3$ [PMNT] single crystals", *J. Appl. Phys.* , **87**, 2312 – 2319 (2000).

[3] Z.-G. Ye, M. Dong and Y. Yamashita, "Thermal stability of the $Pb(Zn_{1/3}Nb_{2/3})O_3$-$PbTiO_3$ [PZNT91/9] and $Pb(Mg_{1/3}Nb_{2/3})O_3$-$PbTiO_3$ [PMNT68/32] single crystals", *J. Crystal Growth*, **211**, 247 - 251 (2000).

[4] A. A. Bokov, N. P. Protsenko and Z.-G. Ye, "Relationship between ionicity, ionic radii and order/disorder in complex perovskites", *J. Phys. Chem. Solids*, **61**, 1519 – 1527 (2000).

[5] A. A. Bokov and Z.-G. Ye, "Freezing of dipole dynamics in relaxor ferroelectric $Pb(Mg_{1/3}Nb_{2/3})O_3$-$PbTiO_3$ as evidenced by dielectric spectroscopy", *J. Phys.: Condens. Matter*, **12**, L541 – L548 (2000).

[6] A. Bokov and Z.-G. Ye, "Phenomenological description of dielectric permittivity peak in relaxor ferroelectrics", *Solid State Commun.*, **116**, 105-108 (2000).

[7] A. Bokov and Z.-G. Ye, "Dielectric dispersion and critical behavior in relaxor ferroelectric $Pb(Mg_{1/3}Nb_{2/3})O_3$-$PbTiO_3$", *Appl. Phys. Lett.*, **77**, 1888-1890 (2000).

[8] Y. Hosono, K. Harada, Y. Yamashita, M. Dong & Z.-G. Ye, "Growth and electric and thermal properties of lead magnesium niobate – lead scandium niobate – lead titanate ternary single crystals", *Jpn. J. Appl. Phys.*, **39**, 5589 – 5592 (2000).

[9] L. Zhang, M. Dong and Z.-G. Ye, "Flux growth and characterization of the relaxor-based $Pb(Zn_{1/3}Nb_{2/3})_{1-x}Ti_xO_3$ [PZNT] single crystals", *Mater. Sci. & Eng. B*, **78**, 96-104 (2000).

[10] V. Yu. Topolov and Z.-G. Ye, "Elastic matching of the morphotropic phases in polydomain (1-x)$Pb(Zn_{1/3}Nb_{2/3})O_3$-x$PbTiO_3$ single crystals", *Ferroelectrics*, **253**, 71-78 (2001).

[11] Z.-G. Ye and V. Yu. Topolov, "Complex domain and heterophase structures in (1-x) $Pb(Mg_{1/3}Nb_{2/3})O_3$-x$PbTiO_3$ single crystals", *Ferroelectrics*, **253**, 79 – 86 (2001).

[12] W. Chen and Z.-G. Ye, "Top-Cooling-Solution-Growth and characterization of piezoelectric $0.955Pb(Zn_{1/3}Nb_{2/3})O_3$ - $0.045PbTiO_3$ [PZNT] single crystals", *J. Mater. Sci.*, **36** (18), 4393 – 3499 (2001).

[13] M. Dong and Z.-G. Ye, "High temperature thermodynamic properties and pseudo-binary phase diagram for the (1-x) $Pb(Zn_{1/3}Nb_{2/3})O_3$ – $xPbTiO_3$ system", *Jpn. J. Appl. Phys.*, **40**, Part 1, 4604 – 4610 (2001).

[14] W. Chen and Z.-G. Ye, "Top-seeded solution growth and characterization of piezo-/ferroelectric (1-x)$Pb(Zn_{1/3}Nb_{2/3})O_3$–$xPbTiO_3$ single crystals", *J. Crystal Growth*, **233**, 503 – 511 (2001).

[15] Z.-G. Ye, B. Noheda, M. Dong, D. Cox and G. Shirane, "Monoclinic phase in the relaxor-based piezo-/ ferroelectric $Pb(Mg_{1/3}Nb_{2/3})O_3$ - $PbTiO_3$ system", *Phys. Rev. B*, **64**, 184114/1-5 (2001).

[16] D. La-Orauttapong, J. Toulouse, J. L. Robertson and Z.-G. Ye, "Diffuse neutron scattering study of a disordered perovskite $Pb(Zn_{1/3}Nb_{2/3})O_3$ crystal", *Phys. Rev. B*, **64**, 212101/1-4 (2001).

[17] P. M. Gehring, S. Wakimoto, Z.-G. Ye and G. Shirane, "Soft mode dynamics above and below the Burns temperature in the relaxor $Pb(Mg_{1/3}Nb_{2/3})O_3$", *Phys. Rev. Lett.*, **87**, 277601-1-4 (2001).

[18] K. Hirota, Z.-G. Ye, S. Wakimoto, P. M. Gehring and G. Shirane, "Neutron Diffuse Scattering from Polar Nano Regions in the Relaxor $Pb(Mg_{1/3}Nb_{2/3})O_3$", *Phys. Rev. B*, **65**, 104105/1-7 (2002).

[19] D. La-Orauttapong, B. Noheda, Z.-G. Ye, P. M. Gehring, J. Toulouse, D. Cox and G. Shirane, "Phase Diagram of Relaxor Ferroelectric (1-x)$Pb(Zn_{1/3}Nb_{2/3})O_3$ – $xPbTiO_3$", *Phys. Rev. B*, **65**, 144101/1-7 (2002).

[20] A. A. Bokov and Z.-G. Ye, "Low Frequency Dielectric Spectroscopy of Relaxor Ferroelectric $Pb(Mg_{1/3}Nb_{2/3})O_3$ - $PbTiO_3$", *Phys. Rev. B*, **65**, 144112/1-10 (2002).

[21] S. Wakimoto, C. Stock, R. J. Birgeneau, Z.-G. Ye, W. Chen, W. J. L. Buyers, P. M. Gehring and G. Shirane, "Ferroelectric Ordering in the Relaxor $Pb(Mg_{1/3}Nb_{2/3})O_3$ as Evidenced by Low-Temperature Phonon Anomalies", *Phys. Rev. B*, **65**, 172105/1-4 (2002).

[22] A. A. Bokov and Z.-G. Ye, "Giant Electrostriction and Stretched Exponential Electromechanical Relaxation in $0.65Pb(Mg_{1/3}Nb_{2/3})O_3$ – $0.35PbTiO_3$ Single Crystals", *J. Appl. Phys.*, **91**, 6656 – 6661 (2002).

[23] B. Noheda, D. E. Cox, G. Shirane, J. Gao and Z.-G. Ye, "Phase Diagram of the Ferroelectric-Relaxor (1-x)$Pb(Mg_{1/3}Nb_{2/3})O_3$ –$xPbTiO_3$", *Phys. Rev. B*, **66**, 054104/1-10 (2002).

[24] A. A. Bokov and Z.-G. Ye "Universal Relaxor Polarization in $Pb(Mg_{1/3}Nb_{2/3})O_3$ and Related Materials", *Phys. Rev. B*, **66**, 064103/1-9 (2002).

[25] P. M. Gehring, S. Wakimoto, Z.-G. Ye and G. Shirane, "Ferroelectric Dynamics in the Perovskite Relaxor PMN", *American Institute of Physics Conference Proceedings* ["Fundamental Physics of Ferroelectrics 2002", Ed. R. E. Cohen], Vol. **626**, pp. 99 -107 (2002).

[26] D. La-Orauttapong, J. Toulouse, Z.-G. Ye, R. Erwin and J.L. Robertson, and W. Chen, "Diffuse Neutron Scattering Study of Relaxor Ferroelectric (1-x)$Pb(Zn_{1/3}Nb_{2/3})O_3$-$xPbTiO_3$ (PZN-xPT)", *American Institute of Physics Conference Proceedings* ["Fundamental Physics of Ferroelectrics 2002", Ed. R. E. Cohen], Vol. **626**, pp. 89 – 98 (2002).

[27] A. A. Bokov and Z.-G. Ye, "Ferroelectric Properties of Monoclinic $Pb(Mg_{1/3}Nb_{2/3})O_3$ - $PbTiO_3$ Crystals", *Phys. Rev. B*, **66**, 094112/1-5 (2002).

[28] S. Wakimoto, C. Stock, Z.-G. Ye, W. Chen, P. M. Gehring, and G. Shirane, "Mode-coupling and Polar Nanoregions in the Relaxor Ferroelectric $Pb(Mg_{1/3}Nb_{2/3})O_3$", *Phys. Rev. B*, **66**, 224102/1-8 (2002).

[29] Y. Bing and Z.-G. Ye, "Effects of Chemical Compositions on the Growth of Relaxor Ferroelectric $Pb(Sc_{1/2}Nb_{1/2})_{1-x}Ti_xO_3$ Single Crystals", *J. Crystal Growth,* **250**, 118 – 125 (2003).

[30] G. Xu, Z. Zhong, Y. Bing, Z.-G. Ye, C. Stock, and G. Shirane, "New Ground State of Relaxor Ferroelectric $Pb(Zn_{1/3}Nb_{2/3})O_3$", *Phys. Rev. B*, **67**, 104102/1-5 (2003).

[31] Z.-G. Ye, Y. Bing, J. Gao, A. A. Bokov, P. Stephens, B. Noheda, and G. Shirane, "Development of the Ferroelectric Order in Relaxor $(1-x)Pb(Mg_{1/3}Nb_{2/3})O_3 - xPbTiO_3$ $(0 \leq x \leq 0.15)$", *Phys. Rev. B,* **67**, 104104/1-8 (2003).

[32] Y. Bing and Z.-G. Ye, "Growth and Characterization of Relaxor Ferroelectric $Pb(Sc_{1/2}Nb_{1/2})O_3$-$PbTiO_3$ Single Crystals", in "*Proceedings of the 2002 13th IEEE International Symposium on Applications of Ferroelectrics*", IEEE, pp. 447-450 (2003).

[33] D. La-Orauttapong, J. Toulouse, Z.-G. Ye, W. Chen, R. Erwin and J.L. Robertson, "Neutron Scattering Study of Relaxor Ferroelectric $(1-x)Pb(Zn_{1/3}Nb_{2/3})O_3$-$xPbTiO_3$", *Phys. Rev. B*, **67**, 134110/1-10 (2003).

[34] A. A. Bokov, Y.-H. Bing, W. Chen, Z.-G. Ye, S. A. Bogatina, I. P. Raevski, S. I. Raevskaya, and E.V. Sahkar, "Empirical Scaling of the Dielectric Permittivity Peak in Relaxor Ferroelectrics", *Phys. Rev. B*, **68**, 052102/1-5 (2003).

[35] O. Svitelskiy, J. Toulouse, G. Yong and Z.-G. Ye, "Polarized Raman Study of the Phonon Dynamics in $Pb(Mg_{1/3}Nb_{2/3})O_3$ Crystal", *Phys. Rev. B*, **68**, 104107/1-10 (2003).

[36] C. Stock, R. J. Birgeneau, S. Wakimoto, J. S. Gardner, W. Chen, Z.-G. Ye, and G. Shirane, "Universal Static and Dynamic Properties of the Structural Transition in $Pb(Zn_{1/3}Nb_{2/3})O_3$", *Phys. Rev. B*, **69**, 094104/1-10 (2004).

[37] A. A. Bokov and Z.-G. Ye, "Domain structure in the Monoclinic *Pm* Phase of $Pb(Mg_{1/3}Nb_{2/3})O_3$ – $PbTiO_3$ Single Crystals", *J. Appl. Phys.*, **95**, 6347 – 6359 (2004).

[38] W. M. Zhu and Z.-G. Ye, "Effects of Chemical Modification on the Electrical Properties of $0.67BiFeO_3 - 0.33PbTiO_3$ Ferroelectric Ceramics", *Ceram. Intl.*, **30**, 1435 – 1442 (2004).

[39] W. M. Zhu and Z.-G. Ye, "Ternary $Pb(Yb_{1/2}Nb_{1/2})O_3$–$PbZrO_3$–$PbTiO_3$ System as High-T_C/High-Piezoelectric Materials", *Ceram. Intl.*, **30**, 1443 – 1448 (2004).

[40] G. Xu, Z. Zhong, Y. Bing, Z.-G. Ye, C. Stock and G. Shirane, "An Anomalous Phase in the Relaxor Ferroelectric $Pb(Zn_{1/3}Nb_{2/3})O_3$", *Phys. Rev. B,* **70**, 064107/1-6 (2004).

[41] Z.-G. Ye and A. A. Bokov, "Dielectric and Structural Properties of Relaxor Ferroelectrics", *Ferroelectrics*, **302**, 227 - 231 (2004).

[42] V. Yu. Topolov and Z.-G. Ye, "Coexistence of Morphortropic Phases in $(1-x)$ $Pb(Mg_{1/3}Nb_{2/3})O_3$ – $xPbTiO_3$ Solid Solution", *Phys. Rev. B*, **70**, 094113/1-8 (2004).

[43] P. M. Gehring, W. Chen, Z.-G. Ye and G. Shirane, "The Non-Rhombohedral Low-Temperature Structure of PMN-10%PT", *J. Phys.: Condens. Matter*, **16**, 7113 - 7121 (2004).

[44] Y. Bing, A. Bokov, Z.-G. Ye, B. Noheda and G. Shirane, "Structural Phase Transition and Dielectric Relaxation in $Pb(Zn_{1/3}Nb_{2/3})O_3$ Single Crystals", *J. Phys.: Condens. Matter*, **17**, 2493 – 2507 (2005).

[45] A. A. Bokov and Z.-G. Ye, "Polar Nanodomains and Relaxor Behavior in $(1-x)Pb(Mg_{1/3}Nb_{2/3})O_3 - xPbTiO_3$ Crystals with $x = 0.3 - 0.5$", *Mater. Sci. Eng. B*, **120**, 206 – 209 (2005). H.-Y. Guo and Z.-G. Ye, "Electric Characterization and Microstructure of HfO_2 Thin Films Prepared by Chemical Solution Deposition", *Mater. Sci. Eng. B*, **120**, 68 – 71 (2005).

[46] T. R. Welberry, M. J. Gutmann, H. Woo, D. J. Goossens, G. Xu, C. Stock, W. Chen and Z.-G. Ye, "Single-Crystal Neutron Diffuse Scattering and Monte Carlo Study of the Relaxor Ferroelectric $Pb(Zn_{1/3}Nb_{2/3})O_3$ (PZN)", *J. Appl. Crystallogr.*, **38**, 639 – 647 (2005).

[47] J. Toulouse, F. Jiang, O. Svitelskiy, W. Chen, and Z.-G. Ye, "Temperature Evolution of the Relaxor Dynamics in $Pb(Zn_{1/3}Nb_{2/3})O_3$ (PZN): A Critical Raman Analysis", *Phys. Rev. B.*, **72**, 184106 (2005).

[48] Y.-H. Bing and Z.-G. Ye, "Synthesis, Phase Segregation and Properties of Piezo-/Ferroelectric $(1-x)Pb(Sc_{1/2}Nb_{1/2})O_3$–$xPbTiO_3$ Single Crystals", *J. Crystal Growth*, **287** (2), 326-329 (2006).

[49] G. Xu, Z. Zhong, Y. Bing, Z.-G. Ye, and G. Shirane, "Electric Field-Induced Redistribution of Polar Nano-Regions in a Relaxor Ferroelectric", *Nature Materials*, **5**, 134 – 140 (2006).

[50] C. Lei, A. A. Bokov and Z.-G. Ye, "Relaxor Behavior in $Ba(Ti_{0.72}Sn_{0.28})O_3$ Solid Solution", *Ferroelectrics* (in press).

[51] A. Hilczer, M. Szafrański, A. A. Bokov and Z.-G. Ye, "Effect of Hydrostatic Pressure on the Dielectric Properties of PMN-0.31PT Single Crystal", *Ferroelectrics* (in press).

[52] Y.-H. Bing and Z.-G. Ye, "Synthesis and Characterizations of the $(1-x)Pb(Sc_{1/2}Nb_{1/2})O_3$–$xPbTiO_3$ Solid Solution Ceramics", *J. Electroceram.* (in press).

[53] E. L. Venturini, R. K. Grubbs, G. A. Samara, Y. Bing and Z.-G. Ye, "The Ferroelectric and Relaxor Properties of $Pb(Sc_{0.5}Nb_{0.5})O_3$: Influence of Pressure and Biasing Electric Field", *Phys. Rev. B* (in press).

4.1.2) List of Invited Review Articles / Book Chapters (*Refereed*)

[1] Y. J. Yamashita, Y. Hosono, K. Harada and Z.-G. Ye, "Relaxor Ferroelectric Crystals – Recent Development and Applications", in "*Piezoelectric Materials in Devices*", N. Setter (Editor and Publisher), ISNB: 2-9700346-3, Lausanne, pp. 455 – 466, 2002.

[2] Z.-G. Ye, "Crystal Chemistry and Domain Structure of Relaxor Piezocrystals", *Current Opinions in Solid State and Materials Science*, **6**, 35 – 44 (2002).

[3] A. A. Bokov and Z.-G. Ye, "Morphotropic Phase Boundary and Related Properties in Relaxor-Based Piezoelectric Perovskite Solid Solutions", *Ceramics Transaction*, **136**, 37 – 53 (2003).

[4] Y. Yamashita, Y. Hosono, and Z.-G. Ye, "Recent Development Trend of Piezoelectric Single Crystals: A Review", *Transac. Mater. Res. Soc. Jpn.*, **29** [4], 1059 – 1066 (2004).

[5] Z.-G. Ye, "Relaxor-Based Piezo-/Ferroelectric Single Crystals: Synthesis, Properties and Understanding", in "*Ferroelectric Single Crystals*", pp. 297 – 322, Ed. S. Trolier-McKinstry, L. E. Cross, and Y. Yamashita, Penn State University (2004).

[6] A. A. Bokov and Z.-G. Ye, "Recent Progress in Relaxor Ferroelectrics and Related Materials with Perovskite Structure", *J. Mater. Sci.*, **41**, 31 – 52 (2006) [a special issue on ***Frontiers of Ferroelectricity***].

4.2) List of Invited Talks / Lectures

(At national or international conferences and at other universities or research institutions, where the ONR support was acknowledged)

[1] Y. Yamashita, K. Harada, S. Saitoh and Z.-G. Ye, "Growth and Application of Relaxor Single Crystals", 11th American Conference on Crystal Growth and Epitaxy (ACCGE-11), Tucson, Arizona, August 1-6, **1999**.

[2] Z.-G. Ye, "Relaxor-Based Piezo-/Ferroelectric Single Crystals: Microstructure, Domain Engineering and Applications", Department of Materials Sciences, Tsinghua University, Beijing, China, May 24, **2000**.

[3] Z.-G. Ye, "Morphotropic Domain Structures and Related Properties of Relaxor-Based PiezoCrystals", 6th International Symposium on Ferroic Domains and Mesoscopic Structures", Nanjing, China, May 29 – June 2, **2000**.

[4] Z.-G. Ye, "Relaxor-Based PiezcoCrystals: from Microsctructure and Domain Engineering to Enhanced Properties and Applications", Fujian Institute of Research on the Structures of Matter, Chinese Academy of Sciences, June 7, **2000**.

[5] Z.-G. Ye, "Relaxor-Based PiezoCrystals: from Microsctructure and Domain Engineering to Enhanced Properties and Applications", Shanghai Institute of Ceramics, Chinese Academy of Sciences, June 16, **2000**.

[6] Z.-G. Ye, "Thermodynamic Behavior, Growth and Anisotropic Properties of PiezoCrystals", 12th IEEE International Symposium on the Applications of Ferroelectrics (ISAF'2000), Hawaii, July 30 – August 3, **2000**.

[7] Z.-G. Ye, "Relaxor-Based PiezoCrystals: Design, Synthesis and Anisotropic Properties", 3rd Asian Meeting on Ferroelectrics (AMF-3), Hong Kong, Dec. 12 - 15, **2000**.

[8] Y. Yamashita, K. Harada, Y. Hosono and Z.-G. Ye, "Crystal Growth of Two Inch-Sized Lead Zinc Niobate – Lead Titanate Single Crystals", 2001-ONR Meeting on Acoustic Transducer Materials and Devices", Baltimore, MD, May 13 - 16, **2001**.

[9] Z.-G. Ye, "Recent Developments in Relaxor Ferroelectric-Based High Strain Piezoelectric Single Crystals", 84th CSC Conference and Exhibition, Montreal, May 26 -30, **2001**.

[10] Z.-G. Ye, "Relaxor Ferroelectric Materials: Structure, Properties and Present Understanding", Institute of Physics, Autonomy University of Puebla, Mexico, June 13, **2001**.

[11] Z.-G. Ye, "Innovative Relaxor Ferroelectrics-Based High Strain Piezoelectric Single Crystals: Design, Synthesis and Characterization", Institute of Physics, Autonomy University of Puebla, Mexico, June 15, **2001**.

[12] Z.-G. Ye, "Morphotropic Phase Diagram, Domain Structure and Properties of Relaxor Piezoelectric Single Crystals", The 104th American Ceramic Society Meeting, St. Louis, MO April 28 – May 1, **2002**.

[13] Z.-G. Ye, "Relaxor Ferroelectric Single Crystals: Recent Developments and New Challenges", The 14th American Conference on Crystal Growth and Epitaxy, Seattle, WA, Aug. 5 –9 , **2002**.

[14] Z.-G. Ye, "Morphotropic Phase Boundary-related Domain Structures and Properties of Relaxor Ferroelectric Single Crystals", The 7th International Symposium on Ferroic Domains and Mesoscopic Structures (ISFD-7), Giens, France, Sept. 15-19, **2002**.

[15] Z.-G. Ye, "Polar Nanostructure and Relaxor Ferroelectric Materials", Centre for Nano Technology, University of Washington, Seattle, Feb. 18, **2003**.

[16] Z.-G. Ye, "Relaxor Ferroelectrics-Based PiezoCrystals: Materials Technology and Fundamental Understanding", UK Ferroelectrics Conference 2003, Belfast, April 10, **2003**.

[17] Z.-G. Ye and A. Bokov, "Dielectric and Structural Properties of Relaxor Ferroelectrics", 10th European Meeting of Ferroelectricity (EMF-10), Cambridge, UK, Aug. 2-8, **2003**.

[18] Z.-G. Ye, "Développement Récent de Monocristaux de Haute Piézoélectricité Dérivés de Relaxeurs Ferroélectriques", Institut de Chimie de la Matière Condensée de Bordeaux, France, Oct. 26, **2003**.

[19] Z.-G. Ye, "Relaxor-Based Piezoelectric Single Crystals: Recent Development and Present Understanding", International Conference on Materials for Advanced Technology / 3rd Asian Meeting on Electroceramics (ICMAT/AMEC-3), Singapore, Dec. 8, **2003**.

[20] Z.-G. Ye, "High Piezo-/Ferroelectric Single Crystals: Materials Development and Fundamental Understanding", Shanghai Institute of Ceramics, Chinese Academy of Sciences, Shanghai, July 20, **2004**.

[21] Z.-G. Ye, "Recent Development and Present Understanding of High Piezo-/Ferroelectric Single Crystals", Fujian Institute of Research on the Structures of Matter, Chinese Academy of Sciences, Fuzhou, China, August 4, **2004**.

[22] Z.-G. Ye, "Crystal Chemistry and Materials Physics of Relaxor Ferroelectrics", Xiamen University, Xiamen, China, August 6, **2004.**

[23] Z.-G. Ye, "High Piezo- and Ferroelectric Single Crystals: Recent Development and Present Understanding", Advanced Institute of Science & Technology (AIST), Tsukuba, Japan, August 24, **2004**.

[24] Z.-G. Ye, "Domain Structures and Properties of the MPB Phases in Piezo-/Ferroelectric Single Crystals", The 8th International Symposium on Ferroic Domains and Meso- to Nanoscopic Structures (ISFD-8), Tsukuba, Japan, August 24, **2004**.

[25] Z.-G. Ye, "Recent Development and Future Directions in Materials for Electromechanical Transducers", Nippon Electronic Company (NEC) Tokin, Sendai, Japan, August 26, **2004**.

[26] Z.-G. Ye, "High T_C, High Performance PiezoCrystals for Medical Ultrasonic Transducers", Toshiba Medical Corporation (TMSC), Nasu Shiobar, Japan, August 26, **2004**.

[27] Z.-G. Ye, "Growth and Characterization of PZT Single Crystals", Aloka Corp., Tokyo, Japan, Aug. 31, **2004**.

[28] Z.-G. Ye, "High Piezo-/Ferroelectric Single Crystals", The 7th European Conference on Applications of Polar Dielectrics (ECAPD7), Liberec, Czech Republic, Sept. 6-9, **2004.**

[29] Z.-G. Ye, "Structural and Dielectric Properties of Relaxor Ferroelectrics", Institute of Physics, Czech Academy of Sciences, Prague, Czech Republic, Sept. 10, **2004.**

[30] Z.-G. Ye, "High Performance Piezo- and Ferroelectric Single Crystals I: Materials Development and Applications", The International School on Crystal Growth (ISCG-2005), Puebla, Mexico, March 7 - 11, **2005**.

[31] Z.-G. Ye, "High Performance Piezo- and Ferroelectric Single Crystals II: Properties and Present Understanding", The International School on Crystal Growth (ISCG-2005), Puebla, Mexico, March 7 - 11, **2005**.

[32] Z.-G. Ye, "Recent Developments in Relaxor Ferroelectrics Single Crystals", Shanghai Institute of Ceramics, Chinese Academy of Sciences, Shanghai, China, June 10, **2005**.

[33] Z.-G. Ye, "Growth, Characterization and Applications of High Piezo-/ Ferroelectric Single Crystals", Fujian Institute of Research on the Structures of Matter, Chinese Academy of Sciences, Fuzhou, China, June 13, **2005**.

[34] Z.-G. Ye, "Relaxor Ferroelectric Materials: from *chimie-douce* Preparation to Fundamental Understanding", State Key Laboratory of Physical Chemistry, Xiamen University, Xiamen, China, June 24, **2005.**

[35] Z.-G. Ye, and A. A. Bokov, "Recent Progress in Relaxor Ferroelectrics and Related Materials with Perovskite Structures", 4th Asian Meeting on Electroceramics (AMEC-4), Hangzhou, China, June 27 – 30, **2005.**

[36] Z.-G. Ye, "Recent Development & Present Understanding of Relaxor Ferroelectrics & Related Materials", The China University of Petroleum (East China), Dongying, July 2, **2005**.

[37] Z.-G. Ye, "Relaxor-Based High Performance Piezo-/ Ferroelectric Single Crystals: Materials Development & Present Understanding", Institute of Crystal Materials, Shangdong University, Jinan, China, July 4, **2005.**

[38] Z.-G. Ye, "Recent Progress in Materials Physics of Relaxor Ferroelectrics", Department of Materials Sciences, Tsinghua University, Beijing, July 6, **2005.**

[39] Z.-G. Ye, "Polar Nanostructure and Dynamics of Relaxor Ferroelectrics", Symposium on "Solid State Chemistry" at the 88th Canadian Society for Chemistry Conference and Exhibition, Halifax, NS, May 27 – 31, **2006**.

4.3) List of Contributed Oral or Poster Presentations and Technical Reports

(At regional, national or international meetings / conferences, where the ONR support was acknowledged)

[1] Z.-G. Ye, M. Dong, L. Zhang and A. Bokov, "Composition-Induced Morphotropic Domain Structures and Phase Transitions in the Relaxor-Based Piezo- / Ferroelectric Materials", 82nd Canadian Society for Chemistry Conference & Exhibition" Toronto, May 30 - June 2, **1999**.

[2] M. Dong, L. Zhang, Y. Yamashita and Z.-G. Ye, "Optimized Growth, Thermal Stability and Characterization of Relaxor-Based PMNT and PZNT Single Crystals", 11th American Conference on Crystal Growth and Epitaxy (ACCGE-11), Tucson, Arizona, August 1-6, **1999**.

[3] A. Bokov, Z.-G. Ye and N. P. Protsenko, "Relationship between Ionicity, Ionic Radii and Order/Disorder in Complex Perovskites", Piezotechnique'99 / 15th Russian Conference on Physics of Ferroelectrics, Azov, Russia, Sept. 14 – 18, **1999**.

[4] A. Bokov and Z.-G. Ye, "Relaxor and Normal Ferroelectric Behavior in $Pb(Mg_{1/3}Nb_{2/3})O_3$-$PbTiO_3$", Piezotechnique'99 / 15th Russian Conference on Physics of Ferroelectrics, Azov, Rostov-on-Don, Russia, Sept. 14 – 18, **1999**.

[5] M. Dong and Z.-G. Ye, "Microstructure and Electric Characterization of Sol-Gel Derived PZT and PZT/MgO Nanocomposite Ceramics", Materials Research Society Fall Meeting, Boston, Nov. 28 - Dec. 3, **1999**.

[6] M. Dong & Z.-G. Ye, "Electrical Properties of Sol-Gel Derived $Pb(Zr,Ti)O_3$ Nanocomposites", 4th Annual Meeting of the Pacific Center for Advanced Materials and Microstructure (PCAMM), SFU, December 11, **1999.**

[7] Z.-G. Ye, "Innovative Relaxor-Based PiezoCrystals: Phase Diagrams, Crystal Growth, Domain Structure and Electric Properties" (O), ONR PiezoCrystal Workshop, Washington DC, Jan. 18-21, **2000**.

[8] Z.-G. Ye, M. Dong, L. Zhang & A. Bokov, "Relaxor-Based Piezocrystals; from Phase Diagram to Crystal Growth and Characterization" (O & P), 2000-ONR Meeting on Acoustic Transducer Materials and Devices", PennState, PA, April 10-13, **2000**.

[9] Y. Yamashita, Y. Hosono and Z.-G. Ye, "Growth and Characterization of New Piezocrystals from Lead Magnesium Niobate – Lead Scandium Niobate – Lead Titanate Ternary System", 2000-ONR Meeting on Acoustic Transducer Materials and Devices" (P), PennState, PA, April 10-13, **2000**.

[10] L. Zhang, M. Dong & Z.-G. Ye, "Synthesis and Properties of the Relaxor-Based Piezo-/ferroelectrics Single Crystals" (P), 83rd Canadian Society for Chemistry Conference & Exhibition", Calgary, May 26 - 30, **2000**.

[11] Y. Hosono, K. Harada, Y. Yamashita, M. Dong & Z.-G. Ye, "Growth and Electric and Thermal Properties of Lead Magnesium Niobate – Lead Scandium Niobate – Lead Titanate Ternary Single Crystals", 17th Meeting on Ferroelectric Materials and Applications (FMA-17), Kyoto, Japan, May 24, **2000**.

[12] V. Yu. Topolov and Z.-G. Ye, "Elastic Matching of the Mophotropic Phases in Polydomain (1-x)$Pb(Zn_{1/3}Nb_{2/3})O_3$-x$PbTiO_3$ Single Crystals", 6th International Symposium on Ferroic Domains and Mesoscopic Structures, Nanjing, China, May 29 – June 2, **2000.**

[13] Z.-G. Ye and V. Yu. Topolov, "Complex Domain and Heterophase Structures in (1-x) $Pb(Mg_{1/3}Nb_{2/3})O_3$-x$PbTiO_3$ Single Crystals" (*Excellent Poster Award*), 6th International Symposium on Ferroic Domains and Mesoscopic Structures, Nanjing, China, May 29 – June 2, **2000.**

[14] M. Dong, W. Chen and Z.-G. Ye, "Thermodynamic Properties and Top-Cooling Growth of Relaxor-Based PiezoCrystals", 12th IEEE International Symposium on the Applications of Ferroelectrics (ISAF'2000), Hawaii, July 30 – August 3, **2000**.

[15] A. Bokov and Z.-G. Ye, "New Critical Behavior in Relaxor Ferroelectric $Pb(Mg_{1/3}Nb_{2/3})O_3$-$PbTiO_3$", 3rd Asian Meeting on Ferroelectrics (AMF-3), Hong Kong, Dec. 12 - 15, **2000**.

[16] M. Dong and Z.-G. Ye, "Microstructure and Electrical Properties of Sol-Gel Derived $Pb(Zr_{0.53}Ti_{0.47})O_3$/MgO Nanoparticles and Composite Ceramics", 3rd Asian Meeting on Ferroelectrics (AMF-3), Hong Kong, Dec. 12 - 15, **2000**.

[17] Z.-G. Ye, "High-Temperature Phase Diagrams and Growth of Relaxor-Based PiezoCrystals", Symposium on the Growth and Characterization of Piezoelectric Relaxor Crystals", PennState University, State College, April 27, **2001**.

[18] Z.-G. Ye, "Low-Temperature Phase Diagrams and Properties of Relaxor-Based PiezoCrystals", Symposium on the Growth and Characterization of Piezoelectric Relaxor Crystals", PennState University, PA, April 27, **2001**.

[19] Z.-G. Ye, "Towards a More Complete Characterization of Relaxor Ferroelectric Single Crystal Systems", 2001-ONR Meeting on Acoustic Transducer Materials and Devices, Baltimore, MD, May 13 - 16, **2001**.

[20] Z.-G. Ye, "Innovative Relaxor-Based PiezoCrystals: Phase Diagrams, Crystal Growth, Domain Structure and Electric Properties", ONR/DARPA PiezoCrystal Workshop, Washington DC, July 24-27, **2001**.

[21] J. Gao, M. Dong and Z.-G. Ye, "Study of the High Temperature Phase Diagram of the Relaxor Ferroelectric $Pb(Mg_{1/3}Nb_{2/3})O_3$-$PbTiO_3$ Solid Solution System", 6th Annual Meeting of the Pacific Center for Advanced Materials and Microstructure (PCAMM), SFU, Dec. 8, **2001**.

[22] Y. Bing and Z.-G. Ye, "Growth and Characterization of Complex Perovskite (1-x)$Pb(Sn_{1/2}Nb_{1/2})O_3$-x$PbTiO_3$ Single Crystals of MPB Composition", 6th Annual Meeting of the Pacific Center for Advanced Materials and Microstructure (PCAMM), SFU, Dec. 8, **2001**.

[23] J. Gao, M. Dong and Z.-G. Ye, "High Temperature Phase Diagrams of the Relaxor Ferroelectric $Pb(Mg_{1/3}Nb_{2/3})O_3$-$PbTiO_3$ and Related Systems", 2nd Annual Student Conference on Materials Science, UBC, Jan. 24-25, **2002**.

[24] K. Hirota, Z.-G. Ye, S. Wakimoto, P. Gehring and G. Shirane, "Neutron Diffuse Scattering from Polar Nanoregions in the Relaxor $Pb(Mg_{1/3}Nb_{2/3})O_3$", America Physical Society Meeting, Indianapolis, ID, March 18-22, **2002.**

[25] O. Svitelskiy, J. Toulouse and Z.-G. Ye, "Raman Study of Phonon Dynamics in $Pb(Mg_{1/3}Nb_{2/3})O_3$ (PMN) Crystal", America Physical Society Meeting, Indianapolis, ID, March 18-22, **2002.**

[26] Z.-G. Ye, "Growth, Structure and Properties of Relaxor-Based Piezocrystals", 2002-ONR Meeting on Acoustic Transducer Materials and Devices, Baltimore, MD, May 12 - 15, **2002**.

[27] Y. Bing and Z.-G. Ye, "Growth and Characterization of $Pb[(Sc_{1/2}Nb_{1/2})_{1-x}Ti_x]O_3$ Single Crystals with MPB Composition", The 104th American Ceramic Society Meeting, St. Louis, MO, April 28 – May 1, **2002**.

[28] Y. Yamashita, K. Harada, Y. Hosono and Z.-G. Ye, "Effects of Stoichiometry of Charging Raw Materials on Crystal Growth Results of Lead Zinc Niobate – Lead Titanate Single Crystals by a Solution Bridgman Process", 2002-ONR Meeting on Acoustic Transducer Materials and Devices", Baltimore, MD, May 12 - 15, **2002**.

[29] J. Gao, M. Dong and Z.-G. Ye, "Synthesis and Phase Behaviour of the Piezo-/Ferroelectric Solid Solution (1-x)$Pb(Mg_{1/3}Nb_{2/3})O_3$-x$PbTiO_3$", 85th CSC Conference and Exhibition, Vancouver, June 1-5, **2002**.

[30] Y. Bing, W. Chen and Z,-G. Ye, "Top-Seeded and Flux Growth and Characterization of the Piezo-/Ferroelectric Single Crystals", International Joint Conferences on the Applications of Ferroelectrics (IFFF'2002), Nara, Japan, May 28 – 31, **2002**.

[31] Z.-G. Ye and A. A. Bokov, "Morphotropic Phase Boundary and Related Properties of Relaxor Piezoelectric Single Crystals", International Joint Conferences on the Applications of Ferroelectrics (IFFF'2002), Nara, Japan, May 28 – 31, **2002**.

[32] Y. Bing, W. Chen and Z,-G. Ye, "High-Temperature Solution Growth and Characterization of Relaxor-Based Ferroelectric Single Crystals", The 14th American Conference on Crystal Growth and Epitaxy, Seattle, WA, Aug. 5 –9 , **2002**.

[33] Z.-G. Ye, V. Yu. Topolov and A.A Bokov, "Effects of the Monoclinic Phase on the Morphotropic Domain Structures in (1–x)$Pb(Mg_{1/3}Nb_{2/3})O_3$ – x$PbTiO_3$", The 7th International Symposium on Ferroic Domains and Mesoscopic Structures (ISFD-7), Giens, France, Sept. 15-19, **2002**.

[34] J. Gao and Z.-G. Ye, Synthesis and Phase Diagrams of $Pb(Mg_{1/3}Nb_{2/3})O_3$-$PbTiO_3$-PbO Systems", 7th Annual Meeting of the Pacific Center for Advanced Materials and Microstructure (PCAMM), NRC at UBC, Dec. 7, **2002**.

[35] W. Zhu and Z.-G. Ye, "Study of Electrical Conduction in $BiFeO_3$-$PbTiO_3$ Ferroelectric Ceramics", 7th Annual Meeting of the Pacific Center for Advanced Materials and Microstructure (PCAMM), NRC / UBC, Dec. 7, **2002**.

[36] Z.-G. Ye, "Piezo- and Ferroelectric Materials Based on Morphotropic Phase Boundary: Synthesis, Characterization and Structure–Property Relations", ONR/DARPA PiezoCrystal Workshop, Washington DC, Jan. 27-30, **2003**.

[37] P. Gehring, G. Shirane and Z.-G. Ye, "$Pb(Mg_{1/3}Nb_{2/3})O_3$-$10PbTiO_3$ is Not Rhombohedral", Fundamental Physics of Ferroelectrics 2003, Williamsburg, VA. USA, Feb. 2 – 5, **2003**.

[38] D. La-Orauttapong, J. Toulouse, B. Hennion, W. Chen, Z.-G. Ye, R. Erwin and J.L. Robertson, "Phonon Anomaly of Relaxor Ferroelectric $(1-x)Pb(Zn_{1/3}Nb_{2/3})O_3$-$xPbTiO_3$ Studied by Inelastic Neutron Scattering", Fundamental Physics of Ferroelectrics 2003, Williamsburg, VA. USA, Feb. 2 – 5, **2003**.

[39] D. La-Orauttapong, J. Toulouse, B. Hennion, W. Chen, Z.-G. Ye, R. Erwin and J.L. Robertson, "Inelastic Neutron Scattering Study of the Relaxor Ferroelectric PZN-*x*PT", America Physical Society Meeting, Austin, TX, USA, March 3–7, **2003**.

[40] Z.-G. Ye and A. Bokov, "Morphotropic Domain Structure of $Pb(Mg_{1/3}Nb_{2/3})O_3$-$PbTiO_3$ Crystals", 2003-ONR Meeting on Acoustic Transducer Materials and Devices, Penn State University, PA, May 6 - 10, **2003**.

[41] Y. Yamashita, Y. Hosono, S. Tezuka and Z.-G. Ye, "High Piezoelectric Constant, High Curie Temperature $Pb(In_{1/2}Nb_{1/2})O_3$-$Pb(Mg_{1/3}Nb_{2/3})$-$PbTiO_3$ Ternary Single Crystals near MPB", 2003-ONR Meeting on Acoustic Transducer Materials and Devices", Penn State University, PA, May 6 - 10, **2003**.

[42] Y.-H. Bing and Z.-G. Ye, "High-T_C Piezoelectric Materials: $Pb(Sc_{1/2}Nb_{1/2})_{1-x}Ti_xO_3$", 2003-ONR Meeting on Acoustic Transducer Materials and Devices, Penn State University, PA, May 6 - 10, **2003**.

[43] W. Zhu and Z.-G. Ye, "Dielectric and Piezoelectric Properties of $Pb(Yb_{1/2}Nb_{1/2})O_3$ – $PbZrO_3$ – $PbTiO_3$ Ternary System", 2003-ONR Meeting on Acoustic Transducer Materials and Devices, Penn State University, PA, May 6 - 10, **2003**.

[44] W. Chen and Z.-G. Ye, "Growth and Characterization of $Pb(Zr_{1-x}Ti_x)O_3$ Single Crystals", 2003-ONR Meeting on Acoustic Transducer Materials and Devices, Penn State University, PA, May 6 - 10, **2003**.

[45] Y.-H. Bing and Z.-G. Ye, "Growth and Properties of $(1-x)Pb(Sc_{1/2}Nb_{1/2})O_3$ – $xPbTiO_3$ Single Crystals: A Relaxor-Based High-T_C Piezoelectric Material", 15th American Conference on Crystal Growth and Epitaxy (ACCGE-15), Keystone, Colorado, July 20 – 24, **2003**.

[46] W. Chen, J. Gao, L. C. Lim and Z.-G. Ye, "Top-Seeded Solution Growth and Characterization of PMN-PT and PZN-PT Single Crystals", 15th American Conference on Crystal Growth and Epitaxy (ACCGE-15), Keystone, Colorado, July 20 – 24, **2003**.

[47] A. Bokov and Z.-G. Ye, "Domain Structure of the Monoclinic Phase in $Pb(Mg_{1/3}Nb_{2/3})O_3$-$PbTiO_3$ Crystals", 10th European Meeting of Ferroelectricity (EMF-10), Cambridge, UK, Aug. 2-8, **2003**.

[48] Z.-G. Ye, A. Bokov and M. Maglione, "Dielectric and Structural Properties of Relaxor Ferroelectrics", 55 Years of Ferroelectrics, Leeds, UK, Sept. 21 – 23, **2003**.

[49] W. Zhu and Z.-G. Ye, "Preparation and Electrical Properties of $Pb(Yb_{1/2}Nb_{1/2})O_3$ – $PbZrO_3$ – $PbTiO_3$ Ternary System as High-T_C / High-Piezoelectric Materials", International Conference on Materials for Advanced Technology / 3rd Asian Meeting on Electroceramics (ICMAT/AMEC-3), Singapore, Dec. 7 - 12, **2003**.

[50] W. Zhu and Z.-G. Ye, "Effects of Chemical Modification on the Electrical Properties of $0.67BiFeO_3$ –$0.33PbTiO_3$ Ferroelectric Ceramics", International Conference on Materials for Advanced Technology / 3rd Asian Meeting on Electroceramics (ICMAT/AMEC-3), Singapore, Dec. 7 - 12, **2003**.

[51] F. Jiang, O.Svitelskiy, W. Chen, Z.-G.Ye and J. Toulouse, "A Critical Analysis of the Low Frequency Raman Spectra of Relaxor Ferroelectrics Containing Nb: Two-Time Scale Dynamics", Fundamental Physics of Ferroelectrics 2004, Williamsburg, VA. USA, Feb. 2 – 5, **2004**.

[52] R. K. Grubbs, E. L. Venturini, P. G. Clem, J. J. Richardson, G. A. Samara, Y. Bing and Z.-G. Ye, "Pressure Study of Complex Perovskites: $Pb(Sc_{0.5}Nb_{0.5})O_3$ and $CaCu_3Ti_4O_{12}$", Fundamental Physics of Ferroelectrics 2004, Williamsburg, VA. USA, Feb. 2 – 5, **2004**.

[53] Z.-G. Ye, W. Chen and A. Bokov, "$Pb(Zr_{1-x}Ti_x)O_3$ Single Crystals: Improved Growth and Characterization", 2004-ONR Meeting on Acoustic Transducer Materials and Devices, Penn State University, PA, May 11 - 13, **2004.**

[54] Y.-H. Bing, and Z.-G. Ye, "A New Family of Piezoelectric Single Crystals: $(1-x)PbSnO_3–xPbTiO_3$" (O & P), 2004-ONR Meeting on Acoustic Transducer Materials and Devices, Penn State University, PA, May 11 - 13, **2004**.

[55] Z.-G. Ye, J. Gao, W. Chen, Y.-H. Bing, A. A. Bokov, and L. C. Lim, "Synthesis and Characterization of Relaxor-Based PiezoCrystals" (P), 2004-ONR Meeting on Acoustic Transducer Materials and Devices, Penn State University, PA, May 11 - 13, **2004**.

[56] W.-Z. Zhu and Z.-G. Ye, "Effects of Chemical Modifications on the Electrical Properties of $0.67BiFeO_3 – 0.33PbTiO_3$ Ferroelectric Ceramics" (P), 2004-ONR Meeting on Acoustic Transducer Materials and Devices, Penn State University, PA, May 11 - 13, **2004**.

[57] Z.-G. Ye, "Novel Piezo- and Ferroelectric Single Crystals Based on Morphotropic Phase Boundary", Workshop on "Future Directions in Materials for Electromechanical Transducers", Arlington, VA, July 11 – 13, **2004.**

[58] Z.-G. Ye and J. Gao, "Complex Phase Behaviour in High-Piezoelectric $(1-x)Pb(Mg_{1/3}Nb_{2/3})O_3–xPbTiO_3$ Solid Solutions" (O), The 18th IUPAC International Conference on Chemical Thermodynamics", Beijing, China, Aug. 17 – 20, **2004.**

[59] J. Gao and Z.-G. Ye, "High-Temperature Phase Diagram of the Pseudo-Binary $Pb[(Mg_{1/3}Nb_{2/3})_{0.65}Ti_{0.35}]O_3$ – PbO System" (P), The 18th IUPAC International Conference on Chemical Thermodynamics", Beijing, China, Aug. 17 – 20, **2004.**

[60] Y.-H. Bing and Z.-G. Ye, "Effects of Composition and Ordering on Domain Structure of $Pb(Sc_{1/2}Nb_{1/2})O_3$ and $(1-x)Pb(Sc_{1/2}Nb_{1/2})O_3–xPbTiO_3$ Single Crystals" (P), The 8th International Symposium on Ferroic Domains and Meso- to Nanoscopic Structures (ISFD-8), Tsukuba, Japan, August 24 - 27, **2004.**

[61] A. A. Bokov and Z.-G. Ye, "Polar Nanodomains and Universal Relaxor Polarization in $Pb(Mg_{1/3}Nb_{2/3})O_3$ and Related Materials" (P), The 8th International Symposium on Ferroic Domains and Meso- to Nanoscopic Structures (ISFD-8), Tsukuba, Japan, August 24 - 27, **2004.**

[62] L. C. Lim, K. K. Rajan, A. A. Bokov and Z.-G. Ye, "X-ray Diffraction Study and Polarized Light Microscopy of Domain Structures in Flux-grown PZN-(6–7)%PT Single Crystals" (P), The 8th International Symposium on Ferroic Domains and Meso- to Nanoscopic Structures (ISFD-8), Tsukuba, Japan, August 24 - 27, **2004.**

[63] C. Lei, A. A. Bokov and Z.-G. Ye, "Relaxor Ferroelectric Properties of the $BaTiO_3$-$BaSnO_3$ System", The 9th Annual Meeting of the Pacific Center for Advanced Materials and Microstructure (PCAMM), NRC / UBC, Dec. 4, **2004.**

[64] A. A. Bokov, M. Maglione and Z.-G. Ye, "Low-Frequency Dielectric Dispersion and Freezing in Relaxor Ferroelectrics", 2005 Workshop on Fundamental Physics of Ferroelectrics, Williamsburg, VA, USA, Feb. 6 – 9, **2005.**

[65] Y.-H. Bing, A. A. Bokov, Z.-G. Ye, B. Noheda and G. Shirane, "Structural Phase Transition and Dielectric Relaxation in $Pb(Zn_{1/3}Nb_{2/3})O_3$ Single Crystals", 2005 Workshop on Fundamental Physics of Ferroelectrics, Williamsburg, VA, USA, Feb. 6 – 9, **2005.**

[66] R. K. Grubbs, E .L. Venturini and G. A. Samara, Y.-H. Bing and Z.-G. Ye, "The Ferroelectric and Relaxor Properties of $Pb(Sc_{0.5}Nb_{0.5})O_3$: Effects of Pressure and Biasing Electric Field" (O), 2005 Workshop on Fundamental Physics of Ferroelectrics, Williamsburg, VA, USA, Feb. 6 – 9, **2005.**

[67] Y.-H. Bing, and Z.-G. Ye, "Investigations of $(1-x)Pb(Sc_{1/2}Nb_{1/2})O_3 - xPbTiO_3$ Single Crystals and Ceramics" (O & P), 2005-ONR Meeting on Acoustic Transducer Materials and Devices, Penn State University, PA, May 9 - 12, **2005.**

[68] A. Bokov, and Z.-G. Ye, "Relaxor to Ferroelectric Phase Transition in $(1-x)$ $Pb(Mg_{1/3}Nb_{2/3})O_3 - xPbTiO_3$ Crystals (with $x \leq 0.5$)" (O & P), 2005-ONR Meeting on Acoustic Transducer Materials and Devices, Penn State University, PA, May 9 - 12, **2005.**

[69] W. M. Zhu, and Z.-G. Ye, "Growth and Characterization of $0.33Pb(Yb_{1/2}Nb_{1/2})O_3$–$0.44PbTiO_3$–$0.23PbZrO_3$ Single Crystals" (O & P), 2005-ONR Meeting on Acoustic Transducer Materials and Devices, Penn State University, PA, May 9 - 12, **2005.**

[70] C. Lei, A. A. Bokov, and Z.-G. Ye, "Ferroelectric to Relaxor Transition in the $BaTiO_3$–$BaSnO_3$ System", 88th Canadian Society for Chemistry Conference" (O), Saskatoon, SK, May 28 – June 1, **2005**.

[71] Y.-H. Bing, J. Gao, A. A. Bokov, Z.-G. Ye, B. Noheda and G. Shirane, "Structure and Properties of the High-Piezoelectric $(1-x)Pb(Mg_{1/3}Nb_{2/3})O_3 - xPbTiO_3$ Solid Solution System", 88th Canadian Society for Chemistry Conference", Saskatoon, SK, May 28 – June 1, **2005**.

[72] W. Zhu, and Z.-G. Ye, "Structural and Magnetic Characterization of the $(1-x)PbTiO_3 - xBiFeO_3$ System", 4th Asian Meeting on Electroceramics (AMEC-4), Hangzhou, China, June 27 – 30, **2005.**

[73] Y.-H. Bing, and Z.-G. Ye, "Studies of the Structural and Electrical Properties of $(1-x)Pb(Sc_{1/2}Nb_{1/2})O_3$–$xPbTiO_3$ Ceramics", 4th Asian Meeting on Electroceramics (AMEC-4), Hangzhou, China, June 27 – 30, **2005.**

[74] Y.-H. Bing, and Z.-G. Ye, "Structural Disorder, Dielectric Properties and Phase Transition of Relaxor $Pb(Sc_{1/2}Nb_{1/2})O_3$ Single Crystals", 4th Asian Meeting on Electroceramics (AMEC-4), Hangzhou, China, June 27 – 30, **2005.**

[75] W. Chen, J. Gao, A. A. Bokov, and Z.-G. Ye, "Growth of Perovskite $Pb(Mg_{1/3}Nb_{2/3})O_3$–$PbTiO_3$ Single Crystals and Characterization of Their Structure and Piezo-/Ferroelectric Properties" (O), 16th American Conference on Crystal Growth and Epitaxy (ACCGE-16), Big Sky, Montana, July 11 – 15, **2005.**

[76] Y.-H. Bing, and Z.-G. Ye, "Effects of the Growth Conditions and Composition on the Structure and Properties of the Relaxor Ferroelectric $(1-x)Pb(Sc_{1/2}Nb_{1/2})O_3$–$xPbTiO_3$ Single Crystals" (O), 16th American Conference on Crystal Growth and Epitaxy (ACCGE-16), Big Sky, Montana, July 11 – 15, **2005.**

[77] A. Hilczer, M. Szafrański, A. Bokov, Z.-G. Ye, "Effect of Hydrostatic Pressure on the Dielectric Properties of PMN-0.3PT Single Crystals", 11th International Meeting on Ferroelectrics (IMF-11). Iguassu Falls, Brazil/Argentina, Sept. 5 – 9, **2005.**

[78] A. A. Bokov, M. Maglione and Z.-G. Ye, "Critical Dielectric Behaviour in $Ba(Ti_{1-x}Zr_x)O_3$ Solid Solution" (O), 11th International Meeting on Ferroelectrics (IMF-11). Iguassu Falls, Brazil/Argentina, Sept. 5 – 9, **2005.**

[79] A. A. Bokov, and Z.-G. Ye, "Freezing of the Dielectric Response in Relaxor $Pb(Mg_{1/3}Nb_{2/3})O_3$ Single Crystals" (O), 11th International Meeting on Ferroelectrics (IMF-11). Iguassu Falls, Brazil/Argentina, Sept. 5 – 9, **2005.**

[80] Y. Bing, A.A. Bokov, B. Noheda, G. Shirane, and Z.-G. Ye, "Relaxor-to-Ferroelectric Phase Transition in $Pb(Zn_{1/3}Nb_{2/3})O_3$ Single Crystals" (O), 11th International Meeting on Ferroelectrics (IMF-11). Iguassu Falls, Brazil/Argentina, Sept. 5 – 9, **2005.**

[81] C. Lei, A. A. Bokov, and Z.-G. Ye, "Ferroelectric and Relaxor Properties of the $BaTiO_3$ - $BaSnO_3$ Solid Solutions" (O), 11th International Meeting on Ferroelectrics (IMF-11). Iguassu Falls, Brazil/Argentina, Sept. 5 – 9, **2005.**

[82] A. A. Bokov, and Z.-G. Ye, "Crossover from Critical Behavior to Double Freezing in (1-x)$Pb(Mg_{1/3}Nb_{2/3})O_3$ –x$PbTiO_3$ Relaxors", *2006 Conference on Fundamental Physics of Ferroelectrics*, Colonial Williamsburg, VA, USA, Feb. 12 – 15, **2006**.

[83] Y.-H. Bing, A. A. Bokov, and Z.-G. Ye, "Phase Transition in Ferroelectric Relaxors – A Comparative Study of $Pb(Sc_{1/2}Nb_{1/2})O_3$, $Pb(Zn_{1/3}Nb_{2/3})O_3$ & $Pb(Mg_{1/3}Nb_{2/3})O_3$", *2006 Conference on Fundamental Physics of Ferroelectrics*, Colonial Williamsburg, VA, USA, Feb. 12 – 15, **2006**.

[84] M. Matsuura, K. Hirota, P. M. Gehring, Z.-G. Ye, W. Chen and G. Shirane, "Composition Dependence of the Diffuse Scattering in the Relaxor Ferroelectric Compounds (1-x)$Pb(Mg_{1/3}Nb_{2/3})O_3$–x$PbTiO_3$ ($0 \leq x \leq 0.40$), *American Physical Society Meeting*, Baltimore, MD, March 13 – 17, **2006**.

[85] Z.-G. Ye, Y. Bing and A. Bokov, "Phase Transitions in Relaxor Ferroelectric crystals", 2006-U.S. Navy Workshop on Acoustic Transducer Materials and Devices, Penn State University, PA, May 8 - 11, **2006.**

[86] A. A. Bokov, and Z.-G. Ye, "Crossover from Double-Freezing to Critical Behavior in Relaxor Ferroelectric (1-x)$Pb(Mg_{1/3}Nb_{2/3})O_3$–x$PbTiO_3$ Solid Solution" (O & P), 2006-U.S. Navy Workshop on Acoustic Transducer Materials and Devices, Penn State University, PA, May 8 - 11, **2006.**

[87] W.-M. Zhu and Z.-G. Ye, "Structural and Magnetic Characterization of Multiferroic (1-x)$BiFeO_3$–x$PbTiO_3$ Solid Solution with MPB Compositions" (O & P), 2006-U.S. Navy Workshop on Acoustic Transducer Materials and Devices, Penn State University, PA, May 8 - 11, **2006.**

[88] W.-M. Zhu and Z.-G. Ye, "Effect of Aliovalent Ionic Doping on the Ferroelectric Properties of High-T_C 0.67$BiFeO_3$–0.33$PbTiO_3$ Ceramics" (O & P), 2006-U.S. Navy Workshop on Acoustic Transducer Materials and Devices, Penn State University, PA, May 8 - 11, **2006.**

[89] Y.-H. Bing, H.-Y. Guo, and Z.-G. Ye, "Phase Transitions in Relaxor Ferroelectrics - Kinetics of Polar Nanoregions and Effects of Electric Field" (O), 9th International Symposium on Ferroic Domains and Micro- to Nano-scopic Structures (ISFD-9), June 27 – 31, **2006**.

[90] Y.-H. Bing, H.-Y. Guo, and Z.-G. Ye, "Meso- to Macroscopic Domain Structures and Phase Transitions in $Pb(Sc_{1/2}Nb_{1/2})O_3$ and $Pb(Sc_{1/2}Nb_{1/2})O_3$–$PbTiO_3$ Single Crystals" (*The Best Poster Award*), 9th International Symposium on Ferroic Domains and Micro- to Nano-scopic Structures (ISFD-9), June 27 – 31, **2006**.